Similarity Solution of Unsteady MHD Boundary Layer Flow of a Nanofluid for Free and Forced Convection Around an Inclined Plate

By

S. M. OSMAN GANI

Roll No.: 16MMATH002P

A Thesis submitted in partial fulfillment of the requirement for the degree of

MASTER OF PHILOSOPHY IN MATHEMATICS

Department of Mathematics

CHITTAGONG UNIVERSITY OF ENGINEERING & TECNOLOGY, CHITTAGONG, BANGLADESH

2024

CANDIDATE'S DECLARATION

I hereby declare that the work contained in this Thesis has not been previously submitted to meet requirements for an award at this or any other higher education institute. To the best of my knowledge and belief, the Thesis contains no material previously published or written by another person except where due reference is cited. Furthermore, the Thesis complies with the PLAGIARISM and ACADEMIC INTEGRITY regulation of CUET.

_____

(S. M. OSMAN GANI)

Student ID: 16MMATH002P

Department of Mathematics

CHITTAGONG UNIVERSITY OF ENGINEERING & TECNOLOGY (CUET)

Approval by the Supervisor

This is to certify that S. M. OSMAN GANI, ID: 16MMATH002P has carried out this research work under my supervision, and that he has fulfilled the relevant Academic Ordinance of the Chittagong University of Engineering & Technology, so that he is qualified to submit the following Thesis in the application for the degree of MASTER of PHILOSOPHY in MATHEMATICS. Furthermore, the thesis complies with the PALGIARISM and ACADEMIC regulation of CUET.

Professor Dr. Md. Yeakub Ali

Department of Mathematics

Chittagong University of Engineering and Technology

DEDICATION

Dedicated

To

My dearest Parents and beloved Wife

List of Publication

Published Paper:

The results presented in the following publication are included in the thesis.

1. **Gani, S.M.O.,** Ali, M.Y. and Islam, M.A., 2022. Effects on Unsteady MHD Flow of a Nanofluid for Free Convection past an Inclined Plate. *Journal of Scientific Research*, *14*(3), pp.797-812.

   http://dx.doi.org/10.3329/jsr.v14i3.58301 **(Chapter 2)**

Acknowledgement

Firstly, I want to express my gratitude to Almighty, the most kind and generous for enabling me to accomplish this thesis work.

To my view, acknowledge with sincere appreciation and a deep feeling of respect to my supervisor **Professor Dr. Md. Yeakub Ali**, Department of Mathematics, Chittagong University of Engineering & Technology (CUET) for his kind guideline, motivating discussion and constant guidance I've received through the research work and introduced me such an interesting field of research.

I would want to take this time to thank every one of my beloved mathematics teachers at CUET for their invaluable suggestions and guidance during this endeavor.

I acknowledge and express my gratitude through my respected supervisor and also to the Simulation Lab, Department of Mathematics, and CUET for the technical assistance to complete this work.

I am thankful of all the support; I received during this moment from Chittagong University of Engineering & Technology (CUET) authorities.

Last but not least, I'd like to give thanks to my family, colleagues, relatives, friends and well-wishers for their unwavering encouragement and support.

January 2024 **S. M. OSMAN GANI**

Abstract

This study investigates the unsteady magnetohydrodynamic (MHD) boundary layer flow of electrically conducting nanofluids over an inclined plate, considering both forced and free convection. This flow situation is relevant to various engineering applications, including solar water heaters, inclination sensors, heat removal in industrial processes, and even deterrence, power generation in nuclear reactors, and biomedical applications. The governing equations are transformed into ordinary differential equations using similarity solutions. These equations are then solved numerically with the sixth-order Runge-Kutta method and the Nachtsheim-Swigert iteration technique. The effects of various parameters, such as the buoyancy ratio, magnetic field strength, Brownian motion, thermophoresis, and unsteadiness, on the velocity, temperature, and concentration profiles are analyzed in detail through graphical representations and discussions.

Furthermore, the influence of these parameters on the skin friction coefficient, Nusselt number (heat transfer), and Sherwood number (mass transfer) is presented in tabular form. The numerical results reveal that increasing the nanofluid viscosity leads to a rapid rise in the velocity profiles. Conversely, higher unsteadiness parameters are associated with decreases in both velocity and concentration profiles.

বিমূর্ত

এই গবেষণাটি জোরপূর্বক এবং মুক্ত উভয় পরিচলন বিবেচনা করে একটি ঝোঁকযুক্ত প্লেটের উপর বৈদ্যুতিকভাবে পরিচালিত ন্যানোফ্লুইডগুলির অস্থির চৌম্বকীয়-হাইড্রোডায়নামিক (MHD) সীমানা স্তর প্রবাহের তদন্ত করে। এই প্রবাহ পরিস্থিতি সৌর জল উত্তাপ, প্রবণতা সেন্সর, শিল্প প্রক্রিয়াগুলিতে তাপ অপসারণ এবং এমনকি প্রতিরোধ, পারমাণবিক চুল্লিতে বিদ্যুৎ উৎপাদন এবং বায়োমেডিকাল অ্যাপ্লিকেশন সহ বিভিন্ন প্রকৌশল প্রয়োগের জন্য প্রাসঙ্গিক। পরিচালনাকারী সমীকরণগুলি সাদৃশ্য সমাধান ব্যবহার করে সাধারণ ডিফারেনশিয়াল সমীকরণে রূপান্তরিত হয়। এই সমীকরণগুলি তারপর ষষ্ঠ-ক্রমের Runge-Kutta পদ্ধতি এবং Nachtsheim-Swigert পুনরাবৃত্তি কৌশল দিয়ে সংখ্যাসূচকভাবে সমাধান করা হয়। বেগ, তাপমাত্রা এবং ঘনত্ব প্রোফাইলের উপর বিভিন্ন পরামিতিগুলির প্রভাব, যেমন প্লবতা অনুপাত, চৌম্বক ক্ষেত্রের শক্তি, ব্রাউনিয়ান গতি, থার্মোফোরেসিস এবং অস্থিরতা, গ্রাফিকাল উপস্থাপনা এবং আলোচনার মাধ্যমে বিস্তারিতভাবে বিশ্লেষণ করা হয়।

উপরন্তু, ত্বকের ঘর্ষণ সহগ, নুসেল্ট সংখ্যা (তাপ স্থানান্তর) এবং শেরউড সংখ্যা (ভর স্থানান্তর)-এর উপর এই পরামিতিগুলির প্রভাব ট্যাবুলার আকারে উপস্থাপন করা হয়। সংখ্যাসূচক ফলাফলগুলি প্রকাশ করে যে ন্যানোফ্লুইড সান্দ্রতা বৃদ্ধি বেগ প্রোফাইলগুলিতে দ্রুত বৃদ্ধির দিকে পরিচালিত করে। বিপরীতভাবে, উচ্চতর অস্থিরতা পরামিতিগুলি বেগ এবং ঘনত্ব প্রোফাইল উভয়ের হ্রাসের সাথে যুক্ত।

CONTENTS

List of Figures

List of Tables

Nomenclature

B_0	Uniform magnetic field strength
P	Unsteadiness parameter
Db	Brownian diffusion coefficient
D_T	Thermophoresis diffusion coefficient
f	Dimensionless stream function
g_e	Acceleration due to gravity
h_f	Heat transfer coefficient
k	Thermal conductivity
M	Dimensionless magnetic parameter
Nb	Brownian Motion parameter
Nr	Buoyancy-ration parameter
Nt	Thermophoresis parameter
N_{u_x}	Local Nusselt number
Nur	Reduced Nusselt number
Pr	Prandtl number
R_{a_x}	Local Rayleigh number
$Sh_{x,n}$	Local nanoparticle Sherwood number
$Shrn$	Reduced nanoparticle Sherwood number
T	Fluid temperature
T_f	Hot fluid temperature
T_w	Fluid temperature at the wall
T_∞	Ambient temperature
u, v	Velocity component along x and y-directions
d	Acute angle of the plate to the vertical

Greek symbols

α_m	Thermal diffusivity
β	Thermal expansion coefficient
μ	Viscosity of the nanofluid
ν	Kinematic viscosity of the fluid
ϕ	Dimensionless nanoparticle volume fraction
$\hat{\phi}$	Nanoparticle volume fraction
$\widehat{\phi_w}$	Nanoparticle volume fraction at the wall
$\widehat{\phi_\infty}$	Ambient Nanoparticle volume fraction
Ψ	Steam function
ρ_f	Density of the nanofluid
σ_{nf}	Electrical conductivity of the nanofluid
τ	Ratio between the effective heat capacity of the nanoparticle material and heat capacity of the fluid
θ	Dimensionless temperature

Subscripts

f	Base fluid
nf	Nanofluid
ω, ∞	Condition at the surface and in the free stream, repectively

Chapter 1

1.1 Fluid Mechanics

The science of fluid dynamics is also separated into various classes. The investigation of how fluids transfer can be generally referred to as hydrodynamics, as they are incompressible (including liquids, particularly water, and gases traveling slowly). A specialized branch of hydrodynamics named hydraulics studies liquid flows in pipelines and open channels. The study of fluids that experience large density changes, such as gases passing rapidly through nozzles, is called "gas dynamics. The topic of aerodynamics investigates the flow of gases, especially air, over objects moving at high and low speeds, including automobiles, rockets, and airplanes. Other specialized fields, such as hydrology, meteorology, and oceanography, deal with naturally occurring flows (Çengel et al., 2017)

1.2 Viscosity

The measure that is used to describe a fluid's resistance to flow is referred to as viscosity. The relative movements of immersed objects in fluids as well as the motion of levels with different velocities within them are both difficult. Elastic stresses are those that may be attributed to a material's deformation caused by its rest state. In the shear stress in the x direction for a fluid, where v is the fluid's velocity in the x direction at a distance of y from the boundary and x is the direction of motion, we have Newton's law of viscosity. The viscosity of gases increases as temperature increases, while the viscosity of liquids rapidly decreases as temperature increases. Liquids flow more smoothly when warmed, whereas gases are slower to move. For instance, water has a viscosity of 0.85×10^3 pascal-second at 27 °C (81 °F) and 0.36×10^3 pascal-second at

77 °C (171 °F), respectively, compared to 1.85 × 5 and 2.08 × 10^5 pascal-second for air at the same temperatures (Mosallanezhad et al., 2024)

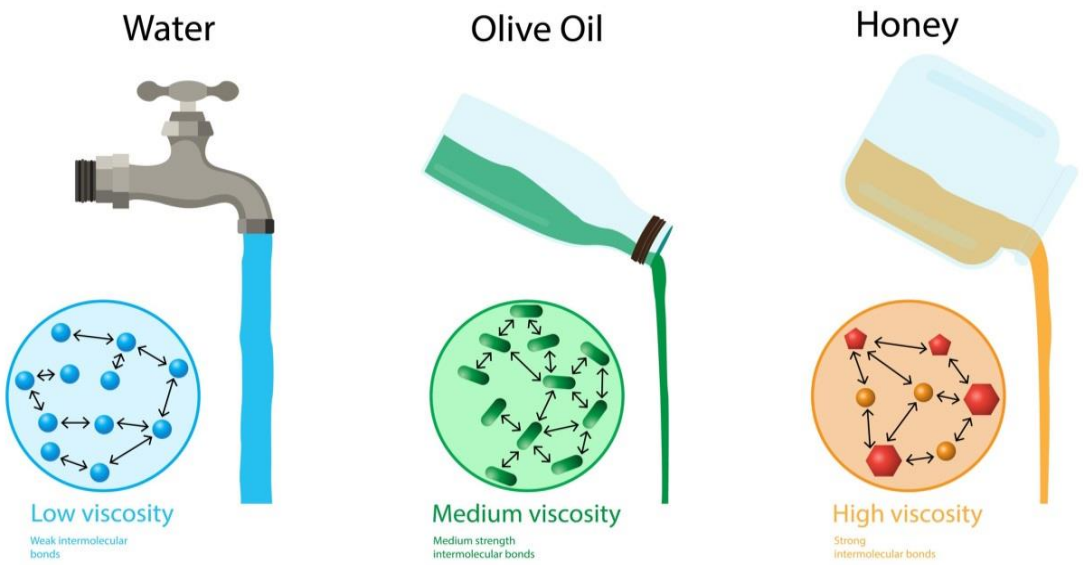

Figure 1.1: Viscosity of Liquid

1.3 Megnetohydrodynamic

Megnetohydrodynamics (MHD) is a branch of physical science that focuses on research into the magnetic properties and behavior of electrically conducting fluids. Electromagnetic theory and fluid dynamics are two established branches of physics. The analysis of hydrodynamic flows is described as magnetodynamics. The word magnetodynamics was first introduced by Hannes Alfyen.

The terms "magnetohydrodynamics" (MHD) and "liquid dynamics" are formed from the words "magneto" and "liquid," respectfully. The essential idea of MHD is that magnetic fields can generate when the fluid is polarized, a current will move through a moving conducting field, changing the magnetic field. This article will give a brief introduction to magnetohydrodynamics and cover some of its fundamental

ideas. Several branches of physics, especially solar physics, Magnetohydrodynamics plays a major role in plasma physics, astrophysics, and other fields where we can study the magnetohydrodynamics of the sun. A magnetic field's impact on a dynamically conducting fluid is indeed the central objective of MHD physics. Later, the MHD also displays relativistic properties; for this purpose, it is sometimes repeatedly alluded to as general relativistic magnetohydrodynamics or classical magnetohydrodynamics. According to its relativistic research, MHD physics does have some applications. Let's analyze a few important magnetohydrodynamic applications. macroscopic balance of forces, equilibrium, and dynamics are generally described by MHD. On an immense scale, ideal MHD characterizes dynamics quite well. A useful measure of plasma stability is ideal MHD. The vast majority catastrophic instabilities are unstable in such an ideal MHD, that is part of interesting facts. It really is established In the large majority of astrophysical plasmas, MHD is an acceptable approximation. So far, sometimes extensions are needed (ALFVÉN, 1942)

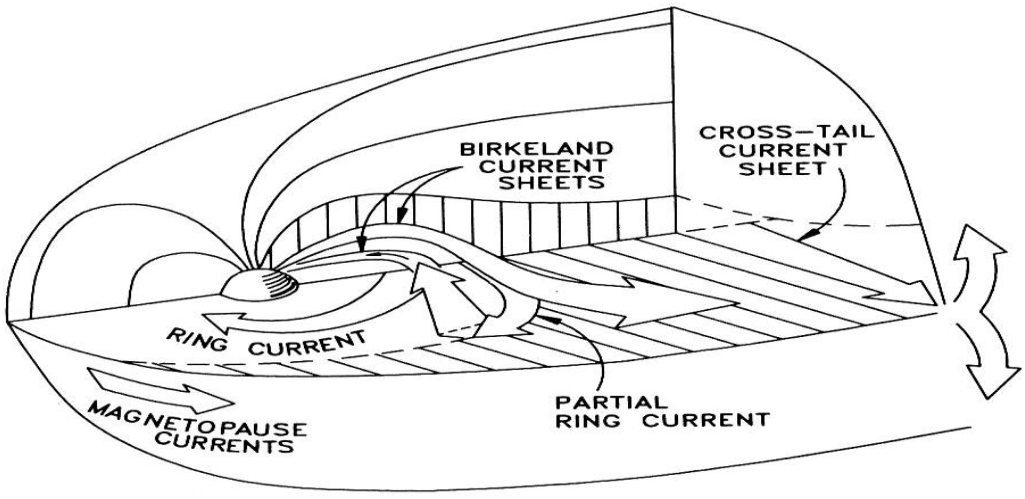

Figure 1.2: Schematic view of the different current system which shapes the Earth's magnetosphere.

1.4 Heat Transfer

We are all aware that a heated, preserved liquid that has been refrigerated cools down, whereas a cold, preserved drink warms up in a room. By transmitting power from a warm medium to a cold one, this is polished. When both mediums are at the same temperature, the energy transfer ceases as it continues to flow from a medium compared with one that is colder in temperature. There are different types of energy. The type of energy that is capable of being switched within systems due to an increase or drop in temperature is what we are specifically interested in. The science of heat transfer is associated with understanding the rates of these kinds of energy transfers. The cumulative effect of these three methods of heat transmission unquestionably regulates how hot or cold a medium is. These are simple descriptions of three categories (Kirkwood, P.E. and Parker-Gibson, 2013)

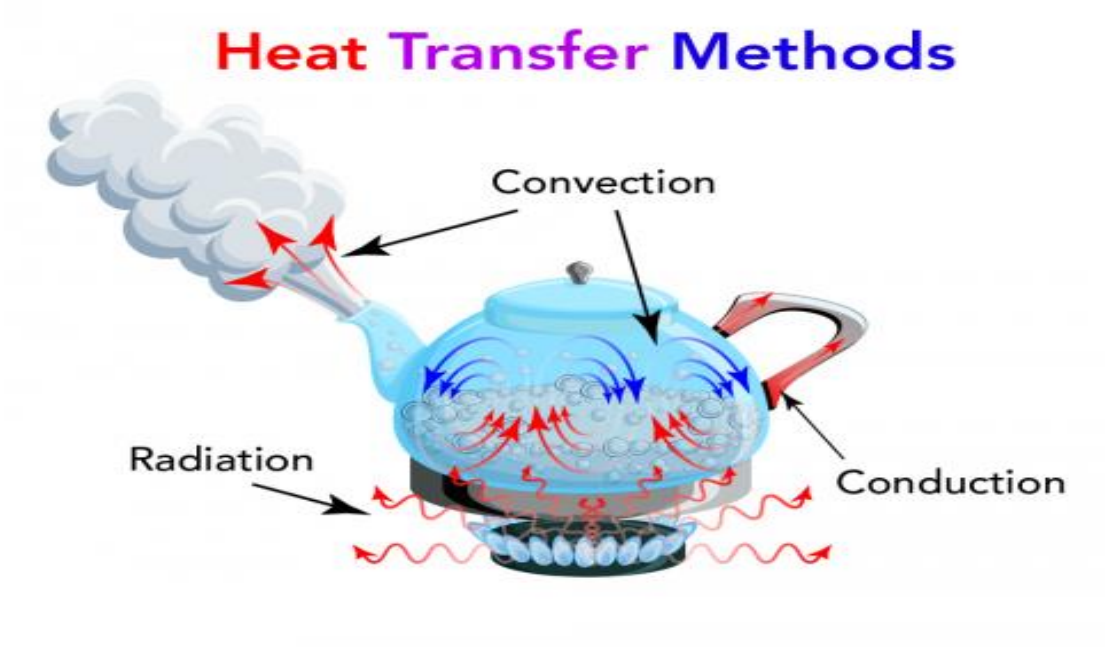

Figure 1.3: Mechanisms of conduction, convection, and radiation for heat transferred.

1.5 Heat Conduction

When two substances are in direct contact with one another, a process called conduction occurs. More rapidly than in a cooler body, the molecules in a warmer one vibrate. The slower molecules clash with the faster vibrating molecules. The object warms up as a consequence of the cooler molecules vibrating at a faster rate. Have you ever sat on a cool couch, for instance? When you stood up, were you aware of how much warmer the seat was? The movement of molecules caused on the couch by the heat from your skin (Kirkwood, P.E. and Parker-Gibson, 2013).

Conduction can actually occur within a particular element as well. Assume a metal rod that has recently been introduced into a fireplace. The end of the rod that has been in touch with the embers becomes incredibly hot. The heated end's energy will travel through the rod to the colder end. The temperature of the entire rod will ultimately be the same. This is why using a hot metal rod demands the use of gloves (Haile, E. and Shankar, 2015)

We can determine that the plane layer's frequency of heat conduction has an inverse relationship with the layer's thickness and corresponds with the temperature deviation all over the layer and around the area of heat transfer, i.e.

$$Q = -K\frac{dT}{dx}$$

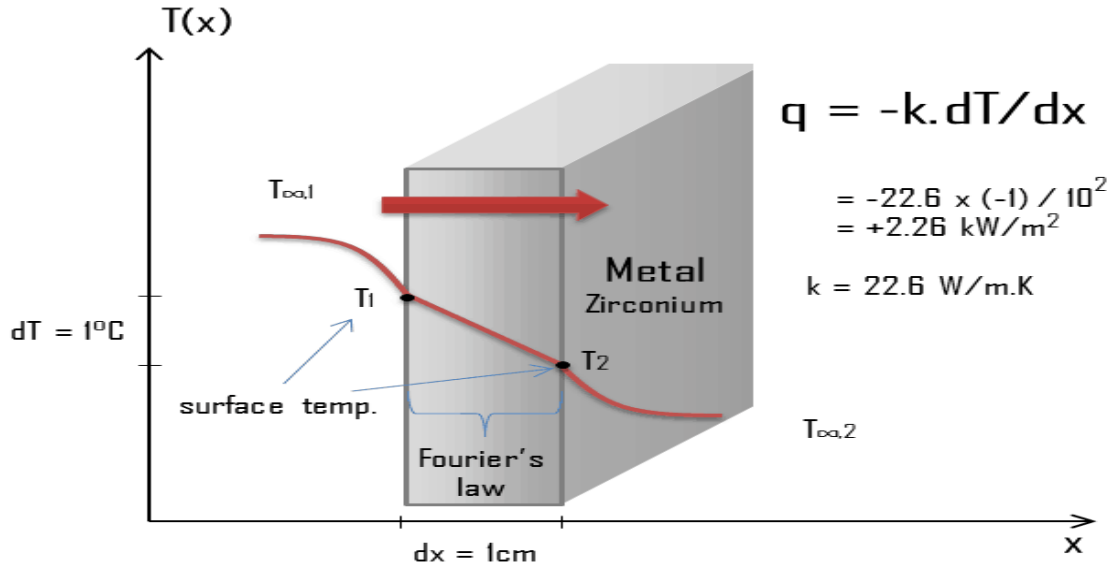

Figure 1.4: Heat conduction in surface area, rate of heat transfer

Heat conduction was first established by J.B.J. Fourier in 1822. K is a measure of a material's capability to conduct heat and indicates the material's thermal conductivity. The rate at which the temperature T rises with respect to the difference in the direction of the heat flow x, known as the temperature gradient at the section, is expressed by dT/dx. The direction of positive heat flow is in the direction of increasing distance x, and this sign convention is necessary for mathematically describing the heat conduction equation. Heat will gradually gravitate from hot spots to lower areas whenever the temperature changes. Correspondingly, when the temperature gradient is negative, heat flow will be positive.

1.6 Heat convection

The movement of thermal energy through fluids has been demonstrated by convective heat transfer. Large-scale molecular movement underneath the liquid,

gas, or liquid-gas mixture is the reason of convection. Conduction is the primary method through which heat is transported between molecules; however, fluid motion also plays a significant role in heat transmission. Both thermal diffusion, in which fluid molecules move randomly, and convection, forms of convective heat transfer, occur when heat is transported through the fluid's expanding current motion. There are two primary mechanisms that make up the convective mode of heat transfer: forced convection and spontaneous or free convection.

1.6.1 Forced Convection

A technique that assists in producing motion in a flowing fluid by applying force externally is known as forced convection of heat transfer, which is a classification of heat transfer caused by forced convection. Forced convection heat transfer is utilized almost everywhere, regardless of whether it's a steam turbine, a heating system, a pump, a suction device, or another device. Buoyancy affects the forced convection flow's temperature and velocities fields, which alter the wall, shear force parameters crucial to the majority of engineering problems (Abin John*, Jithin Thomas*, Jose S Kattukaran*, Relno Baby M*, 2014)

Figure 1.5: Forced convection heat transfer

1.6.2 Natural or Free Convection

Natural convection, also known as "buoyant" or "free" Convection, is a vital process mechanism that is effective in a wide range of circumstances, including cooling electrical circuit boards in computers, creating massive atmospheric circulation, and affecting the weather. It occurs because of the combination of a gravitational field and density gradients. Laminar and turbulent free-convective flows are both possible. A flow throughout a rigid surface with a temperature that is the most prevalent type of free convection occurs when the flow medium is higher or lower than it is. Inversely correlated to fluid flow rate is the quantity of heat transfer brought on by free convection between a surface and a fluid. The flow rate rises in proportion to the rate at which heat transfer (Sun et al., 2012)

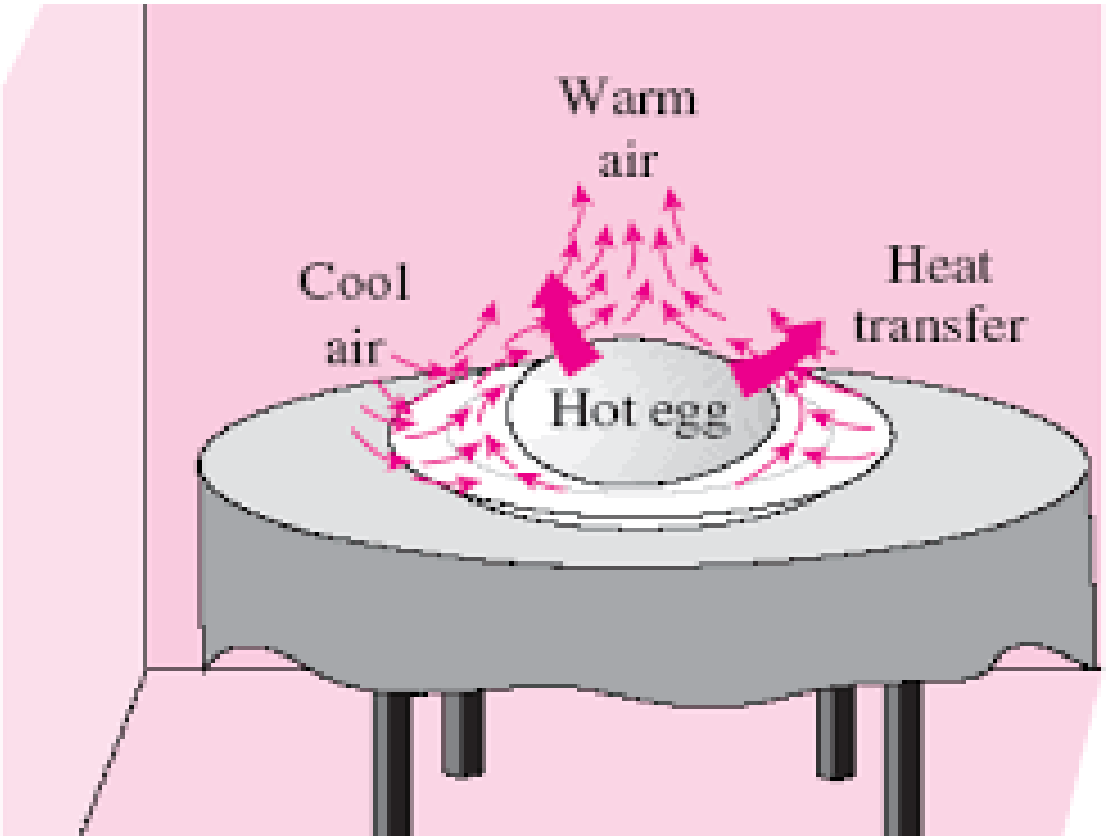

Figure 1.6: Free or Natural heat transfer

1.6.3 Mixed or Combined Convection

Integrating forced and free convection, mixed convection takes place when a particular moment is created concurrently by an external forcing mechanism (i.e., a distant source of energy for the streamlined, fluid framework of the body) and an internal volumetric force. The flow, temperature, form, and orientation each play significant roles in determining whether each type of convection contributes to the movement of heat. It will be expected that the impact of free convection on heat transmission can be discounted for large Reynolds numbers and small Grashof values. On the other hand, free convection should predominate for big Grashof numbers and small Reynolds numbers. The Archimedes number (Ar), which is used to analyze potentially mixed convection, parameterizes the proportional strength of forced and free convection. The Grashof-Reynolds squared ratio determines the Archimedes number.

$$Ar = \frac{Gr}{Re^2}$$

When Ar 1 is present, forced convection takes dominance over natural convection (Sun et al., 2012) .

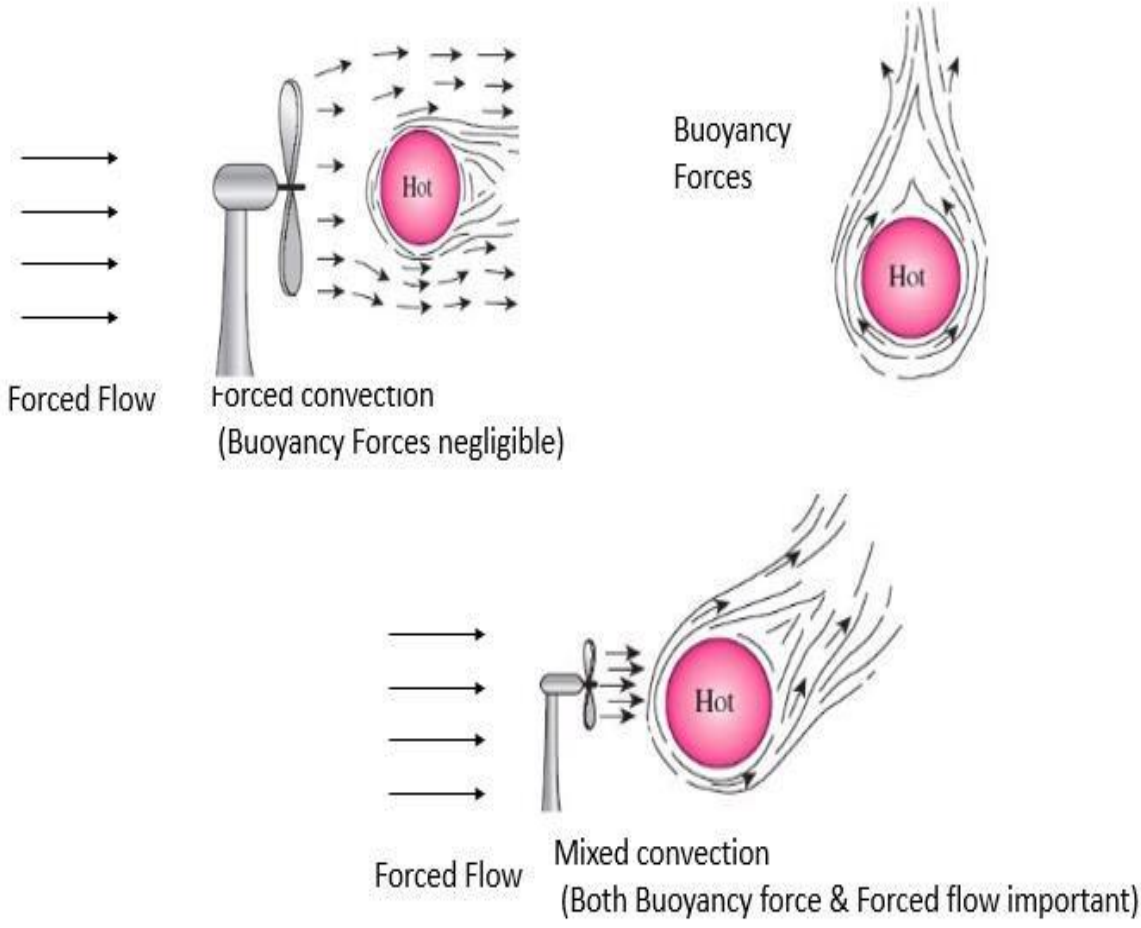

Figure 1.7: Mixed convection heat transfer

1.7 Radiation

All matter consists of photons at temperatures above absolute zero, which are transmitted as electromagnetic waves as a result of modifications in atoms' electronic structures. Radiation does not require an intervening medium to carry it. Radiate heat transfer happens in the vacuum of space. For example, the heating of the earth by the sun is a transfer of energy by radiation (Bazukyan, I.L., Rostomyan, A.V., Hovhannisyan, A.G., Aleksanyan, T.M., Hakobyan, L.L., Dallakyan, A.M. and Haertlé, 2022).

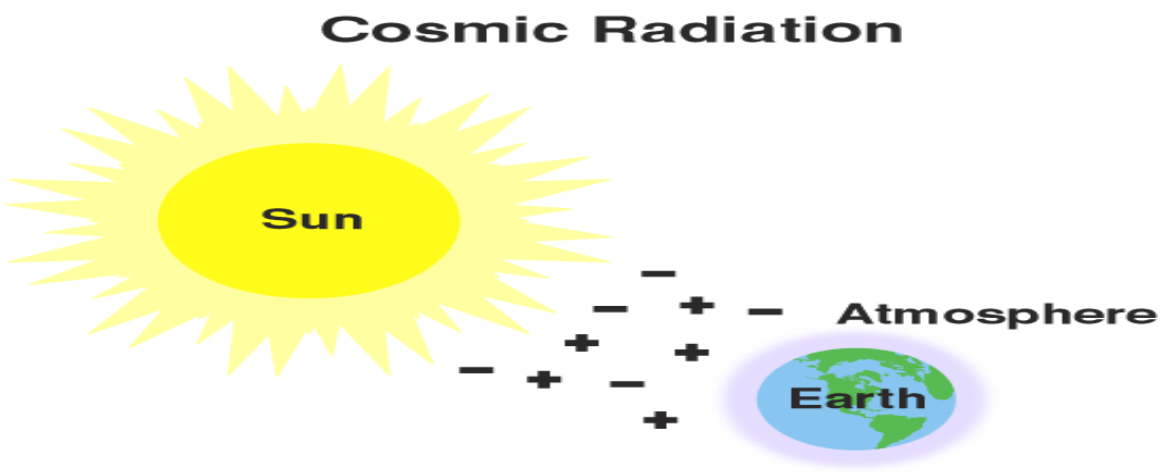

Figure 1.8: Radiation heat transfer

1.8 Thermal Conductivity

Thermal conductivity, denoted by the symbol k, is a measure of a material's capacity to conduct heat. A substance's capability to store thermal energy is gauged by its specific heat capacity (Cp). Different materials store heat in various ways. If the material has a high thermal conductivity value, it is an excellent heat conductor or insulator. For instance, water has a specific heat capacity of 4.18 kJ/kg and iron has a specific heat capacity of 0.45 kJ/kg, suggesting that water can store roughly 10 times the energy per unit mass as iron at ambient temperature. The shape of the medium affects the rate of heat conduction through it. Consider a solid object wedged between two environments with contrasting temperatures. Assuming $T_2 > T_1$, let T_1 be the temperature at $x=0$ and T_2 be the temperature at $x=L$. This situation can appear as a structure on a chilly winter day, with the building wall serving as the solid substance dividing the warm interior space from the cold exterior. Diffusion will cause the temperature differential to equalize, causing heat to pass from the warmed environment to the chilled one. The rate of heat

movement per unit area in a particular direction (in this case, the minus x-direction) can be expressed in terms of a heat flux, or q. In many materials, it has been found that q is inversely connected with separation distance and accurately corresponds to the temperature difference (Hed, G. and Bellander, 2006).

$$q = -k\frac{T_2 - T_1}{L}$$

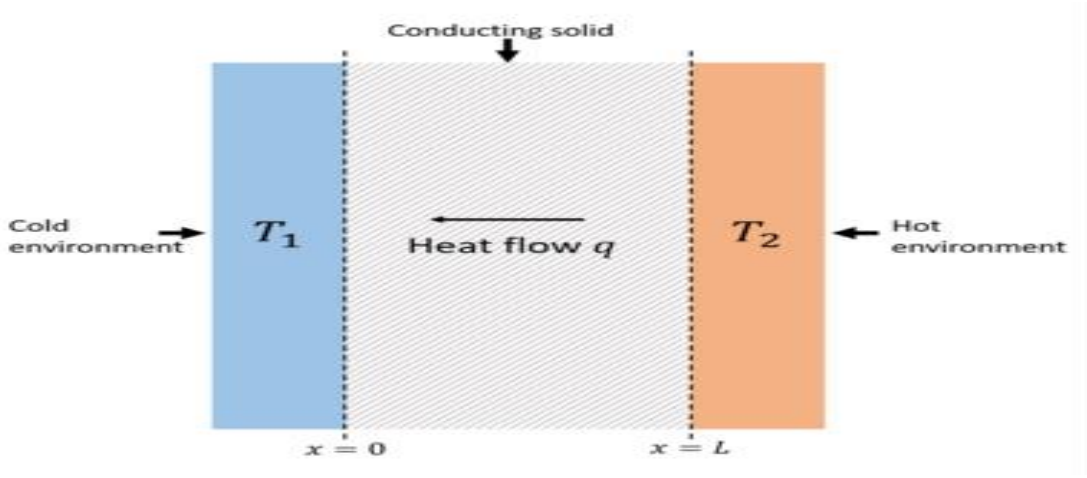

Figure 1.9: Thermal conductivity can be defined in terms of the heat flow q across a temperature difference.

1.9 Thermal Diffusivity

Thermal diffusivity can be determined by dividing thermal conductivity by specific heat capacity and density under constant stress. It calculates the rate at which heat transfers between the hot and cold ends of a material. The scientific description of thermal diffusivity is $\alpha = \frac{k}{\rho C_p}$.

K here refers to thermal conductivity.

The capacity absorbing heat is C_p.

The amount of density there is ρ.

The ratio of heat retained per unit volume to heat transported through a substance is known as its thermal diffusivity. A substance with a high density is made up of atoms and molecules that are tightly packed together. The quantity of heat that can pass through an object and at what speed and distance depends on its density. Imagine a road that has extra toll booths, with the cars representing energy quanta in the form of heat (Hetnarski, R.B., Eslami, M.R. and Gladwell, 2009)

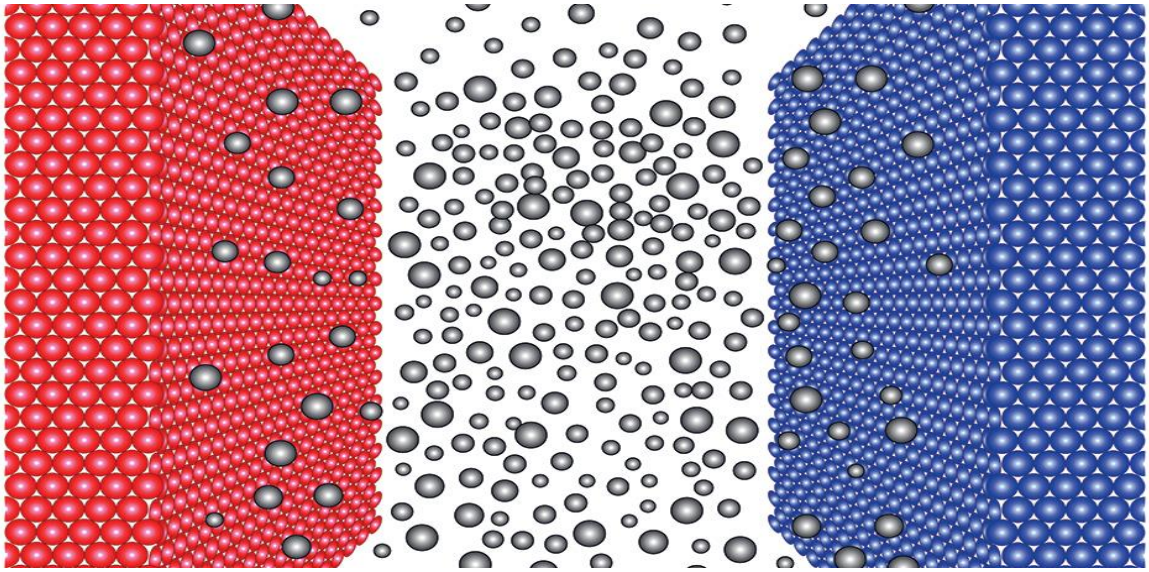

Figure 1.10: Measurement of thermal diffusivity

1.10 Thermophoresis

Thermophoresis, a radiometric force brought on by a temperature differential, accelerates the movement of microscopic particles in one direction toward a cold surface and in the reverse direction away from a hot surface. Velocity is the term used to describe the thermophoretic motion. Particles are transported via thermophoresis from the hot fluid zone to the frigid region. Several engineering uses of this phenomenon involve looking into the material, eliminating tiny

particles from gas steams, adsorption on turbine blade steams, and calculating the trajectories of removed gas particles from combustion devices. Grading index germanium dioxide and silicon dioxide for use in the manufacture of optical fiber for communications can be generated through the thermophoresis technique. Technology incorporating semi-conductive materials, especially for the manufacturing of controlled, high-quality wafers and the creation of magnetohydrodynamic (MHD) energy, is an additional significant mechanism to be investigated. One of the main reasons for nuclear reactor accidents is the deposition of radioactive particles during thermophoresis. Therphoretic force and velocity depend on a number of factors, in particular the aerosol particle's and the carrier gas's thermal conductivity, which have an inverse relationship with the temperature gradient (Talbot, L.R.K.R.W.D.R., Cheng, R.K., Schefer, R.W. and Willis, 1980).

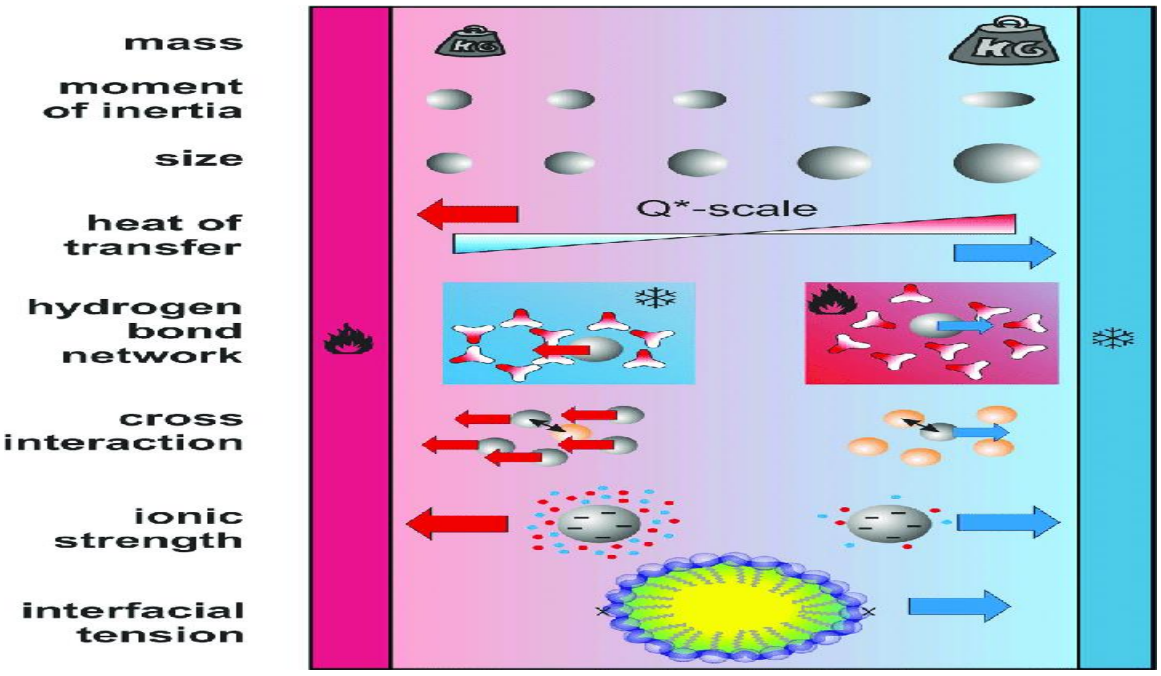

Figure 1.11: Sketch of a roadmap to identify the direction of the thermophoretic motion.

1.11 Compressible and Incompressible Flow

Regardless of being the case that all fluids are compressible, pressure variations alter their density. It is generally possible to simplify the analysis of the flow in steady settings by assuming it is incompressible and has a constant density, as long as the fluctuations in pressure are minor. Since liquids are very difficult to compress, they are generally regarded as incompressible under steady conditions. Very high-pressure differences can arise in some unstable settings, so it's important to consider them. Gases are simply compressed, taking the outcome of compressible and pressure changes into account when the changes in density and pressure are relatively modest.

1.12 Steady Flow

When there is a steady flow, the flow doesn't change over time. Nevertheless, if the rate of change in both pressure and velocity is equal on either side of a fixed average value, the flow is determined to be constant if the average values remain constant. The following lists many flow types*:*

1.12.1 Steady uniform flow:

Every point in the fluid and every cross-section have the same velocity and cross-section area at every given time. As an example, think of the way a liquid flows through a pipe with a uniform windbag at successive full velocities.

1.12.2 Steady non-uniform flow:

Although conditions fluctuate throughout time, they do not always remain so. From cross-section to cross-section, the fluid has a different velocity and cross-section area. For instance, the friction causes water flowing along the channel sides to travel more slowly than water in the channel's center.

1.12.3 Unsteady uniform flow:

The circumstances at every point are the same at a specific point in time, but they will vary throughout time: For instance, when a pump is turned off, the flow of fluid through a pipe with a uniform bore that is running full might accelerate.

1.12.4 Unsteady non-uniform flow:

A process in which the amount of liquid moving per second changes. During water release, for instance, water flows through the system of canals.

1.13 Prandtl Number Pr

The ratio of the diffusivity of momentum (kinematic viscosity) compared with the diffusivity of heat is known as the Prandtl number, which has no dimensions. Ludwig Prandtl, a German physicist, first proposed. It is denoted by:

$Pr = \frac{\nu}{\alpha}.$

$= \frac{viscous\ diffusion\ rate}{thermal\ diffusion\ rate} = \frac{\mu c_p}{k}.$

Where, $\nu = Kinematics\ viscodity, \nu = \frac{\mu}{\rho}$

$\alpha = Thermal\ diffusivity, \alpha = \frac{k}{\rho c_p}.$

$\mu = Changing\ viscosity.$

K, Thermal conductivity

$c_p, The\ Specific\ heat.$

$\rho = Density.$

The Prandtl number is only and has no length scale subject to the fluid and the liquid state, in contrast to the Reynolds and Grashof numbers, which have scale elements subscripted. On property charts, the Prandtl number is usually shown together with additional characteristics like both thermal conductivity and viscosity.

Average values are:

- For molten potassium, 0.003
- 0.015 or so for mercury
- For molten lithium, use 0.065.
- 0.16 to 0.7 for noble gas or noble gas and hydrogen combinations0.63 for oxygen
- For air and many other gases, roughly 0.71
- 1.38 for ammonia gas
- for the refrigerant R-12, between 4 and 5
- 7.56 or so for water (18 °C)
- For seawater, at 0 and 20 degrees Celsius, respectively, 13.4 and 7.2
- For n-butanol, 50
- Engine oil, between 100 and 40,000
- For glycerol, 1000
- 10,000 for melts of polymer
- The mantle of the Earth is about 1×10^{25}.

The Prandtl number, $Pr \ll 1$, indicates that thermal diffusivity predominates, but when $Pr \gg 1$ is high, momentum diffusivity dominates. Heat conduction instead of convection is more significant for liquid mercury, demonstrating that thermal diffusivity is predominant. However, for engine oil, momentum diffusivity

dominates because convection is much more efficient than pure conduction at transferring energy from a region. Gases have Prandtl values close to 1, which means that heat and momentum travel through the fluid exactly at the same frequency. Compared to the velocity boundary layer, Oils have a substantially smaller thermal boundary obstacles than liquid metals, and conversely. The Prandtl number's mass transfer counterpart is known as the Schmidt number, increased by the previous value results in the Lewis number.

1.14 Magnetic Parameter M

The magnetic parameter has been described as a proportion of the force of attraction to magnetic fields to the force of inertia.

$M = \frac{\sigma B_0^2 L}{\rho U}$.

If this is of order 1, then there is a strong magnetic force present, and the flow must be classified as hydromantic flow. If it is significantly under one, the flow can be considered hydrodynamic. When M is little, the magnetic field has little impact on motion; however, when M is large, the magnetic field significantly influences motion.

1.15 Rayleigh number R_{a_x}

The Rayleigh number for a fluid, commonly referred to as the buoyancy drive flow or free convection, is connected to the buoyancy drive flow. It is denoted by

$R_{a_x} = \frac{\beta g(T_f - T_\infty)x^3}{\nu\alpha} = Gr.Pr.$

The unique length is x.

R_{a_x} is the Rayleigh number for the characteristic length x.

g = the acceleration caused by gravity.

β is the thermal expansion coefficient, which is equal to 1/T (T is the absolute temperature) for ideal gases.

Kinematic viscosity is denoted by ν

Thermal diffusivity is α.

T_f is the hot fluid temperature.

T_∞ = fluid temperature (quiescent temperature) at a distance from the object's surface.

Grashof number for characteristic length equals x in Gr_x

Pr = Prandtl number

The Grashof and Prandtl numbers multiply to produce the Rayleigh number. The Rayleigh number's significance gives an accurate measure of whether the boundary layer of natural convection is laminar or turbulent. The Rayleigh number is significant for most engineering applications, ranging from 10^6 to 10^8.

1.16 Nusselt Number N_{u_L}

The Nusselt number (Nu) is a dimensionless parameter that quantifies the enhancement of heat transfer across a boundary in a fluid due to convection, relative to pure conduction. Convection encompasses both diffusive (conductive) and advective (fluid motion) heat transfer mechanisms. It is named after the German engineer Wilhelm Nusselt. The Nusselt number is calculated by comparing the convective heat transfer coefficient to the thermal conductivity of the fluid and a characteristic length. A Nusselt number of one signifies purely

conductive heat transfer across the fluid layer, under identical conditions as convective heat transfer (but with a stationary fluid). Higher Nusselt numbers indicate a greater contribution of convection to the overall heat transfer process. Turbulent flows, typically with velocities ranging from 100 to 1000 m/s, are associated with significantly larger Nusselt numbers, reflecting their enhanced heat transfer efficiency.

$N_{u_L} = \frac{hL}{k_f} = \frac{Heat\ transfer\ by\ convection}{Heat\ transfer\ across\ conductors}$.

L=Length of a characteristic.

k_f =Fluid thermal conductivity

h= Coefficient of convective heat transfer.

The Sherwood number is the Nusselt number's mass transfer a comparable one.

1.17 Sherwood Number S_h

In mass-transfer operations, a number without dimensions called the Sherwood number will be used, also known as the mass transfer Nusselt number. Its name honors Thomas Kilgore Sherwood and indicates the ratio of the rate of diffusive mass movement compared to the rate of convective mass transfer. It is defined by

$S_h = \frac{K.L}{D} = \frac{convective\ heat\ transfer}{conductive\ heat\ transfer}$

L= Distinctive length

D is for mass diffusion.

K is the mass transfer parameter.

1.18 Literature survey

Nowadays, nanofluids have been proposed to possess an abundance with advantages in deterrence, applications in medicine and the biomedical sector, nuclear reactor electricity generation, and, perhaps most significantly, any industrial heat-removal applications. The current study will concentrate on the use of nanofluids in nuclear reactor coolants, household refrigerators, chillers, heat exchangers, fuel cells, microelectronics, hybrid-powered generators, thermal control of the vehicle, engine cooling, grinding, machining, ships, boiler flue gas temperature reduction, and space technology (Dai et al., 2016). (Choi, S.U. and Eastman, 1995) When he initially put forth to conduct research with nanofluids, he proposed suspending nanoparticles in a base fluid, such as ethylene glycol, water, or oil. (N. Ali et al., 2018) Studied a review of the production, stability, and thermophysical characteristics of nanofluids. (Li, L., Zhang, Y., Ma, H. and Yang, 2008) Have studied a molecular dynamics simulation investigation into molecular stacking at the liquid-solid interface in nanofluids. (Choi, 2008) Introduced the latest applications of fresh scientific research. (Sreelakshmy, K.R., Nair, A.S., Vidhya, K.M., Saranya, T.R. and Nair, 2014) Examined an overview of recent nanofluid research. (Alam et al., 2009) Analyzed how over an inclined radiating isothermal permeable surface, steady magnetohydrodynamic heat and mass transfer flow are influenced by viscous dissipation and Joule heating when thermophoresis is present. (F. Ali et al., 2013) Investigated the effects of simultaneous mass and heat transfer on MHD-free convection flow through a slanted plate with a porous medium around it. (Anghel, M., Hossain, M.A., Zeb, S. and Pop, 2001) Examined how mass and heats are concurrently moved through an

inclined flat plate using free convection. (Chen, 2004) Due to convection, which naturally happens on a porous, inclining surface with fluctuating wall temperatures and concentrations, analyzed heat and mass transfer occur in MHD flow. (Narahari, M., Akilu, S. and Jaafar, 2013) Examined a nanofluid freely moving across an angled isothermal plate. (A. J. Chamkha et al., 2010) Studied a nanofluid with MHD-free convection and the production of heat effects traveling through a vertical plate. (Hamad, Pop, et al., 2011) Studied the a magnetic field's effects on a nanofluid's free convection flow on a vertical, semi-infinite flat plate. The transport of tiny, small particles go away from a hot surface and toward a cold one is made faster by the radiometric force that is called thermophoresis. Calculations were made to determine how effectively tiny particles deposited owing to temperature fluctuations in a laminar tube flow by (Walker, K.L., Homsy, G.M. and Geyling, 1979). (Rahman, A.T.M.M., Alam, M.S. and Chowdhury, 2012) Studied unsteady forced convection flow surrounding a wedge in two-dimensions with local similarity solutions. (Chiou, 1998) Examined how thermophoresis affected the deposition of submicron particles onto an isothermal moving plate from a forced flow of laminar boundary layers. (Hamad & Pop, 2011) Examined A rotating frame of reference for an unstable MHD-free convection flow in a nanofluid past a permeable vertically flat plate. (Goyal et al., 2013) Heat source/sink solution and partial slip in MHD viscoelastic nanofluid flow has been examined across a stretched sheet. (Kuznetsov et al., 2010) Have investigated a nanofluid that spontaneously passes through a boundary layer, or vertical plate.

1.19 Methodology

We employed the free parameter technique to resolve the regulations for partial differential equations and locate a similarity solution. According to the free parameter technique, the dependent variable in the equations will be explained in terms of "similarity parameters," frequently referred to as similarity variables, and then as a single variable in the end. The quantity of independent variables in the formulas needs to decrease by one as a result of the development of the similarity variable. The ultimate objective of every method is to reduce the number of independent variables, but this technique makes it possible to work with initial assumptions. The boundary values of the transformed equations, which are an ODE, must be constants even though the boundary values of the original PDE may be dependent on other independent variables if the original PDE had two independent variables. The Nachtsheim-Swigertshooting iteration method and the method of Runge-Kutta can be employed to numerically solve the altered similarity equations with boundary conditions.

Chapter 2

Effects on Unsteady MHD Flow of a Nanofluid for Free Convection past an Inclined Plate

2.1. Introduction

Presently, nanofluids are thought to have wide ranges advantage in medical application, biomedical industry, and detergency, power generation in nuclear reactors and more specifically in any heat removal involved industrial applications. The ongoing research will focus on the utilization of nanofluids in microelectronics, fuel cells, pharmaceutical processes, hybrid-powered engines, engine cooling, vehicle thermal management, domestic refrigerator, chillers, heat exchanger, nuclear reactor coolant, grinding, machining, space technology, defense and ships and boiler flue gas temperature reduction (Dai et al., 2016). (Choi, S.U. and Eastman, 1995) First introduced the concept of nanofluids where he proposed the suspension of nanoparticles in a base fluid such as water, oil and ethylene glycol. (Kuznetsov et al., 2010) We have examined the influence of nanoparticles on natural convection boundary-layer flow past a vertical plate. (Mohammed J. Uddin et al., 2012) Discussed Steady two dimensional MHD laminar free convective boundary layer flows of an electrically conducting Newtonian nanofluid over a soid stationary vertical plate. (Mustafa et al., 2014)Studied Nonlinear radiation heat transfer effects in the natural convective boundary layer flow of nanofluid past a vertical plate: a numerical study. (Rana et al., 2012) Studied Flow and heat transfer of a nanofluid over a nonlinearly stretching sheet: a numerical study. (Shit et al., 2016) Have analyzed the viscoelastic nanofluid flow

and heat transfer over a stretching sheet in the presence of magnetic field. (Goyal et al., 2013) Considered Numerical solution of MHD viscoelastic nanofluid flow over a stretching sheet with partial slip and heat source/sink. (Wang et al., 2020) Analyzed the effect of electric fields and magnetic fields on heat transfer of nanofluids, the mechanism of thermal conductivity enhancement of nanofluids, the heat transfer enhancement of nanofluids in the presence of an applied electric feild. (Nandy et al., 2014) Studied two dimensional boundary layer flow of unsteady forced convection nanofluid over a permeable shrinking sheet presence of thermal radiation. (S. M. Ibrahim et al., 2013) Studied Similarity solution of heat and mass transfer for natural convection over a moving vertical plate with internal heat generation and a convective boundary condition in the presence of thermal radiation, viscous dissipation, and chemical reaction. Boundary layer flow and heat transfer of viscoelastic nanofluids past a stretching sheet with partial slip conditions were discussed by (Goyal et al., 2014a). (Goyal et al., 2014b) Analyzed the boundary layer flow of nanofluids over a power law stretching sheet effect on coating and suspensions, movement of biological fluid, cooling of metallic plate, melt-spinning, heat exchangers technology, and oceanography. (F. Ali et al., 2013) Have considered the combined effects of radiation and chemical reaction on the magnetohydrodynamic free convection flow of an electrically conducting incompressible vicous fluid over an inclined plate embedded in a porous medium. A radiometric force by temperature gradient that enhance small micron sized particles moving toward a cold surface and away from the hot surface is termed as thermophoresis. The deposition efficiency of small particles due to thermophoresis in a laminar tube flow was calculated by (Walker, K.L., Homsy, G.M. and Geyling, 1979).

(Hamad, Pop, et al., 2011) Obtained Magnetic field effects on free convection flow of a nanofluid past a vertical semi-infinite flat plate. Steady natural convection boundary-layer flow of a nanofluid consisting of a pure fluid with nanoparticles along a permeable verticle plate in the presence of magnetic field, heat generation or asorption, and suction or injection effects have been analyzed by (A. J. Chamkha et al., 2010). (M. Y. Ali, Uddin, et al., 2016) Hence, it is greatly important to analyze unsteady two dimension free convective boundary layer flow along a permeable inclined flat plate in the presence of magnetic field and thermophorsis. Stability analysis and its direct simulation were analyzed by (Venkatasubbaiah et al., 2009). (Johnson et al., 1978) Investigated possible similarity solutions for free convection boundary layers adjacent to flat plates in porous media. (Kumari, M., Slaouti, A., Takhar, H.S., Nakamura, S. and Nath, 1996) Have studied unsteady free convection flow over a continuous moving vertical surface. (Slaouti et al., 1998) Considered unsteady free convection flow in the stagnation-point region of a three-dimensional body. (Hamad & Pop, 2011) Examined unsteady MHD free convection flow past a vertical permeable flat plate in a rotating frame of reference with constant heat source in a nanofluid.

Very Recently, (M. Y. Ali, Zahed, et al., 2016; Md. Yeakub Ali et al., 2015; M. N. Uddin et al., 2016) Studied similarity solutions for an internal heat generation, thermal radiation and free convection unsteady boundary layer flow over a vertical plate. Further, we also examined similarity solutions of unsteady convective boundary layer flow along isothermal vertical plate with porous medium. Moreover, we considered similarity solutions of unsteady mixed convective boundary layer flow of viscous incompressible fluid along isothermal horizontal plate.

The aim of the present study is to discuss effect of a similarity solution of unsteady MHD boundary layer flow of a nanofluid for free convection around an inclined plate. In this study the governing partial differential equations are transformed to a system of nonlinear ordinary differential equations by using similarity transformation. The similarity solutions of governing equations are discussed for various conditions. The transformed equations are solved by using Shooting Technique. The results of non-dimensional parameters on the velocity, temperature and concentration profiles, magnetic parameter, Prandtl number, Brownian motion parameter, buoyancy-ratio parameter, thermophoresis parameter, Brownian diffusion parameter, unsteadiness and other driving parameters, Skin-friction co-efficient, Nusselt and Sherwood numbers are observed and presented with graphs.

2.2. Mathematical problem, Governing equations and Boundary Conditions

We discussed unsteady, incompressible, two-dimensional, and laminar systems with constant physical properties. The semi-infinite plate is inclined at an acute angle d to the vertical axis. With the x-axis measured along the plate, a magnetic field of uniform strength B_0 is applied in the y-direction (normal to the flow direction). The gravitational acceleration g_e is acting downward. In addition, the buoyancy effects are included in momentum transfer with the usual Boussinesq approximation. It is also assumed that the lower side of the plate is heated by convection through a hot fluid at a temperature T_f with a coefficient of heat transfer h_f. It is assumed that both the nanoparticles and the base fluid are in

thermal equilibrium. In the vicinity of the plate, three different types of boundary layers (momentum, thermal, and nanoparticle volume) are formed.

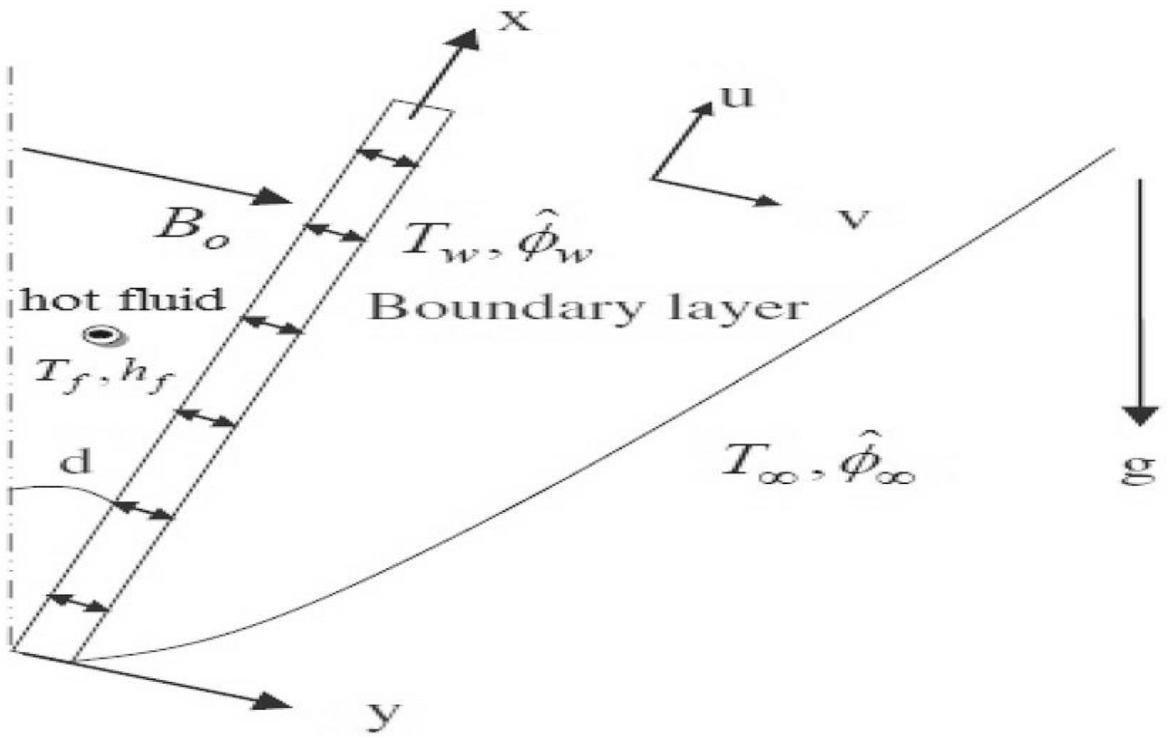

Figure 2.1: Sketch of physical problem

Upon incorporating the main assumptions into the conversation equations for mass, momentum, thermal energy, and nanoparticle species, the dimensional set of governing equations is written as respectively:

$$\frac{\partial u}{\partial x}+\frac{\partial v}{\partial y}=0 \tag{2.1}$$

$$\frac{\partial u}{\partial t}+\rho_f\left(u\frac{\partial u}{\partial x}+v\frac{\partial u}{\partial y}\right)=\mu\frac{\partial^2 u}{\partial y^2}-\sigma_{nf}B_0^2u+[\left(1-\widehat{\emptyset}_\infty\right)\rho_{f_\infty}\beta g_e(T-T_\infty)$$
$$-(\rho_p-\rho_{f_\infty})g_e(\widehat{\emptyset}-\widehat{\emptyset}_\infty)]cosd. \tag{2.2}$$

$$\frac{\partial T}{\partial t}+u\frac{\partial T}{\partial x}+v\frac{\partial T}{\partial y}=\alpha_m\frac{\partial^2 T}{\partial y^2}+\tau[Db\frac{\partial\widehat{\emptyset}}{\partial y}\frac{\partial T}{\partial y}+\frac{D_T}{T_\infty}\left(\frac{\partial T}{\partial y}\right)^2] \tag{2.3}$$

$$\frac{\partial\widehat{\emptyset}}{\partial t}+u\frac{\partial\widehat{\emptyset}}{\partial x}+v\frac{\partial\widehat{\emptyset}}{\partial y}=Db\frac{\partial^2\widehat{\emptyset}}{\partial y^2}+\frac{D_T}{T_\infty}\frac{\partial^2 T}{\partial y^2} \tag{2.4}$$

Where u and v are the velocity components parallel and perpendicular to the plate, respectively, B_0 is uniform magnetic field strength, $\widehat{\emptyset}$ is the local solid volume fraction of the nanoparticles, β is Volumetric thermal expansion coefficient of the base fluid, Db is the Brownian diffusionCoefficient, D_T is the thermophoretic diffusion coefficient, and T is the local temperature. Db Brownian diffusion coefficient. Continuity, momentum, thermal energy, and nanoparticles species equations for nanofluids are represented by equations (2.1) - (2.4).

The boundary conditions may be written as

$$u = 0, v = 0, \widehat{\emptyset} = \widehat{\emptyset}_w, T = T_f \; at \; y = 0. \tag{2.5}$$

$$u = 0, v = 0, \widehat{\emptyset} = \widehat{\emptyset}_\infty, T = T_\infty at \; y \to \infty. \tag{2.6}$$

The continuity equation (1) is satisfied by introducing the steam function$\Psi(x, y)$. Such that

$u = \frac{\partial \Psi}{\partial y}, v = -\frac{\partial \Psi}{\partial x}$.

The momentum, thermal energy, and nanoparticles species equations can be transformed to the corresponding ordinary differential equations by introducing the following

Similarity transformations:

$$\eta = \frac{y}{xt}(R_{a_x})^{1/4}, \;\; \psi = \alpha_m \left(R_{a_x}\right)^{1/4} f(\eta), \;\; \theta(\eta) = \frac{T - T_\infty}{T_f - T_\infty}, \;\; \emptyset(\eta) = \frac{\widehat{\emptyset} - \emptyset_\infty}{\widehat{\emptyset}_w - \widehat{\emptyset}_\infty}. \tag{2.7}$$

With the local Rayleigh number is defined as

$$R_{a_x} = \frac{(1 - \widehat{\emptyset}_\infty)\beta g_e (T_f - T_\infty) x^3 t^3}{\nu \alpha_m} \tag{2.8}$$

$$\frac{\partial \eta}{\partial x} = \frac{y}{t}\left(R_{a_x}\right)^{\frac{1}{4}} \frac{\partial}{\partial x} x^{-1} = \frac{y}{t}\left(R_{a_x}\right)^{\frac{1}{4}} (-1) x^{-1-1} = -\frac{y}{x^2 t}\left(R_{a_x}\right)^{\frac{1}{4}}.$$

$$\frac{\partial \eta}{\partial y} = \frac{1}{xt}\left(R_{a_x}\right)^{\frac{1}{4}}\frac{\partial}{\partial y}y = \frac{1}{xt}\left(R_{a_x}\right)^{\frac{1}{4}}.$$

$$\frac{\partial \eta}{\partial t} = \frac{y}{x}\left(R_{a_x}\right)^{\frac{1}{4}}\frac{\partial}{\partial t}t^{-1} = \frac{y}{t}\left(R_{a_x}\right)^{\frac{1}{4}}(-1)t^{-1-1} = -\frac{y}{xt^2}\left(R_{a_x}\right)^{\frac{1}{4}} = -\frac{y}{xt}\left(R_{a_x}\right)^{\frac{1}{4}}.\frac{1}{t} = -\frac{\eta}{t}.$$

$$u = \frac{\partial \psi}{\partial y} = \alpha_m\left(R_{a_x}\right)^{\frac{1}{4}}\frac{\partial}{\partial y}[f(\eta)] = \alpha_m\left(R_{a_x}\right)^{\frac{1}{4}}f'(\eta)\frac{\partial \eta}{\partial y} = \alpha_m\left(R_{a_x}\right)^{\frac{1}{4}}f'(\eta)\frac{1}{xt}\left(R_{a_x}\right)^{\frac{1}{4}}.$$

$$= \frac{1}{xt}\alpha_m\left(R_{a_x}\right)^{\frac{1}{2}}f'(\eta).$$

$$\frac{\partial u}{\partial y} = \frac{1}{xt}\alpha_m\left(R_{a_x}\right)^{\frac{1}{2}}\frac{\partial}{\partial y}f'(\eta) = \frac{1}{xt}\alpha_m\left(R_{a_x}\right)^{\frac{1}{2}}f''(\eta)\frac{\partial \eta}{\partial y} = \frac{1}{xt}\alpha_m\left(R_{a_x}\right)^{\frac{1}{2}}f''(\eta)\frac{1}{xt}\left(R_{a_x}\right)^{\frac{1}{4}}.$$

$$= \frac{\alpha_m}{x^2t^2}\left(R_{a_x}\right)^{\frac{3}{4}}f''(\eta)\,.$$

$$\frac{\partial^2 u}{\partial y^2} = \frac{\alpha_m}{x^2t^2}\left(R_{a_x}\right)^{\frac{3}{4}}\frac{\partial}{\partial y}f''(\eta) = \frac{\alpha_m}{x^2t^2}\left(R_{a_x}\right)^{\frac{3}{4}}f'''(\eta)\frac{\partial \eta}{\partial y} = \frac{\alpha_m}{x^2t^2}\left(R_{a_x}\right)^{\frac{3}{4}}f'''(\eta)\ \frac{1}{xt}\left(R_{a_x}\right)^{\frac{1}{4}}.$$

$$= \frac{\alpha_m}{x^3t^3}R_{a_x}f'''(\eta)\,.$$

$$\frac{\partial u}{\partial x} = \frac{\alpha_m}{t}\left(R_{a_x}\right)^{\frac{1}{2}}\frac{\partial}{\partial x}\left[\frac{f'(\eta)}{x}\right] = \frac{\alpha_m}{t}\left(R_{a_x}\right)^{\frac{1}{2}}[f'(\eta)\frac{\partial}{\partial x}x^{-1} + \frac{1}{x}\frac{\partial}{\partial x}f'(\eta)].$$

$$= \frac{\alpha_m}{t}\left(R_{a_x}\right)^{\frac{1}{2}}[f'(\eta)(-\frac{1}{x^2}) + \frac{1}{x}f''(\eta)\frac{\partial \eta}{\partial x}].$$

$$= \frac{\alpha_m}{t}\left(R_{a_x}\right)^{\frac{1}{2}}[-\frac{f'(\eta)}{x^2} + \frac{1}{x}f''(\eta)(-\frac{y}{x^2t}\left(R_{a_x}\right)^{\frac{1}{4}})].$$

$$= -\frac{\alpha_m}{x^2t}\left(R_{a_x}\right)^{\frac{1}{2}}f'(\eta) - \frac{y\alpha_m}{x^3t^2}\left(R_{a_x}\right)^{\frac{3}{4}}f''(\eta).$$

$$v = -\frac{\partial \psi}{\partial x} = -\alpha_m\left(R_{a_x}\right)^{\frac{1}{4}}\frac{\partial}{\partial x}[f(\eta)] = -\alpha_m\left(R_{a_x}\right)^{\frac{1}{4}}f'(\eta)\frac{\partial \eta}{\partial x}.$$

$$= -\alpha_m\left(R_{a_x}\right)^{\frac{1}{4}}f'(\eta)\left[-\frac{y}{x^2t}\left(R_{a_x}\right)^{\frac{1}{4}}\right] = \frac{y\alpha_m}{x^2t}\ \left(R_{a_x}\right)^{\frac{1}{2}}f'(\eta).$$

$$\frac{\partial u}{\partial t} = \frac{1}{x}\alpha_m\left(R_{a_x}\right)^{\frac{1}{2}}\frac{\partial}{\partial t}\left[\frac{f'(\eta)}{t}\right] = \frac{1}{x}\alpha_m\left(R_{a_x}\right)^{\frac{1}{2}}[f'(\eta)\frac{\partial}{\partial t}\frac{1}{t} + \frac{1}{t}\frac{\partial}{\partial t}f'(\eta)].$$

$$= \frac{1}{x}\alpha_m\left(R_{a_x}\right)^{\frac{1}{2}}[f'(\eta)\left(-\frac{1}{t^2}\right) + \frac{1}{t}f''(\eta)\frac{\partial \eta}{\partial t}].$$

$$u\frac{\partial u}{\partial x} = \frac{1}{xt}\alpha_m\left(R_{a_x}\right)^{\frac{1}{2}}f'(\eta)[-\frac{\alpha_m}{x^2t}\left(R_{a_x}\right)^{\frac{1}{2}}f'(\eta) - \frac{y\alpha_m}{x^3t^2}\left(R_{a_x}\right)^{\frac{3}{4}}f''(\eta)].$$

$$= -\frac{{\alpha_m}^2}{x^3t^2}R_{a_x}\,f'^2(\eta) - \frac{y{\alpha_m}^2}{x^4t^3}\left(R_{a_x}\right)^{\frac{5}{4}}f'(\eta)f''(\eta).$$

$v\frac{\partial u}{\partial y} = \frac{y\alpha_m}{x^2t}\left(R_{a_x}\right)^{\frac{1}{2}} f'(\eta)\frac{\alpha_m}{x^2t^2}\left(R_{a_x}\right)^{\frac{3}{4}} f''(\eta)$.

$= \frac{y{\alpha_m}^2}{x^4t^3}\left(R_{a_x}\right)^{\frac{5}{4}} f'(\eta)f''(\eta).$

From equation (2.2)

Or, $\frac{\partial u}{\partial t} + \rho_f\left(u\frac{\partial u}{\partial x} + v\frac{\partial u}{\partial y}\right) = \mu\frac{\partial^2 u}{\partial y^2} - \sigma_{nf}B_0^2u + [\left(1-\widehat{\emptyset}_\infty\right)\rho_{f_\infty}\beta g_e(T-T_\infty)$

$-(\rho_p-\rho_{f_\infty})g_e(\widehat{\emptyset}-\widehat{\emptyset}_\infty)]cosd.$

$Or, -\frac{1}{xt^2}\alpha_m\left(R_{a_x}\right)^{\frac{1}{2}}[f'(\eta)+\eta f''(\eta)] +$

$\rho_f\left[-\frac{{\alpha_m}^2}{x^3t^2}R_{a_x}\,f'^2(\eta) - \frac{y{\alpha_m}^2}{x^4t^3}\left(R_{a_x}\right)^{\frac{5}{4}} f'(\eta)f''(\eta) + \frac{y{\alpha_m}^2}{x^4t^3}\left(R_{a_x}\right)^{\frac{5}{4}} f'(\eta)f''(\eta)\right] =$

$\mu\frac{\alpha_m}{x^3t^3}R_{a_x}f'''(\eta) + \frac{(1-\widehat{\emptyset}_\infty)\rho_{f_\infty}\beta g_e(T-T_\infty)x^3t^3}{\mu\alpha_m}.\frac{\mu\alpha_m}{x^3t^3}\,[\theta - Nr\emptyset]cosd -$

$\sigma_{nf}B_0^2\frac{1}{xt}\alpha_m\left(R_{a_x}\right)^{\frac{1}{2}}f'(\eta).$

Or, $-\frac{\alpha_m}{xt^2}\left(R_{a_x}\right)^{\frac{1}{2}}[f'(\eta)+\eta f''(\eta)] - \rho_f.\frac{{\alpha_m}^2}{x^3t^2}R_{a_x}\,f'^2(\eta) = \mu\frac{\alpha_m}{x^3t^3}R_{a_x}f'''(\eta) +$

$R_{a_x}.\frac{\mu\alpha_m}{x^3t^3}\,[\theta - Nr\emptyset]cosd - \sigma_{nf}B_0^2\frac{1}{xt}\alpha_m\left(R_{a_x}\right)^{\frac{1}{2}}f'(\eta).$

Or, $-\frac{x^2t}{\mu}\left(R_{a_x}\right)^{-\frac{1}{2}}[f'(\eta)+\eta f''(\eta)] - \rho_f\frac{\alpha_m t}{\mu}\,f'^2(\eta) = f'''(\eta) + [\theta - Nr\emptyset]cosd -$

$\frac{\sigma_{nf}B_0^2x^2t^2}{\mu\left(R_{a_x}\right)^{\frac{1}{2}}}f'(\eta).$

Or, $-\frac{x^2t}{\mu}\left[\frac{(1-\widehat{\emptyset}_\infty)\rho_{f_\infty}\beta g_e(T-T_\infty)x^3t^3}{\mu\alpha_m}\right]^{-\frac{1}{2}}[f'(\eta)+\eta f''(\eta)] - \rho_f\frac{\alpha_m t}{\mu}\,f'^2(\eta) = f'''(\eta) +$

$[\theta - Nr\emptyset]cosd - \frac{\sigma_{nf}B_0^2x^2t^2}{\mu\left(R_{a_x}\right)^{\frac{1}{2}}}f'(\eta).$

$Or, \frac{1}{\mu}\left[\frac{(1-\widehat{\emptyset}_\infty)\beta g_e(T-T_\infty)}{\mu}\right]^{-\frac{1}{2}} - \frac{1}{Pr}f'^2 = f'''(\eta) + [\theta - Nr\emptyset]cosd - \frac{\sigma_{nf}B_0^2x^2t^2}{\mu\left(R_{a_x}\right)^{\frac{1}{2}}}f'(\eta).$

$Or, f''' + (\theta - Nr\emptyset)cosd - Mf' + \frac{1}{E}[P]^{-1/2}(f'+\eta f'') + \frac{1}{Pr}f'^2 = 0.$

Where, $Pr(Modified\ Prandtl\ Number) = \frac{\mu}{\alpha_m\rho_f t}$

$M(Modified\ Magnetic\ field\ Parameter) = \frac{\sigma_{nf}B_0^2x^2t^2}{\mu(R_{a_x})^{\frac{1}{2}}}.$

$Nr(Buoyancy - ratio\ parameter) = \frac{(\rho_p-\rho_f)(\widehat{\emptyset}_w-\widehat{\emptyset}_\infty)}{\rho_{f_\infty}(1-\widehat{\emptyset}_\infty)(T_f-T_\infty)}.$

$E(Viscosity\ of\ the\ nanofluid) = \mu.$

Unsteadiness parameter $P = \frac{(1-\widehat{\emptyset}_\infty)\beta g_e(T-T_\infty)}{\mu}.$

$\theta(\eta) = \frac{T-T_\infty}{T_f-T_\infty} T = T_\infty + (T_f-T_\infty)\theta(\eta).$

$\frac{\partial T}{\partial t} = 0 + \left(T_f-T_\infty\right)\frac{\partial}{\partial \eta}\theta(\eta)\frac{\partial \eta}{\partial t} = \left(T_f-T_\infty\right)\theta'(\eta)(-\frac{\eta}{t}) = -\frac{\eta\theta'(\eta)}{t}(T_f-T_\infty)..$

$\frac{\partial T}{\partial y} = 0 + (T_f-T_\infty)\frac{\partial}{\partial \eta}\theta(\eta)\frac{\partial \eta}{\partial y} = \left(T_f-T_\infty\right)\theta'(\eta)\frac{1}{xt}\left(R_{a_x}\right)^{\frac{1}{4}} = \frac{(T_f-T_\infty)}{xt}\theta'(\eta)\left(R_{a_x}\right)^{\frac{1}{4}}.$

$\frac{\partial^2 T}{\partial y^2} = \frac{(T_f-T_\infty)}{xt}\left(R_{a_x}\right)^{\frac{1}{4}}\frac{\partial}{\partial \eta}\theta'(\eta)\frac{\partial \eta}{\partial y} = \frac{(T_f-T_\infty)}{xt}\left(R_{a_x}\right)^{\frac{1}{4}}\theta''(\eta)\frac{1}{xt}\left(R_{a_x}\right)^{\frac{1}{4}}.$

$= \frac{(T_f-T_\infty)}{x^2t^2}\theta''(\eta)(R_{a_x})^{\frac{1}{2}}.$

$\frac{\partial T}{\partial x} = 0 + (T_f-T_\infty)\frac{\partial}{\partial \eta}\theta(\eta)\frac{\partial \eta}{\partial x} = \left(T_f-T_\infty\right)\theta'(\eta)(-\frac{y}{x^2t}\left(R_{a_x}\right)^{\frac{1}{4}}).$

$= -\frac{y(T_f-T_\infty)}{x^2t}\theta'(\eta)\left(R_{a_x}\right)^{\frac{1}{4}}.$

$\emptyset(\eta) = \frac{\widehat{\emptyset}-\emptyset_\infty}{\widehat{\emptyset}_w-\widehat{\emptyset}_\infty} \Longrightarrow \widehat{\emptyset} = \emptyset_\infty + (\widehat{\emptyset}_w-\widehat{\emptyset}_\infty)\emptyset(\eta).$

$= \frac{(\widehat{\emptyset}_w-\widehat{\emptyset}_\infty)}{xt}\emptyset'(\eta)\left(R_{a_x}\right)^{\frac{1}{4}}.$

$\frac{\partial^2 \widehat{\emptyset}}{\partial y^2} = \frac{(\widehat{\emptyset}_w-\widehat{\emptyset}_\infty)}{xt}\left(R_{a_x}\right)^{\frac{1}{4}}\frac{\partial}{\partial \eta}\emptyset'(\eta)\frac{\partial \eta}{\partial y} = \frac{(\widehat{\emptyset}_w-\widehat{\emptyset}_\infty)}{xt}\left(R_{a_x}\right)^{\frac{1}{4}}\emptyset''(\eta)\frac{1}{xt}\left(R_{a_x}\right)^{\frac{1}{4}}.$

$= \frac{(\widehat{\emptyset}_w-\widehat{\emptyset}_\infty)}{xt}\left(R_{a_x}\right)^{\frac{1}{4}}\emptyset''(\eta)\frac{1}{xt}\left(R_{a_x}\right)^{\frac{1}{4}} = \frac{(\widehat{\emptyset}_w-\widehat{\emptyset}_\infty)}{x^2t^2}\emptyset''(\eta)\left(R_{a_x}\right)^{\frac{1}{2}}.$

$\frac{\partial \widehat{\emptyset}}{\partial x} = 0 + \left(\widehat{\emptyset}_w-\widehat{\emptyset}_\infty\right)\frac{\partial}{\partial \eta}\emptyset(\eta)\frac{\partial \eta}{\partial x}\left(\widehat{\emptyset}_w-\widehat{\emptyset}_\infty\right)\emptyset'(\eta)\ (-\frac{y}{x^2t}\left(R_{a_x}\right)^{\frac{1}{4}}).$

$= -\frac{y(\widehat{\emptyset}_w-\widehat{\emptyset}_\infty)}{x^2t}\left(R_{a_x}\right)^{\frac{1}{4}}\emptyset'(\eta)\ .$

$\frac{\partial \widehat{\emptyset}}{\partial t} = 0 + \left(\widehat{\emptyset}_w-\widehat{\emptyset}_\infty\right)\frac{\partial}{\partial \eta}\emptyset(\eta)\frac{\partial \eta}{\partial t} = \left(\widehat{\emptyset}_w-\widehat{\emptyset}_\infty\right)\emptyset'(\eta)(-\frac{\eta}{t}).$

$= -\frac{\eta\, \emptyset'(\eta)}{t}\left(\widehat{\emptyset}_w - \widehat{\emptyset}_\infty\right).$

$Or, u\frac{\partial T}{\partial x} = \frac{1}{xt}\alpha_m\left(R_{a_x}\right)^{\frac{1}{2}} f'(\eta)[-\frac{y(T_f - T_\infty)}{x^2 t}\ \theta'(\eta)\left(R_{a_x}\right)^{\frac{1}{4}}].$

$= -\frac{y\alpha_m(T_f - T_\infty)}{x^3 t^2}\ \left(R_{a_x}\right)^{\frac{3}{4}} f'(\eta)\theta'(\eta).$

$v\frac{\partial T}{\partial y} = \frac{y\alpha_m}{x^2 t}\ \left(R_{a_x}\right)^{\frac{1}{2}} f'(\eta)\ \frac{(T_f - T_\infty)}{xt}\theta'(\eta)\left(R_{a_x}\right)^{\frac{1}{4}}.$

$= \frac{y\alpha_m(T_f - T_\infty)}{x^3 t^2}\left(R_{a_x}\right)^{\frac{3}{4}} f'(\eta)\theta'(\eta).$

$\frac{\partial \widehat{\emptyset}}{\partial y}\frac{\partial T}{\partial y} = \frac{(\widehat{\emptyset}_w - \widehat{\emptyset}_\infty)}{xt}\emptyset'(\eta)\left(R_{a_x}\right)^{\frac{1}{4}}\frac{(T_f - T_\infty)}{xt}\theta'(\eta)\left(R_{a_x}\right)^{\frac{1}{4}}.$

$= \frac{(\widehat{\emptyset}_w - \widehat{\emptyset}_\infty)(T_f - T_\infty)}{x^2 t^2}\left(R_{a_x}\right)^{\frac{1}{2}}\theta'(\eta)\emptyset'(\eta).$

From (2.3) we get

$\frac{\partial T}{\partial t} + u\frac{\partial T}{\partial x} + v\frac{\partial T}{\partial y} = \alpha_m\frac{\partial^2 T}{\partial y^2} + \tau[Db\frac{\partial \widehat{\emptyset}}{\partial y}\frac{\partial T}{\partial y} + \frac{D_T}{T_\infty}\left(\frac{\partial T}{\partial y}\right)^2].$

$-\frac{\eta\theta'(\eta)}{t}\left(T_f - T_\infty\right) - \frac{y\alpha_m(T_f - T_\infty)}{x^3 t^2}\ \left(R_{a_x}\right)^{\frac{3}{4}} f'(\eta)\theta'(\eta) + \frac{y\alpha_m(T_f - T_\infty)}{x^3 t^2}\left(R_{a_x}\right)^{\frac{3}{4}} f'(\eta)\theta'(\eta) =$

$\alpha_m\frac{(T_f - T_\infty)}{x^2 t^2}\theta''(\eta)\left(R_{a_x}\right)^{\frac{1}{2}} +$

$\tau[\frac{(\widehat{\emptyset}_w - \widehat{\emptyset}_\infty)(T_f - T_\infty)Db}{x^2 t^2}\left(R_{a_x}\right)^{\frac{1}{4}}\theta'(\eta)\emptyset'(\eta) + \frac{D_T}{T_\infty}(\frac{(T_f - T_\infty)}{xt}\theta'(\eta)\left(R_{a_x}\right)^{\frac{1}{4}})^2].$

$-\frac{\eta\theta'(\eta)}{t}\left(T_f - T_\infty\right) = \frac{\alpha_m}{x^2 t^2}\left(T_f - T_\infty\right)\theta''(\eta)\left(R_{a_x}\right)^{\frac{1}{2}} + \tau\frac{(\widehat{\emptyset}_w - \widehat{\emptyset}_\infty)(T_f - T_\infty)Db}{x^2 t^2}\left(R_{a_x}\right)^{\frac{1}{4}}\theta'(\eta)\emptyset'(\eta).$

$+\tau\frac{D_T}{T_\infty}\ \frac{(T_f - T_\infty)^2}{x^2 t^2}\left(R_{a_x}\right)^{\frac{1}{2}}(\theta'(\eta))^2.$

$-\frac{x^2 t}{\alpha_m}\ \eta\theta'(\eta)\left(R_{a_x}\right)^{-\frac{1}{2}} = \theta''(\eta) + Nb\theta'(\eta)\emptyset'(\eta) + Nt(\theta'(\eta))^2.$

$-\left(\frac{(1 - \widehat{\emptyset}_\infty)\beta g_e(T - T_\infty)}{\mu}\right)^{-\frac{1}{2}}.\frac{1}{\alpha_m}\eta\theta'(\eta) = \theta''(\eta) + Nb\theta'(\eta)\emptyset'(\eta) + Nt(\theta'(\eta))^2.$

$\theta'' + Nb\theta'\emptyset' + Nt\theta'^2 + \frac{1}{Bm}[P]^{-1/2}\eta\theta' = 0.$

Where, $Nb(Brownian\ motion\ parameter) = \frac{\tau Db(\widehat{\emptyset}_w - \widehat{\emptyset}_\infty)}{\alpha_m}$

$Nt(thermophoresis\ parameter) = \frac{\tau D_T(T_f - T_\infty)}{T_\infty \alpha_m}.$

Bm $(thermal\ diffusivity\ parameter) = \alpha_m$

$u\frac{\partial\hat{\emptyset}}{\partial x} = \frac{1}{xt}\alpha_m\left(R_{a_x}\right)^{\frac{1}{2}}f'(\eta)(-\frac{y(\hat{\emptyset}_w-\hat{\emptyset}_\infty)}{x^2t}\left(R_{a_x}\right)^{\frac{1}{4}}\emptyset'(\eta)).$

$= -\frac{y\alpha_m(\hat{\emptyset}_w-\hat{\emptyset}_\infty)}{x^3t^2}\left(R_{a_x}\right)^{\frac{3}{4}}f'(\eta)\emptyset'(\eta).$

$v\frac{\partial\hat{\emptyset}}{\partial y} = \frac{y\alpha_m}{x^2t}\left(R_{a_x}\right)^{\frac{1}{2}}f'(\eta)\frac{(\hat{\emptyset}_w-\hat{\emptyset}_\infty)}{xt}\emptyset'(\eta)\left(R_{a_x}\right)^{\frac{1}{4}}.$

$= \frac{y\alpha_m(\hat{\emptyset}_w-\hat{\emptyset}_\infty)}{x^3t^2}\left(R_{a_x}\right)^{\frac{3}{4}}f'(\eta)\emptyset'(\eta).$

$\frac{\partial\hat{\emptyset}}{\partial t} + u\frac{\partial\hat{\emptyset}}{\partial x} + v\frac{\partial\hat{\emptyset}}{\partial y} = Db\frac{\partial^2\hat{\emptyset}}{\partial y^2} + \frac{D_T}{T_\infty}\frac{\partial^2T}{\partial y^2}.$

Or, $-\frac{\eta\theta'(\eta)}{t}\left(T_f-T_\infty\right) = \frac{\alpha_m}{x^2t^2}\left(T_f-T_\infty\right)\theta''^{(\eta)}\left(R_{a_x}\right)^{\frac{1}{2}}$

$+\tau\frac{(\hat{\emptyset}_w-\hat{\emptyset}_\infty)(T_f-T_\infty)}{x^2t^2}\left(R_{a_x}\right)^{\frac{1}{4}}\theta'(\eta)\emptyset'(\eta).$

Or,$-\frac{\eta\,\emptyset'(\eta)}{t}\left(\hat{\emptyset}_w-\hat{\emptyset}_\infty\right) - \frac{y\alpha_m(\hat{\emptyset}_w-\hat{\emptyset}_\infty)}{x^3t^2}\left(R_{a_x}\right)^{\frac{3}{4}}f'(\eta)\emptyset'(\eta) +$

$\frac{y\alpha_m(\hat{\emptyset}_w-\hat{\emptyset}_\infty)}{x^3t^2}\left(R_{a_x}\right)^{\frac{3}{4}}f'(\eta)\emptyset'(\eta)$

$= Db\frac{(\hat{\emptyset}_w-\hat{\emptyset}_\infty)}{x^2t^2}\emptyset''^{(\eta)}\left(R_{a_x}\right)^{\frac{1}{2}} + \frac{D_T}{T_\infty}\frac{(T_f-T_\infty)}{x^2t^2}\theta''(\eta)\left(R_{a_x}\right)^{\frac{1}{2}}.$

Or, $-\frac{\eta\,\emptyset'(\eta)}{t}\left(\hat{\emptyset}_w-\hat{\emptyset}_\infty\right) = Db\frac{(\hat{\emptyset}_w-\hat{\emptyset}_\infty)}{x^2t^2}\emptyset''^{(\eta)}\left(R_{a_x}\right)^{\frac{1}{2}} + \frac{D_T}{T_\infty}\frac{(T_f-T_\infty)}{x^2t^2}\theta''(\eta)\left(R_{a_x}\right)^{\frac{1}{2}}.$

$Or,\ \frac{\eta\,\emptyset'(\eta)}{t}\left(R_{a_x}\right)^{-\frac{1}{2}}\frac{x^2t^2}{Db} = \emptyset''^{(\eta)} + \frac{Nt}{Nb}\theta''(\eta).$

$Or,\ -\frac{1}{Db}\left(\frac{\left(1-\hat{\emptyset}_\infty\right)\beta g_e(T-T_\infty)}{\mu}\right)^{-\frac{1}{2}}\eta\,\emptyset'(\eta) = \emptyset''^{(\eta)} + \frac{Nt}{Nb}\theta''(\eta).$

$Or,\ \emptyset'' + \frac{Nt}{Nb}\theta'' + \frac{1}{Db}[P]^{-1/2}\eta\emptyset' = 0.$

Where, Db=Brownian motion parameter.

The momentum, thermal energy and nanoparticles species equations are the following forms:

$$f''' + (\theta - Nr\emptyset)cosd - Mf' + \frac{1}{E}[P]^{-1/2}(f' + \eta f'') + \frac{1}{Pr}f'^2 = 0 \quad (2.9)$$

$$\theta'' + Nb\theta'\emptyset' + Nt\theta'^2 + \frac{1}{Bm}[P]^{-1/2}\eta\theta' = 0 \quad (2.10)$$

$$\emptyset'' + \frac{Nt}{Nb}\theta'' + \frac{1}{Db}[P]^{-1/2}\eta\emptyset' = 0 \quad (2.11)$$

The corresponding boundary conditions are:

$$f(\eta) = 0,\ f'(\eta) = 0,\ \theta(\eta) = 1,\ \theta'(\eta) = 0,\ \emptyset(\eta) = 1,\ at\ \eta = 0 \quad (2.12)$$

$$f'(\eta) = 0,\ \theta(\eta) = 0,\ \emptyset(\eta) = 0\ \ as\ \ \eta \to \infty \quad (2.13)$$

Where the prime (′) denotes differentiation with respect to η.

The above equations with boundary condition are solved numerically by using shooting technique.

Skin-friction co-efficient, Nusselt and Sherwood number evaluation.

The quantities we interested in studying are the Skin-friction co-efficient C_f, local Nusselt number Nu_x and the local Sherwood number $Sh_{x,n}$. These parameters respectively characterize wall heat and mass transfer rates. The quantities are defined as:

$$C_f = \frac{\tau_w}{\rho u^2},\ Nu_x = \frac{xq_w}{k(T_f - T_\infty)},\ Sh_{x,n} = \frac{xq_{np}}{D_B(\widehat{\emptyset_w} - \widehat{\emptyset_\infty})}$$

Where τ_w, q_m and q_{np} are the local shearing stress, the wall heat and nano mass fluxes respectively.

The modified Skin-friction co-efficient C_f, Nusselt number Nur and modified nanoparticle Sherwood number $Shrn$ can be written as:

$$C_f {Ra_x}^{1/4} = f''(0),\ Nur = {Ra_x}^{1/4}\, Nu_x = -\theta'(0),\ Shrn = {Ra_x}^{1/4} Sh_{x,n} = -\emptyset'(0)$$

2.3. Numerical Solution

The systems of nonlinear ordinary differential equations, together with boundary conditions, are coupled. Firstly, higher-order non-linear differential equations are converted into linear differential equations of the first order, and these are further transformed into initial value problems solved numerically by applying the shooting method, namely the Nachtsheim-Swigert (1965) iteration technique

(guessing the missing value), along with the sixth-order Runga-Kutta integration technique. The Nachtsheim-Swigert iteration technique is used as the main tool for the numerical approach. The dimensionless similarity equations for momentum, temperature, and concentration are solved numerically by using the iteration technique. In the shooting technique, the missing initial condition at the initial point of the interval is assumed, and the differential equations are also integrated numerically as an initial value problem to the terminal point. The accuracy of the assumed missing initial condition is then checked by comparing the calculated value of the dependent variable at the terminal point with its given value. If a difference exists, another value of the missing initial condition must be assumed, and thus the process is repeated. This process is continued until agreement is reached between the calculated and the given condition for the specified degree of accuracy. The corresponding velocity, temperature, and concentration profiles are shown in the figures.

2.4. Results and Discussions

We studied the unsteady MHD boundary layer flow of a nanofluid for free convection past an inclined plate. The transformed sets of nonlinear ordinary differential equations with boundary conditions are solved numerically by using the shooting method. The velocity, temperature, and concentration profiles, as well as the skin-friction coefficient, Nusselt number, and Sherwood number, were discussed for the different flow parameters involved in the problem. The effects of various parameters are shown graphically and in tabular form.

The effect of the difference parameters is shown graphically when M = 0.10, Pr = 5.00, Nr = 0.50, E = 0.01; Nb = 0.50; P = 0.60; Nt = 0.50; Bm = 0.10; Db = 0.10; d = 60.0.

Figures 2.2, illustrate the velocity profile for different values of the Brownian diffusion coefficient Db. The key property of Brownian diffusion is the thermal motion of droplets. The increasing Brownian diffusion coefficient Db causes an increasing velocity profile. Figure 2.3 represents the dimensionless temperature profile for several values of the Brownian diffusion coefficient Db; the temperature profile decreases with increases in Db. Figure 2.4 displays the effects of the Brownian diffusion coefficient Db on the concentration profile. This is represented in the increase in the concentration profile as the Brownian diffusion coefficient Db increases.

In Figure 2.5, the effect of the velocity profile for different values of the thermal diffusivity parameter Bm is shown. Thermal diffusivity is the thermal conductivity separated by density and specific heat capacity at constant pressure. The thermal diffusivity slightly increased with increasing temperature. The velocity profile decreases with increasing Bm. Figure 2.6 reveals the effect of the thermal diffusivity parameter Bm on the temperature profile. It is evident from the figure that an increase in the thermal diffusivity parameter Bm improves the temperature profile. Figure 2.7 shows the effect of the thermal diffusivity parameter Bm on the concentration profile. As Bm increases, the concentration profile decreases, but at a certain point, the concentration profile reverse.

The thermophoresis parameter is the conveyance force that arises due to the existence of a temperature gradient. Figure 2.8 illustrates the influence of the thermophoresis parameter Nt on the velocity profile of the flow. It is clear from the figure that an increase in the thermophoresis parameter Nt raises the velocity profile of the flow. Figure 2.9 shows the influence of the thermophoresis parameter

Nt on the temperature profile of the flow. The temperature profile is enhanced with an increase in the thermophoresis parameter Nt. The influence of the thermophoresis parameter Nt on the concentration profile is plotted in Figure 2.10. As the thermophoresis parameter Nt increases, the concentration profile increases.

Figure 2.11 illustrates the velocity profile for different values of the unsteadiness parameter P. This figure reveals that an increase in the unsteadiness parameter P results in a decrease in the velocity profile. Figure 2.12 shows the effect of the unsteadiness parameter P on the temperature profile. The unsteadiness parameter increases, but there is no significant variation in the temperature profile. Figure 2.13 represents the variation of the concentration profile with the unsteadiness parameter. It was noted that as P increases, the concentration profile decreases.

Brownian motion is the random motion of nanoparticles inside the base fluid due to the nonstop collision of nanoparticles with the molecules of the base fluid. This motion of the particles is defined by the parameter Nb, Also known as the Brownian motion coefficient. Figure 2.14 elucidate the velocity profile for several values of the Brownian motion parameter Nb. It is clearly shown in the figure that as the Brownian motion parameter increases, the velocity profile increases. Figure 2.15 illustrates the effect of the Brownian motion parameter on the temperature profile. As shown in the figure, the temperature profile increases with increasing values of the Brownian motion parameter. The effect of the Brownian motion parameter Nb on the concentration profile is shown in figure 2.16. It is observed that an increase in the Brownian motion parameter decreases the concentration profile, but at a certain time the concentration profile reverses.

The viscosity of the nanofluid is created on the hypothesis of a viscous fluid containing spherical particles at a very low volume fraction. Figure 2.17 displays the variation of velocity profiles for different values of the viscosity of the nanofluid E. We observe that the velocity profiles increase swiftly with the increase in viscosity of the nanofluid E. The effect of the viscosity of the nanofluid (E) on temperature profiles is shown in figure 2.18. It is clear that there is an enhancement in the viscosity of the nanofluid, but there is no variation in the temperature profiles. Figure 2.19 reveals the effect of the viscosity of the nanofluid (E) on the concentration profiles. It is evident from the figure that there has been an increase in the viscosity of the nanofluid, but it does not show any effect on the concentration profiles.

As the ratio of the variation of the fluid density to the variation of the nanofluid is defined by buoyancy-ration parameter Nr. Figure 2.20 shows the effect of the Buoyancy-ratio parameter Nr on velocity profiles. As shown in the figure, velocity profiles increase with increasing values of Buoyancy-ratio parameter Nr. The influence of the buoyancy-ratio parameter Nr on the temperature profiles is plotted in figure 2.21. With the increasing Buoyancy-ratio parameters, there is no significant variation in the temperature profiles. Figure 2.22 represents typical profiles for the concentration for various values of the Buoyancy-ratio parameter Nr. We see that the concentration profiles increase with the increase of the Buoyancy-ratio parameter Nr, but the increment is very small.

The Lorentz force is a resistive force that is created due to the magnetic field and decreases the fluid motion in the boundary layer region. Figure 2.23 depicts the effect of the magnetic field parameter (M) on the velocity profiles. It is observed

that the velocity profile of the magnetic field is reduced with increasing values of the magnetic field parameter (M). Figure 2.24 exhibits the magnetic field parameter (M) on the temperature profiles. The temperature profile is accelerated with the increase of the magnetic field parameter (M), and the increment is very small. Figure 2.25 displays the effect of the magnetic field parameter (M) onconcentration profiles. As the magnetic field parameter (M) increases, there is no variation in the concentration profiles. The influence of angle (d) on the velocity profile is shown in figure 2.26. It is observed that the velocity profile of the fluid decreases with increasing angle (d). It is clear that as the angle of inclination increases, the influence of the buoyancy force due to thermal diffusion decreases. Figures 2.27 and 2.28 show the effect of the temperature profiles and the concentration profiles, respectively. It is obvious that in the presence of an angle, there is no variation in the temperature profiles or the concentration profiles.

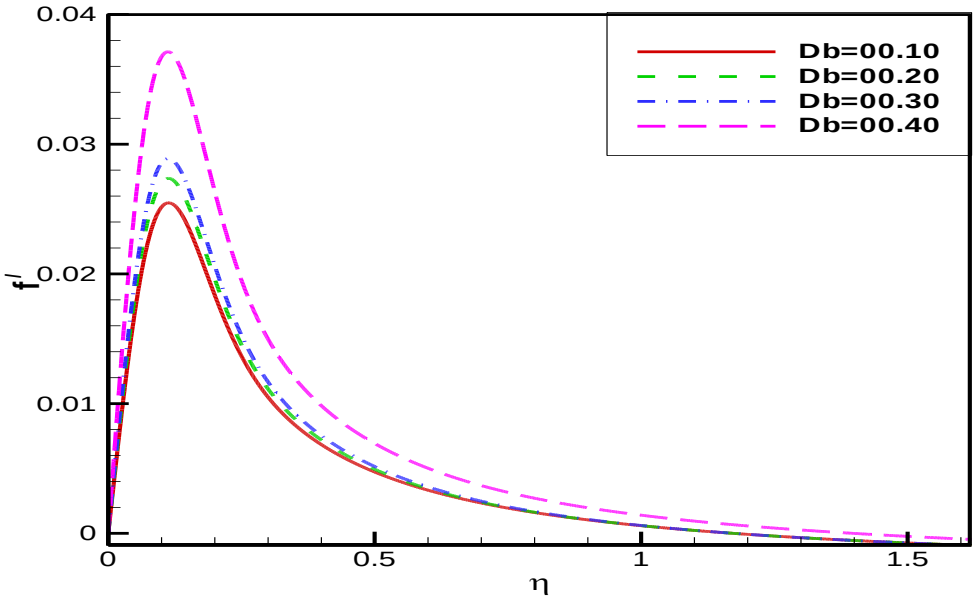

Fig. 2.2: Velocity profile for different values of Brownian diffusion coefficient (Db).

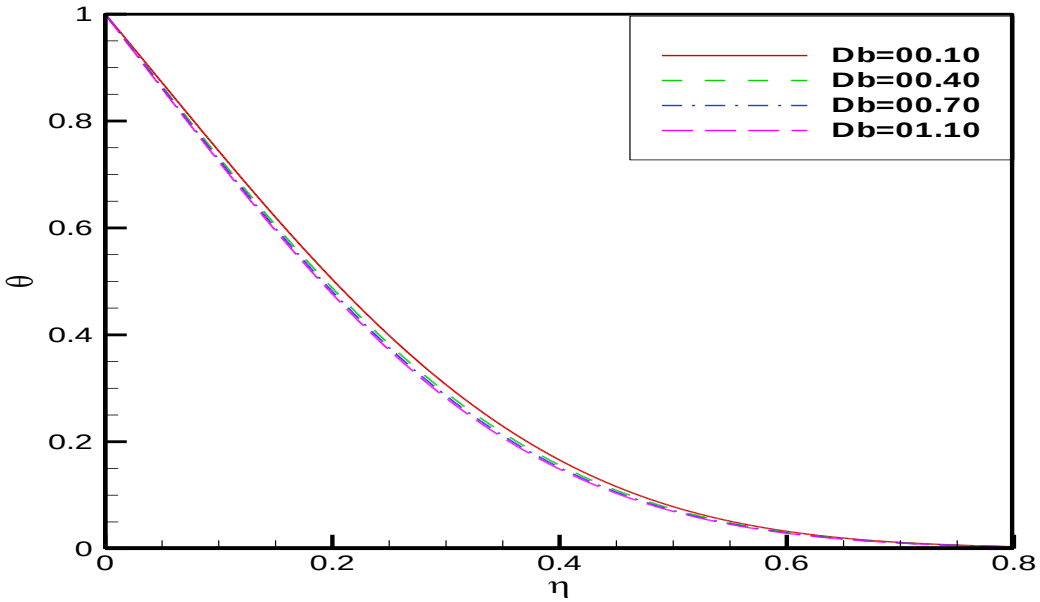

Fig. 2.3: Temperature profile for different values of Brownian diffusion coefficient (Db).

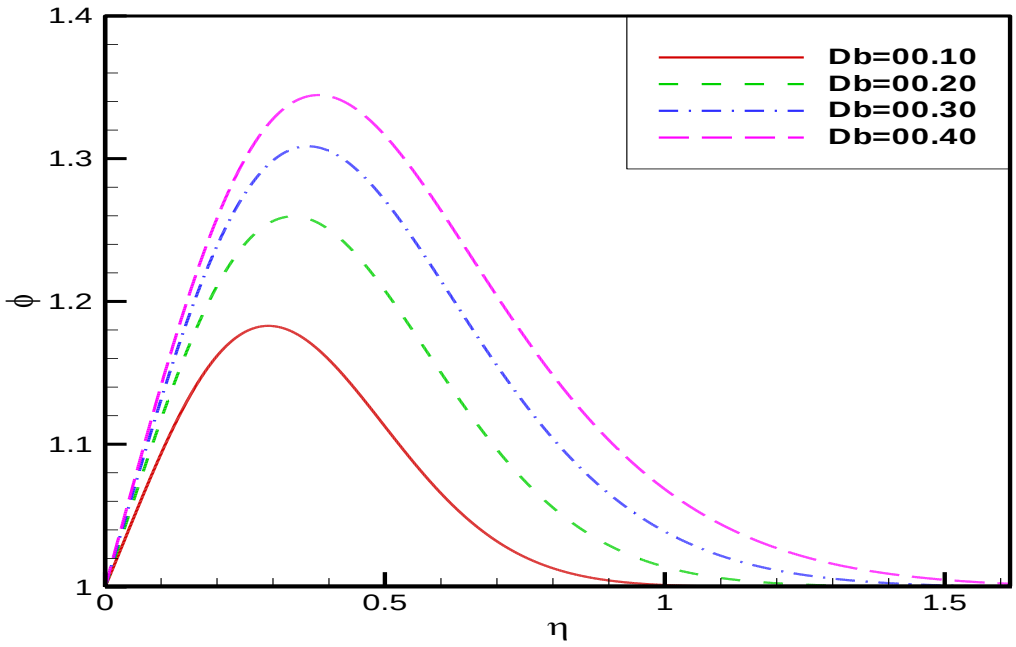

Fig. 2.4: Concentration profile for different values of Brownian diffusion coefficient (Db).

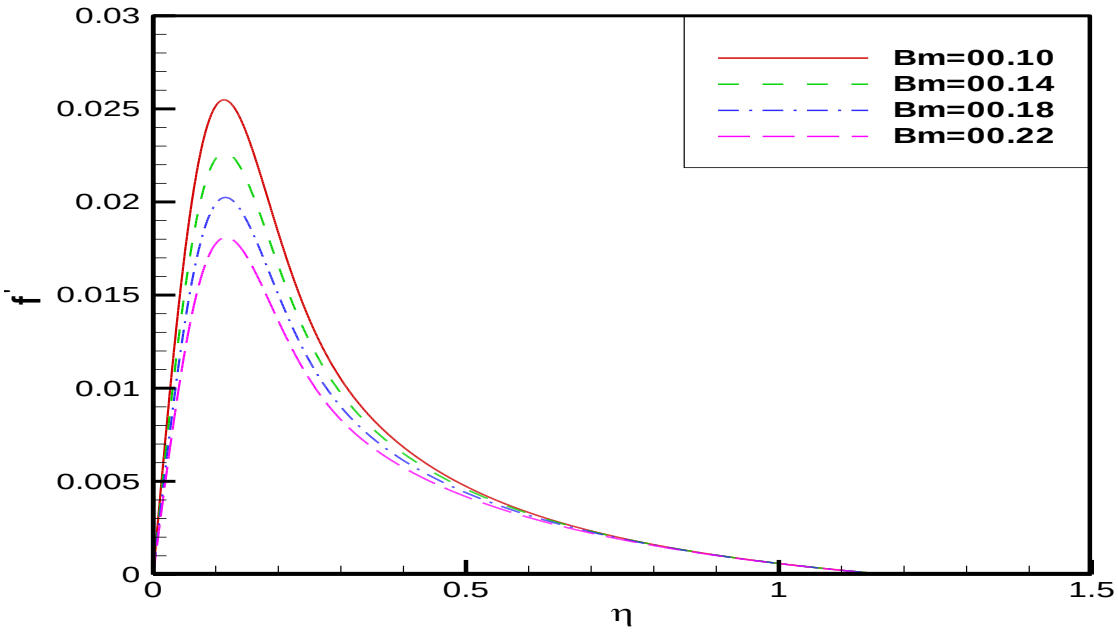

Fig. 2.5: Velocity profile for different values of thermal diffusivity parameter (Bm).

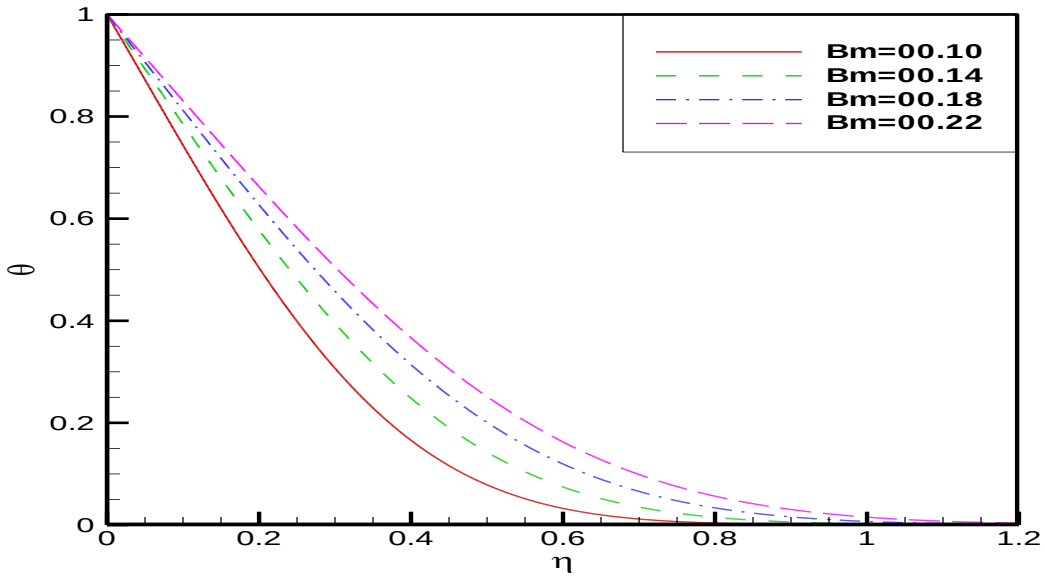

Fig. 2.6: Temperature profile for different values of thermal diffusivity parameter (Bm).

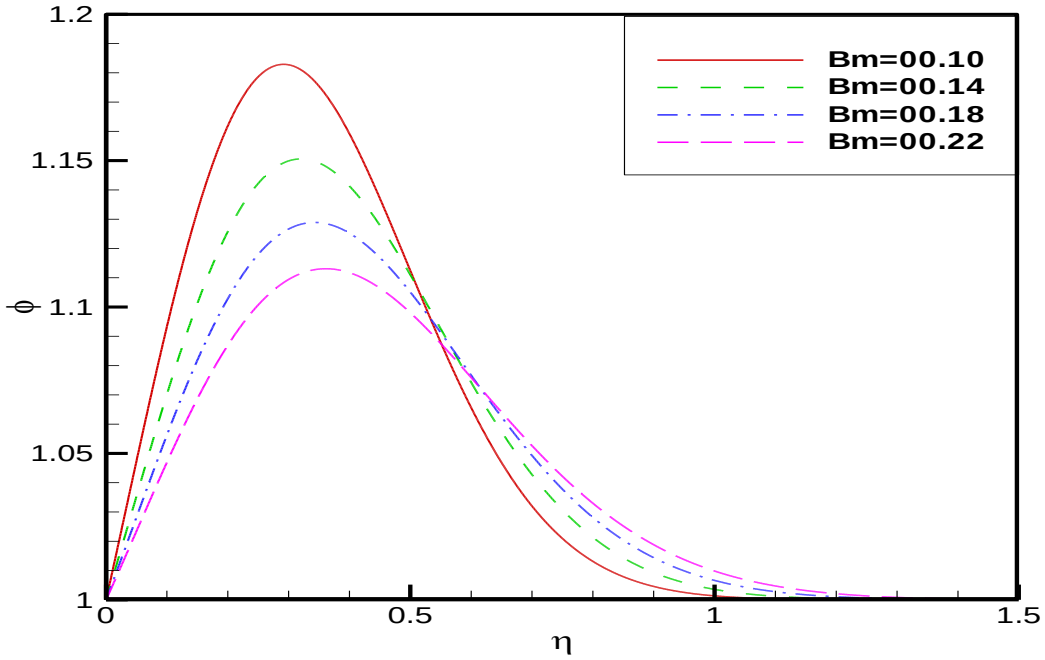

Fig. 2.7: Concentration profile for different values of thermal diffusivity parameter (Bm).

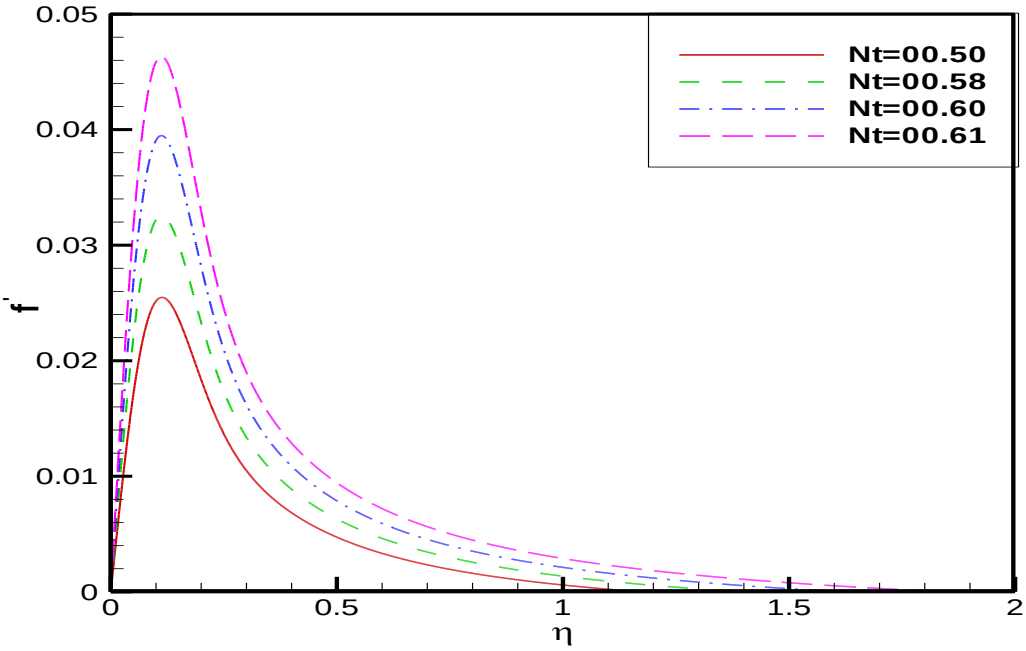

Fig. 2.8: Velocity profile for different values of thermophoresis parameter (Nt).

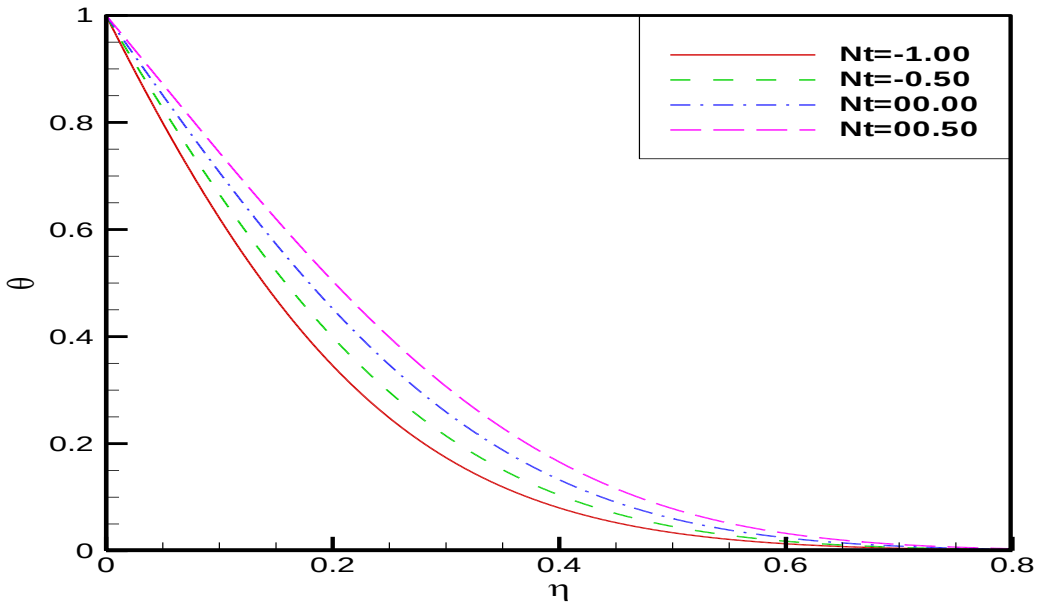

Fig. 2.9: Temperature profile for different values of thermophoresis parameter (Nt).

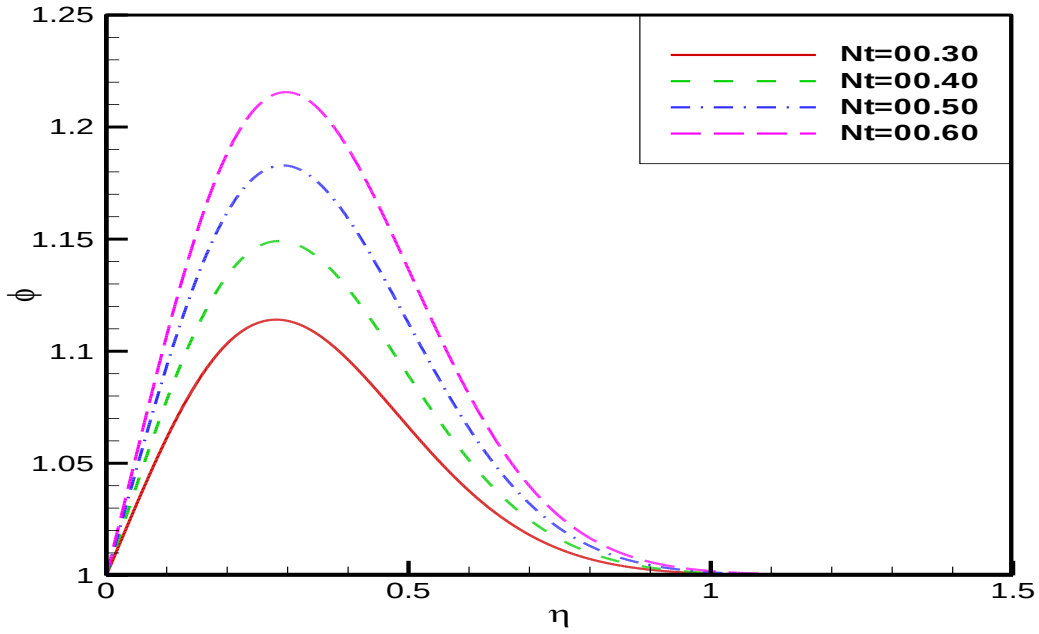

Fig. 2.10: Concentration profile for different values of thermophoresis parameter (Nt).

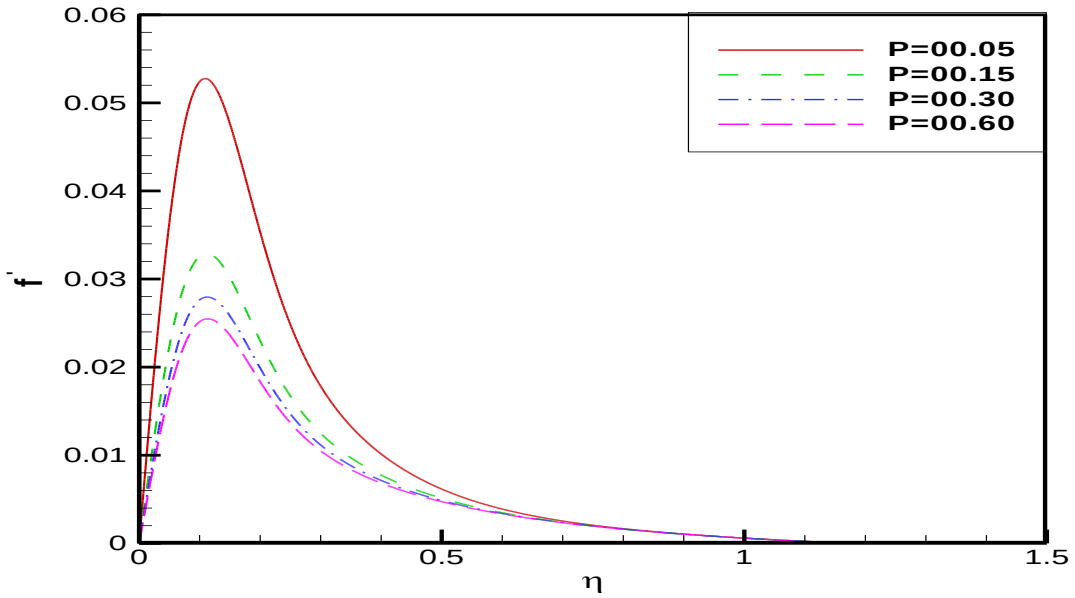

Fig. 2.11: Velocity profile for different values of unsteadiness parameter (P).

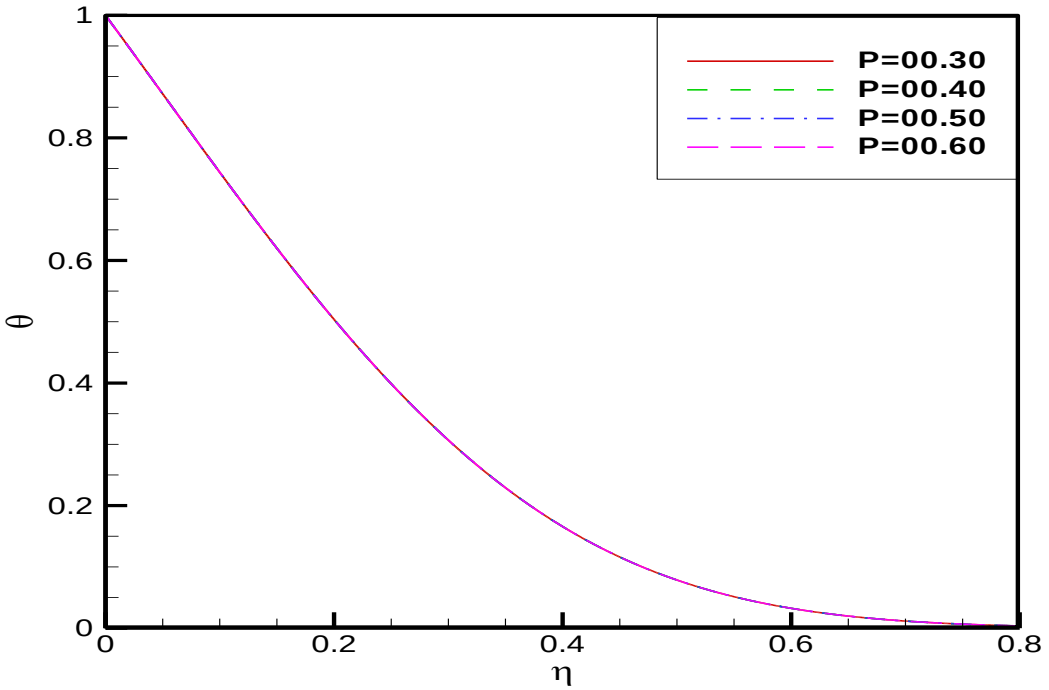

Fig. 2.12: Temperature profile for different values of unsteadiness parameter (P).

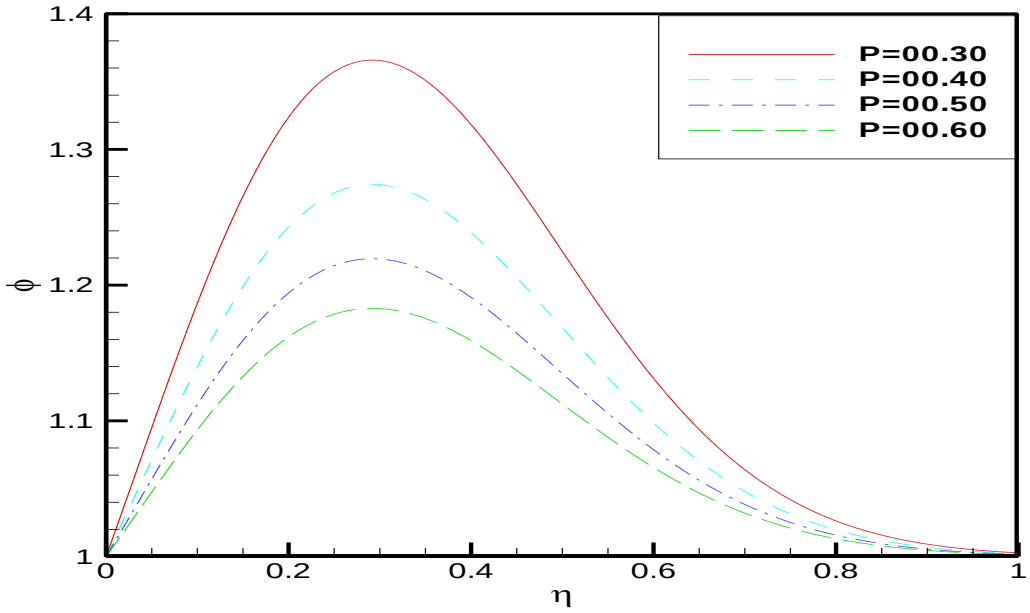

Fig. 2.13: Concentration profile for different values of unsteadiness parameter (P).

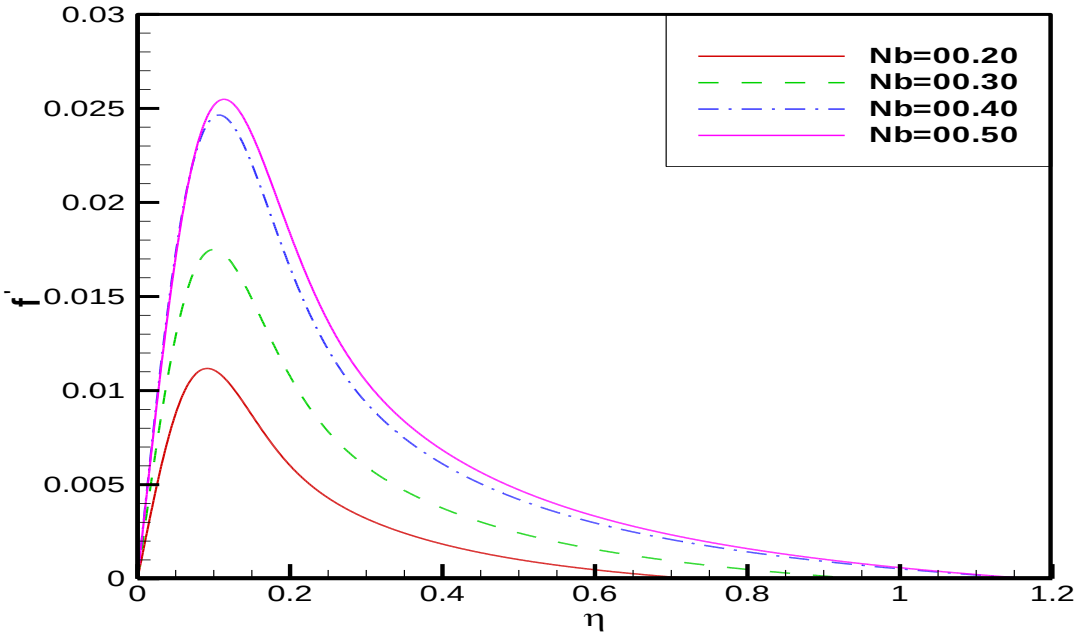

Fig. 2.14: Velocity profile for different values of Brownian motion parameter (Nb).

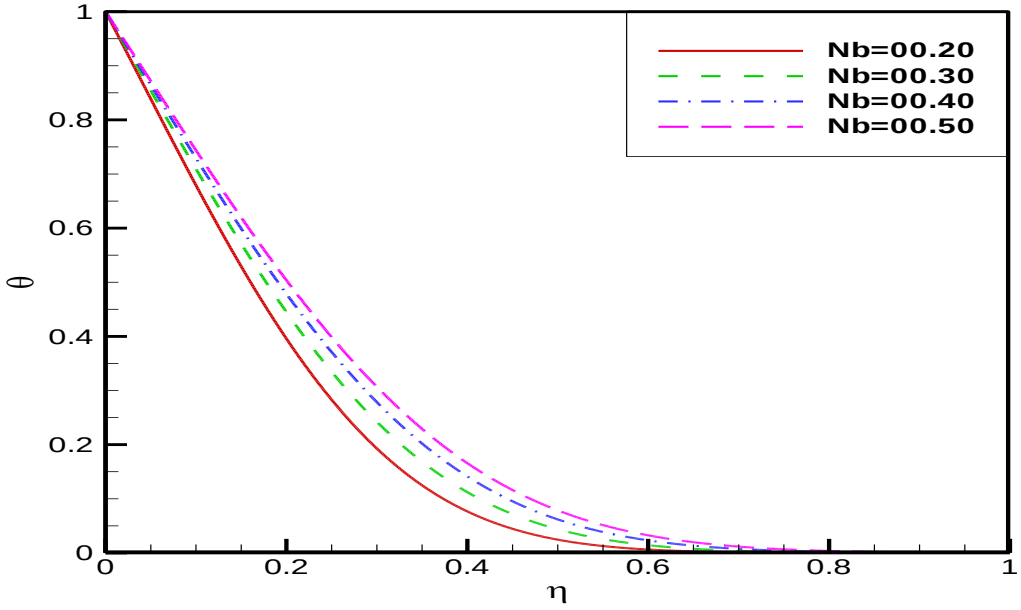

Fig. 2.15: Temperature profile for different values of Brownian motion parameter (Nb).

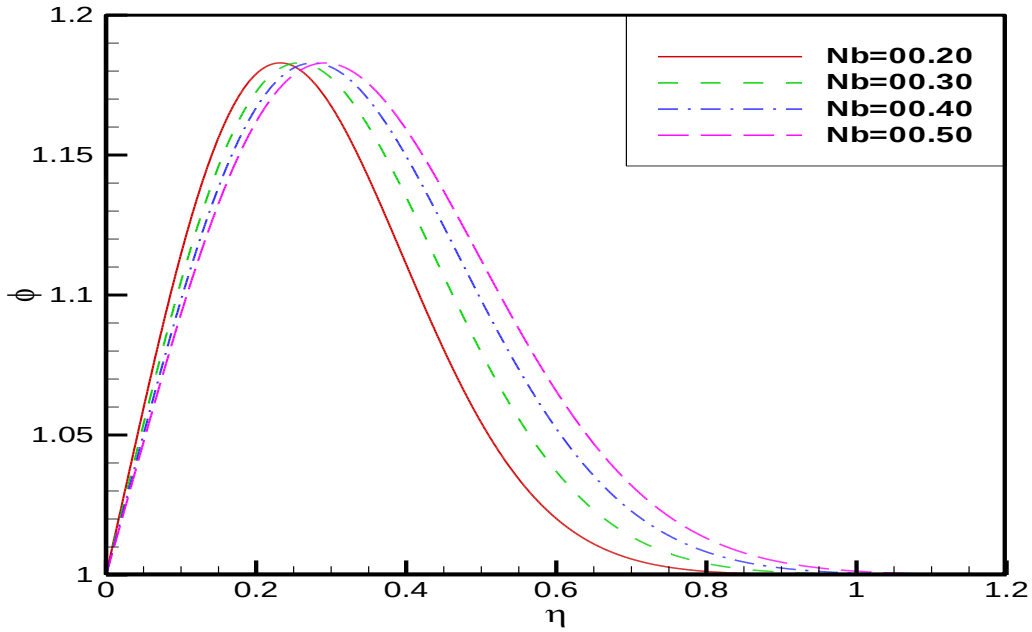

Fig. 2.16: Concentration profile for different values of Brownian motion parameter (Nb).

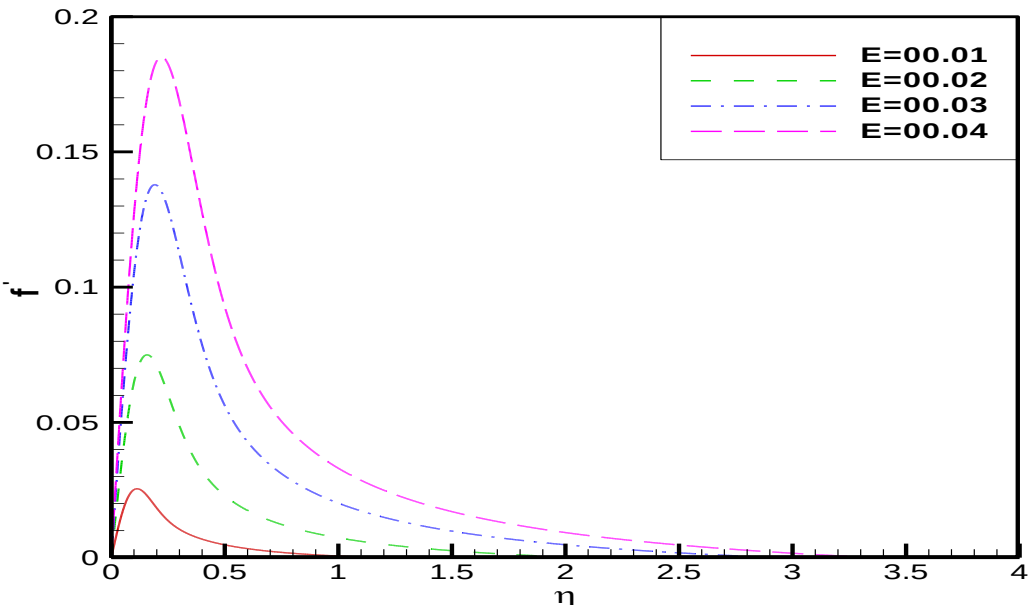

Fig. 2.17: Velocity profile for different values of viscosity of the nanofluid (E).

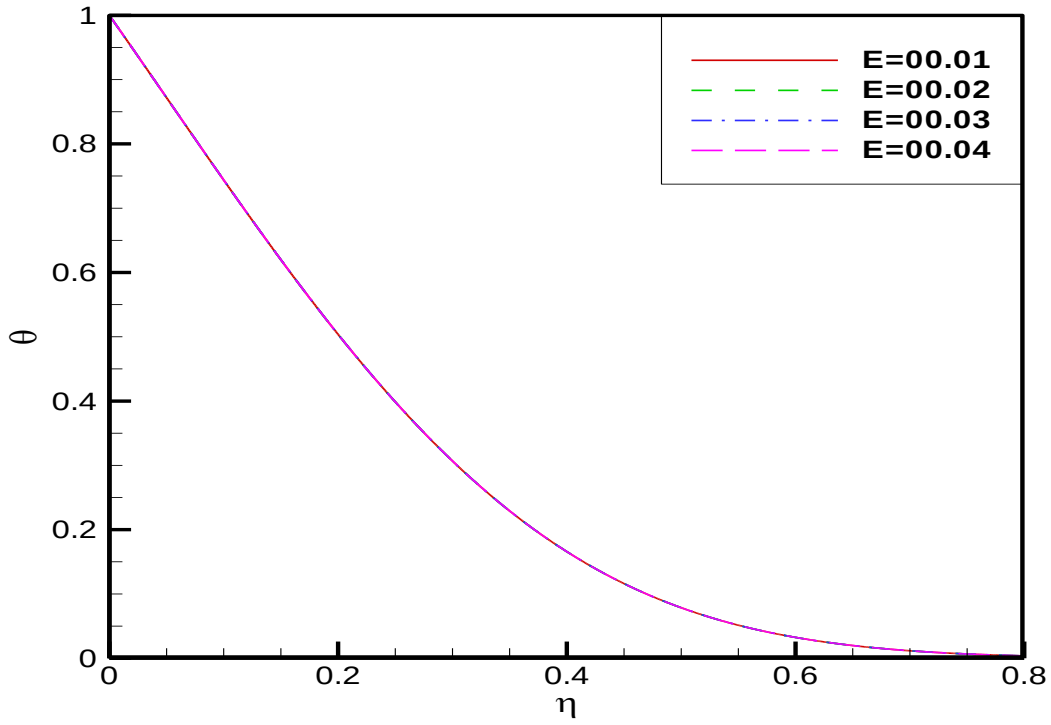

Fig. 2.18: Temperature profile for different values of viscosity of the nanofluid (E).

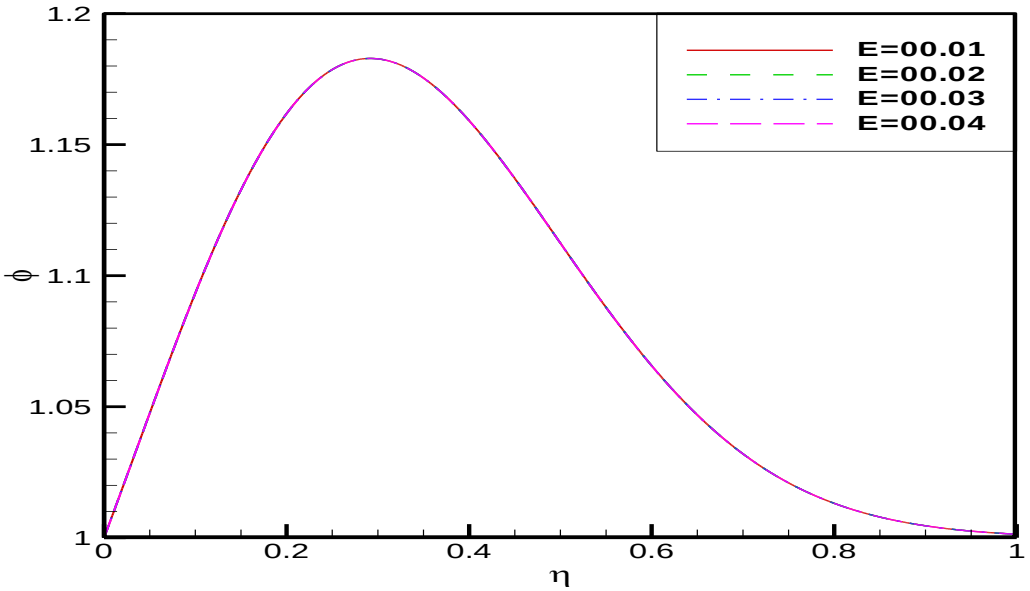

Fig. 2.19: Concentration profile for different values of viscosity of the nanofluid (E).

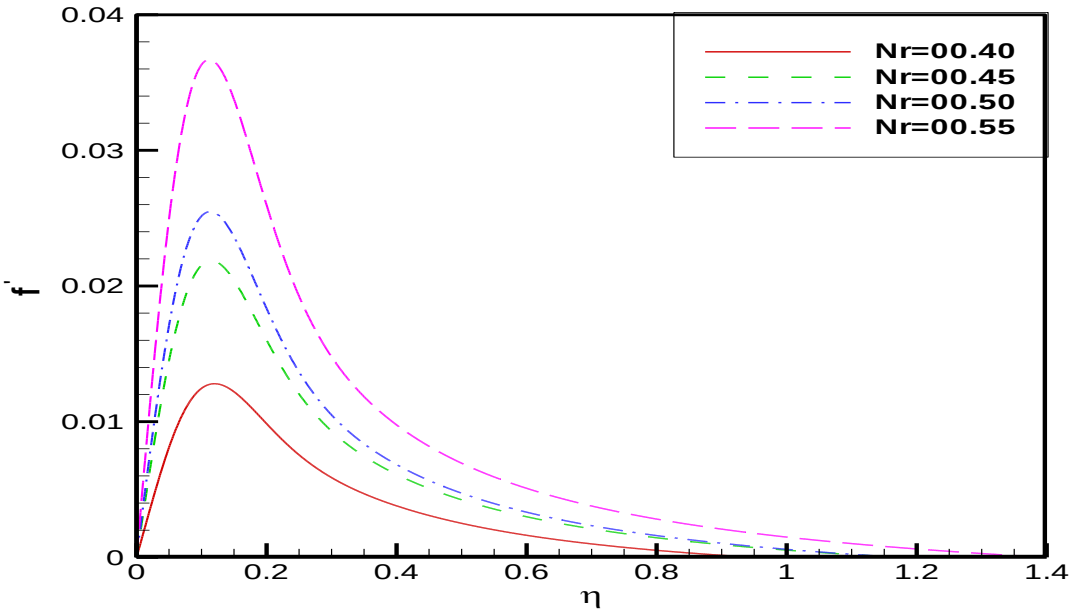

Fig. 2.20: Velocity profile for different values of buoyancy-ration parameter (Nr).

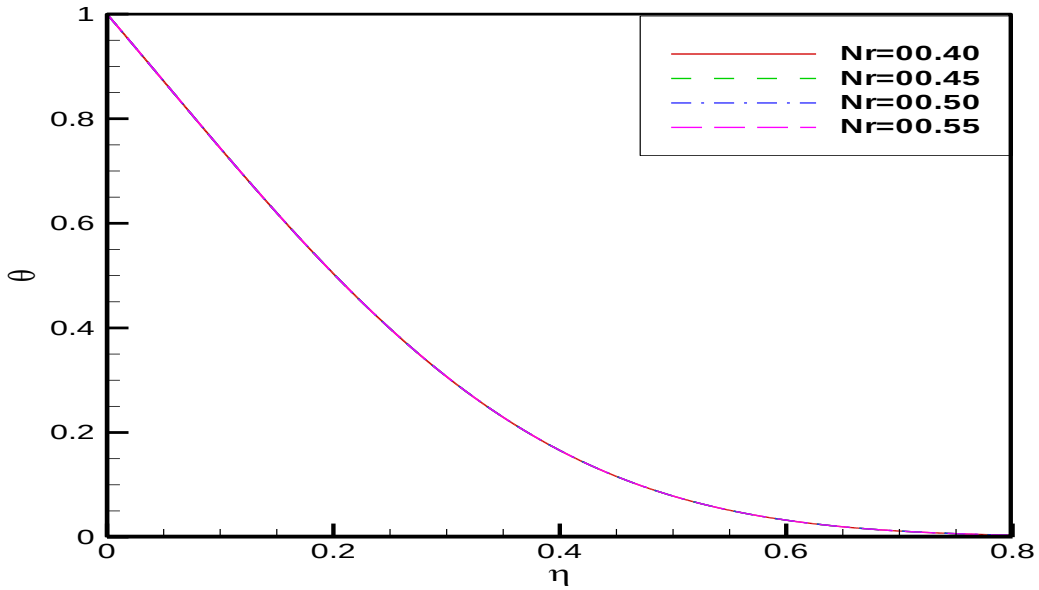

Fig. 2.21: Temperature profile for different values of buoyancy-ration parameter (Nr).

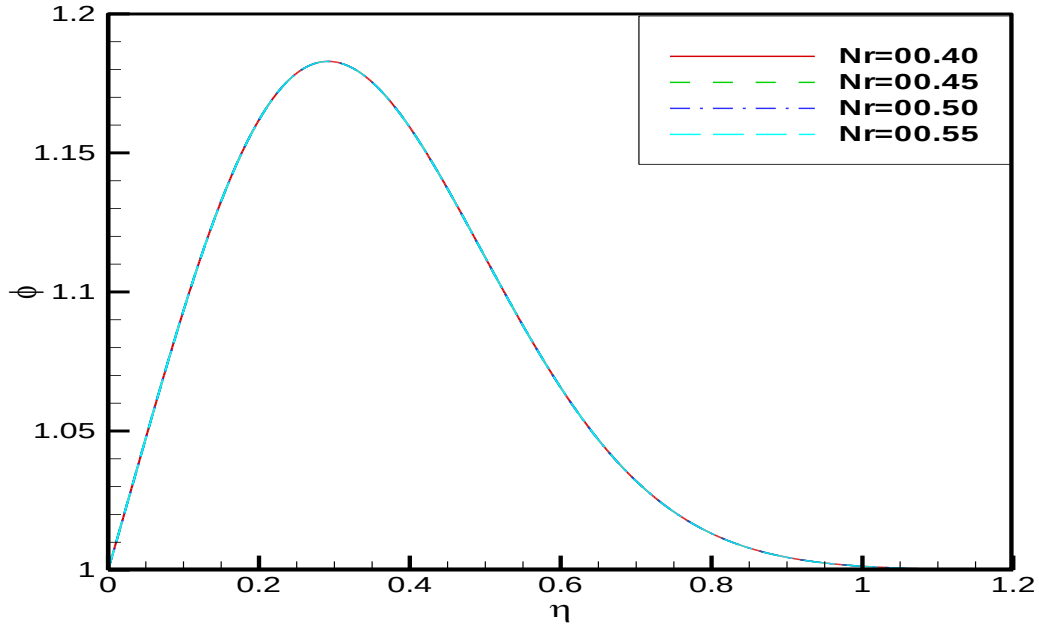

Fig. 2.22: Concentration profile for different values of buoyancy-ration parameter (Nr).

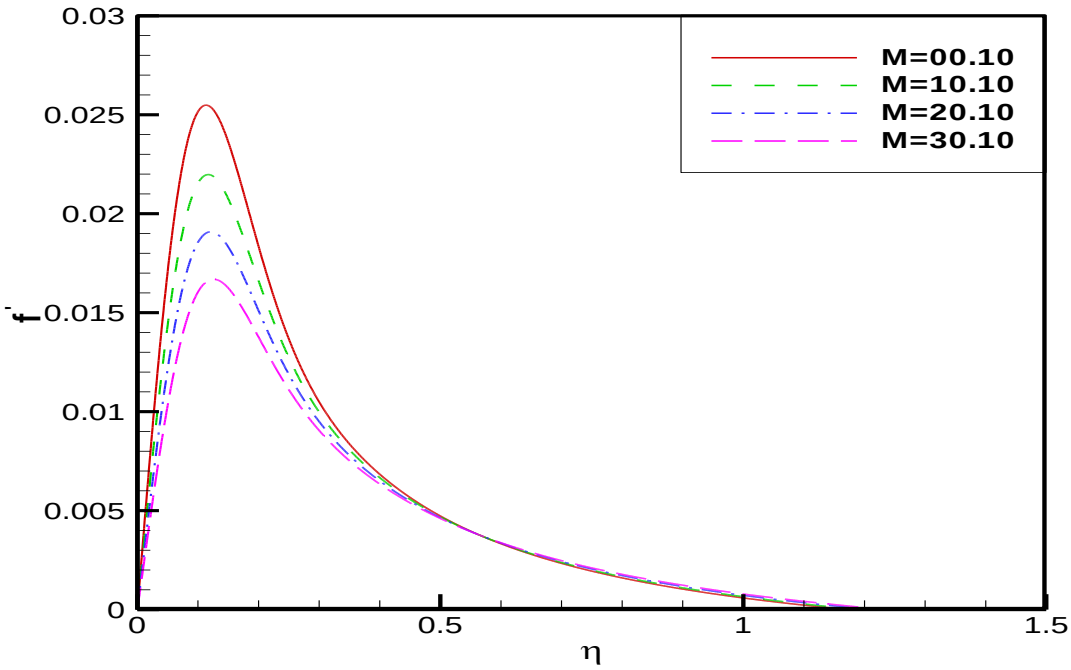

Fig. 2.23: Velocity profile for different values of magnetic field parameter (M).

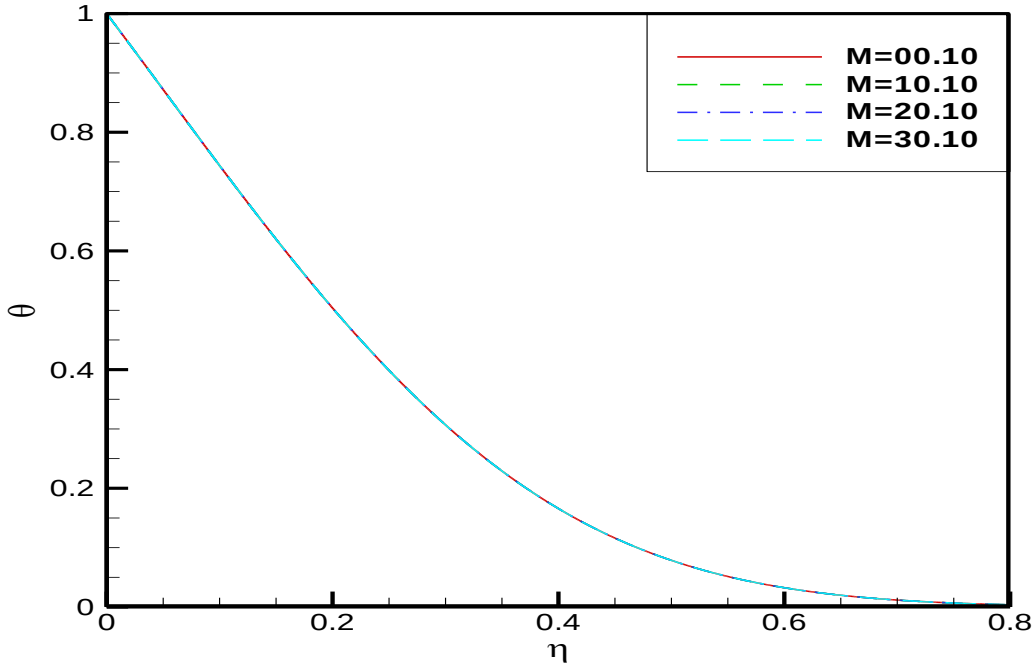

Fig. 2.24: Temperature profile for different values of magnetic field parameter (M).

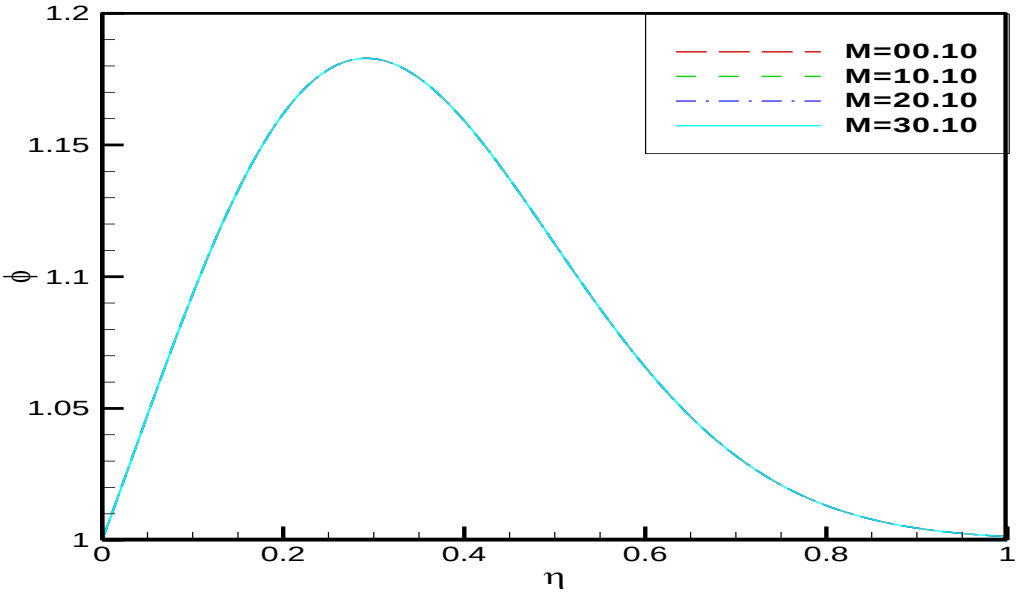

Fig. 2.25: Concentration profile for different values of magnetic field parameter (M).

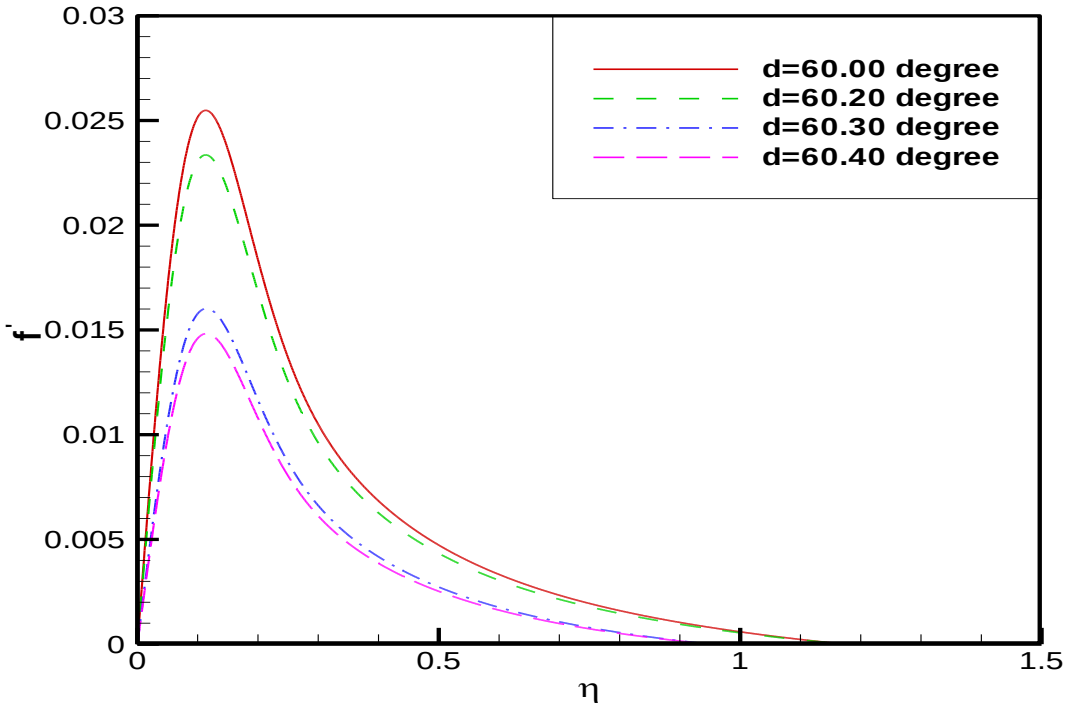

Fig. 2.26: Velocity profile for different values of angle of inclination (d).

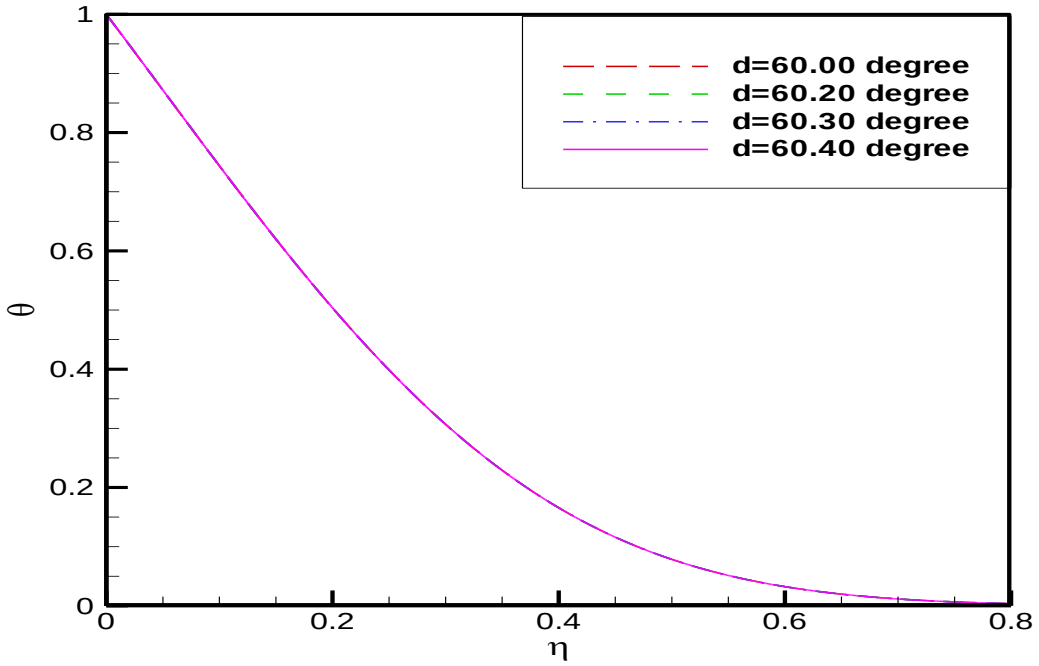

Fig. 2.27: Temperature profile for different values of angle of inclination (d).

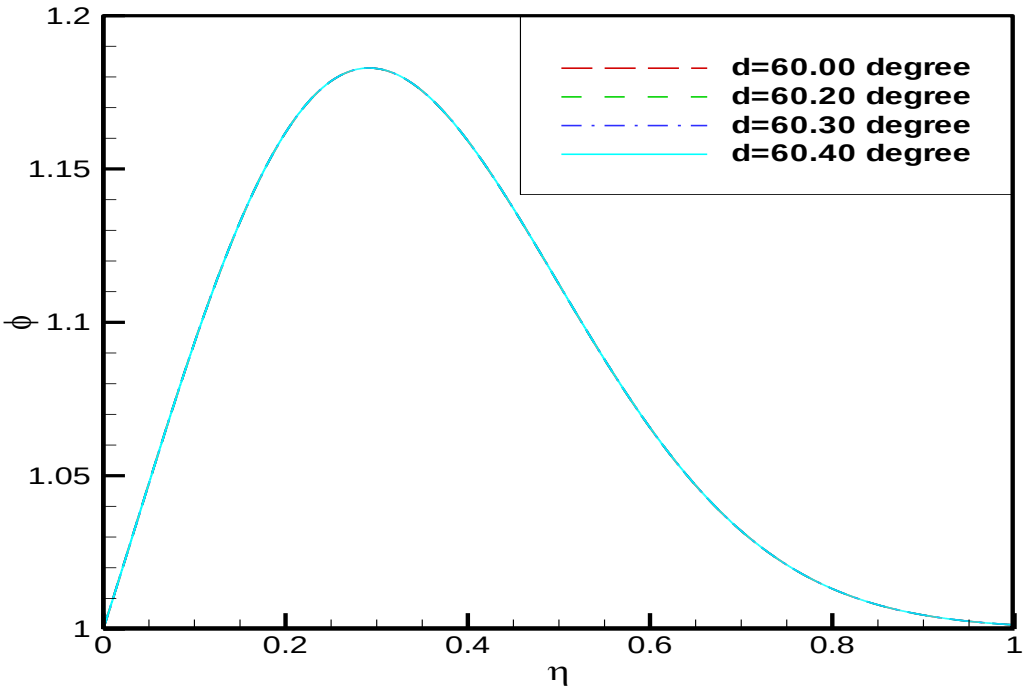

Fig. 2.28: Concentration profile for different values of angle of inclination (d).

The computed numerical values of Sherwood number $\emptyset'(0)$ are presented in Table 2.1 and are compared with the published results of (Aziz et al., 2012; Goyal et al., 2018) The results are found in close agreement.

Table 2.1. Comparison values of $[\emptyset'(\mathbf{0})]$for, $Pr = 5.0,\ M = 0.10,\ E = 0.01, Nb = 0.50,\ P = 0.60,\ Nt = 0.50,\ Bm = 0.10,\ Db = 0.10\ ,\ d = 60.$

Nt	(Aziz, 2012)	(Goyal M. a., 2018)	Present
0.20	1.0584	1.0585	1.1686
0.30	1.0353	1.0355	1.0562
0.40	1.0230	1.0233	0.9829
0.50	1.0102	1.0105	0.9296

At last, numerical results are discussed in Tables 2.2-2.11 for the effect of several parameters on the Skin-friction coefficient, Nusselt number, and Sherwood number. Tables 2.2 and 2.3 delineate that the skin-friction coefficient, Nusselt number, and Sherwood number decrease with the increase of the magnetic and thermal diffusivity parameters Bm.

Table: 2.2. The Skin-friction coefficient $f''(0)$, Nusselt number $\theta'(0)$, Sherwood number $\emptyset'(0)$for several values of M.

$\boldsymbol{M}$	$\boldsymbol{f''(0)}$	$\boldsymbol{-\theta'(0)}$	$\boldsymbol{\emptyset'(0)}$
0.0	0.266488435	2.531689832	0.929650407
5.0	0.244718248	2.531689370	0.929649963
10.0	0.224986956	2.531688902	0.929649513
15.0	0.207060224	2.531688431	0.929649061

Table: 2.3. The Skin-friction coefficient $f''(0)$, Nusselt number $\theta'(0)$, Sherwood number $\emptyset'(0)$for several values of Bm.

$\boldsymbol{Bm}$	$\boldsymbol{f''(0)}$	$\boldsymbol{-\theta'(0)}$	$\boldsymbol{\emptyset'(0)}$
0.10	0.266031360	2.531689823	0.929650398
0.14	0.220738952	2.114057097	0.691134212
0.18	0.182209924	1.849258998	0.550078139
0.22	0.148353839	1.663009380	0.456181391

Table: 2.4. The Skin-friction coefficient $f''(0)$, Nusselt number $\theta'(0)$, Sherwood number $\emptyset'(0)$for several values of Nr.

$\boldsymbol{Nr}$	$\boldsymbol{f''(0)}$	$\boldsymbol{-\theta'(0)}$	$\boldsymbol{\emptyset'(0)}$
0.50	0.266031360	2.531689823	0.929650398
0.51	0.275779650	2.531689377	0.929649751
0.52	0.285527958	2.531688930	0.929649094
0.53	0.295276284	2.531688479	0.929648426

Table: 2.5. The Skin-friction coefficient $f''(0)$, Nusselt number $\theta'(0)$, Sherwood number $\emptyset'(0)$for several values of E.

$\boldsymbol{E}$	$\boldsymbol{f''(0)}$	$\boldsymbol{-\theta'(0)}$	$\boldsymbol{\emptyset'(0)}$
0.01	0.266031360	2.531689823	0.929650398
0.02	0.690348449	2.531683368	0.929645489
0.03	1.104280109	2.531671157	0.929633656
0.04	1.305288981	2.531649821	0.929613008

Table: 2.6. The Skin-friction coefficient $f''(0)$, Nusselt number $\theta'(0)$, Sherwood number $\emptyset'(0)$for several values of Nb.

$\boldsymbol{Nb}$	$\boldsymbol{f''(0)}$	$\boldsymbol{-\theta'(0)}$	$\boldsymbol{\emptyset'(0)}$
0.20	0.099776187	3.183129091	1.168692247
0.30	0.183871508	2.876531178	1.056266214
0.40	0.276322421	2.676949180	0.982999931
0.50	0.266031360	2.531689823	0.929650398

Table: 2.7. The Skin-friction coefficient $f''(0)$, Nusselt number $\theta'(0)$, Sherwood number $\emptyset'(0)$for several values of P.

$\boldsymbol{P}$	$\boldsymbol{f''(0)}$	$\boldsymbol{-\theta'(0)}$	$\boldsymbol{\emptyset'(0)}$
0.30	0.305714003	2.531659128	1.859268112
0.40	0.285872732	2.531676328	1.394466753
0.50	0.273967924	2.531685012	1.115578607
0.60	0.266031360	2.531689823	0.929650398

Table: 2.8. The Skin-friction coefficient $f''(0)$, Nusselt number $\theta'(0)$, Sherwood number $\emptyset'(0)$for several values of Nt.

$\boldsymbol{Nt}$	$\boldsymbol{f''(0)}$	$\boldsymbol{-\theta'(0)}$	$\boldsymbol{\emptyset'(0)}$
0.50	0.266031360	2.531689823	0.929650398
0.58	0.375637496	2.463419235	1.025241113
0.60	0.483590968	2.446061898	1.046625872
0.61	0.590892660	2.437506675	1.057081417

Table: 2.9. The Skin-friction coefficient $f''(0)$, Nusselt number $\theta'(0)$, Sherwood number $\emptyset'(0)$for several values of Pr.

$\boldsymbol{Pr}$	$\boldsymbol{f''(0)}$	$\boldsymbol{-\theta'(0)}$	$\boldsymbol{\emptyset'(0)}$
1.0	0.266076166	2.531689823	0.929650398
3.0	0.266038826	2.531689823	0.929650398
5.0	0.266031360	2.531689823	0.929650398
7.0	0.266028160	2.531689823	0.929650398

Table: 2.10. The Skin-friction coefficient $f''(0)$, Nusselt number $\theta'(0)$, Sherwood number $\emptyset'(0)$for several values of Db.

$\boldsymbol{Db}$	$\boldsymbol{f''(0)}$	$\boldsymbol{-\theta'(0)}$	$\boldsymbol{\emptyset'(0)}$
0.10	0.266031360	2.531689823	0.929650398
0.20	0.295658171	2.601408880	1.171644545
0.30	0.318400656	2.641942002	1.310210182
0.40	0.446227040	2.673229753	1.411489454

Table: 2.11. The Skin-friction coefficient $f''(0)$, Nusselt number $\theta'(0)$, Sherwood number $\emptyset'(0)$for several values of d.

$\boldsymbol{d}$	$\boldsymbol{f''(0)}$	$\boldsymbol{-\theta'(0)}$	$\emptyset'(\mathbf{0})$
60.00	0.266031360	2.531689823	0.929650398
60.05	0.261443641	2.531690480	0.929651033
60.10	0.256202447	2.531691217	0.919651744
60.20	0.243813625	2.531692900	0.929653369

It is noted in Tables 2.4–2.6 that, with the increases of the buoyancy ratio (Nr), the viscosity of the nanofluid (E) and Brownian motion (Nb) parameters, both Nusselt number and Sherwood number decrease while the skin-friction coefficient increases. Moreover, Table-2.7 depicts that with an increase in the unsteadiness parameter (P), both the skin-friction coefficient and Sherwood number decrease while the Nusselt number increases. From Table 2.8, it is observed that the increases in the thermophoresis parameter (Nt), Skin-friction coefficient, and Sherwood number increase while the Nusselt number decreases. It is also seen in Table 2.9 that, with the increases in the Prandtl number (Pr), both the Nusselt number and the Sherwood number are fixed but the Skin friction coefficient decreases. It is shown in Table 2.10 that, with the increase of the Brownian diffusion coefficient parameter (Db), the skin-friction coefficient, Nusselt number, and Sherwood number increase. In Table 2.11, it is clear that Nusselt number and Sherwood number increase while skin friction coefficient decreases with the increased angle (d).

2.5. Conclusions

This study is focused on the similarity solution for the unsteady MHD boundary layer flow of a nanofluid for free convection around an inclined plate. With the help of similarity transformation, the leading time-dependent non-linear partial differential equations are transformed into a set of ordinary differential equations, which are then solved numerically using the shooting method, namely the Nachtsheim-Swigert iteration technique, using FORTRAN software. The effects of governing non-dimensional parameters on velocity, temperature, and concentration gradient are shown graphically, displayed in tabulated form, and discussed from a physical point of view.

The particular conclusions drawn from this study can be summarized as follows:

I. The mathematical problem has been solved numerically using the Nachtsheim-Swigert iteration technique, and the numerical results are shown graphically.
II. The fluid velocity and concentration increase while the fluid temperature decreases due to an increase in the Brownian diffusion coefficient.
III. The fluid velocity and concentration decrease while the fluid temperature increases due to the increase in the thermal diffusivity parameter.
IV. The fluid velocity, temperature, and concentration increase due to the increase in the thermophoresis parameter. The Brownian motion parameter, like the thermophoresis parameter, has the same effect on velocity, temperature, and concentration profiles.

V. The fluid velocity and concentration decrease, while the fluid temperature shows no significant variation due to the increase in the unsteadiness parameter.

VI. The fluid velocity increased while the fluid temperature and concentration showed no significant variation due to the increased viscosity of the nanofluid. Angle, like the thermophoresis parameter, has the same effect on velocity, temperature, and concentration profiles.

VII. The fluid velocity increased while the fluid temperature showed no significant variation, and the fluid concentration increment was very small due to the increase in the buoyancy ratio parameter.

VIII. The fluid velocity decreased while the fluid concentration showed no significant variation, and the fluid temperature increment was very small due to the increase in the magnetic parameter.

IX. The Skin-friction coefficient, Nusselt number, and Sherwood number decrease with the increase of the magnetic parameter and thermal diffusivity parameter.

X. Both Nusselt number and Sherwood number decrease, while skin friction coefficient increases due to an increase in the Bouyancy-ratio parameter, the viscosity of the nanofluid, and the Brownian motion parameter.

XI. Both the Nusselt number and the Sherwood number are fixed, while the skin friction coefficient decreases due to an increase in the Prandlt number.

XII. The skin-friction coefficient and Sherwood number increase while the Nusselt number decreases due to an increasing thermophoresis parameter.

XIII. Skin-friction coefficient, Nusselt number, and Sherwood number increase due to an increasing Brownian diffusion parameter.

Chapter 3

Study of unsteady MHD flow of a Nanofluid for Forced convection over a plate

3.1 Introduction

The investigation of forced convection boundary layer travels has significance for many engineering processes and the production of fiber-glass and condensation in the polymer sector. The possible applications for this time-forced convection flow through boundary layers over inclined plates through thermophoresis while a magnetic field is present include film vaporization on ablative surfaces, cross-hatching in combustion chambers, transportation cooling for rocket boosters, and re-entry vehicles. This particular issue has fascinated many researchers. Numerous significant theoretical and practical fields, including solar physics, geophysics, the production of paper, wire, and fiver coatings, and the storage of agricultural products, can benefit from forced convective boundary layer flows (Md. Jashim Uddin et al., 2016). The effects of thermophoresis on boundary layer flow in mass transfer over flat plates and unsteady forced convective heat in two dimensions have been examined. Regarding a range of physical factors, including mass and heat transfer characteristics, local heat production parameters, magnetic parameters, thermophoretic parameters, Prandtl numbers, Schmidt numbers, and local magnetic field parameters. (Aldoss et al., 1995) Examined the effect of convective conditions of the boundary on the transfer of heat and mass in hydromagnetic mixed convection through a porous material-encased vertical plate. (Kim, 2000) We study the unstable two-dimensional laminar flow while there is a transverse magnetic field present an

incompressible viscous electrically conducting fluid close to a moving semi-infinite vertical porous plate.

Several studies have investigated various aspects of heat and mass transfer in boundary layer flows. Literature (Aldoss et al., 1995) examined the influence of convective boundary conditions on heat and mass transfer in hydromagnetic mixed convection through a porous medium-encased vertical plate. Similarly, studies (Kim, 2000; Selim et al., 2003) explored mixed convection flows past vertical plates, with literature (Kim, 2000) focusing on the stability of laminar flow under a magnetic field and literature (Selim et al., 2003) investigating the effect of surface mass transfer with thermophoresis. Boundary layer flows along various geometries have also been a subject of research. A forced convection heat transfer boundary layer flow along a convergent channel was analyzed using similarity methods in literature (Alam, 2013). The effect of thermophoresis on particle deposition from a laminar forced convection boundary layer flow was studied in Literature (Chiou et al., 1996). (Roşca et al., 2014) Analyzed the problem involves solving the numerical flow of the boundary layer of steady mixed convection through a vertical flat plate incorporated in a fluid-saturated porous medium that included a nanofluid. (Ali J. Chamkha et al., 2000) Examine the effects on coupled heat and mass transfer via mixed convection in a linearly stratified stalemate flow (Hiemenz flow) of internal heat generation or the absorption as well as an externally applied magnetic field. (Hossain et al., 2000) Examined a two-dimensional mixed convection flow of a viscous incompressible substance with temperature-dependent viscosity through a vertical impermeable fluid.

Nanofluids have attracted significant attention in heat transfer research. Literatures (W. Ibrahim et al., 2014; Nasrin et al., 2013) investigated the influence of Prandtl number on forced convection heat transfer in a nanofluid-filled cavity and heat transfer with double diffusion in a nanofluid boundary layer flow, respectively. Numerical methods have been employed to solve complex boundary layer flow problems. Literatures (Ali J. Chamkha et al., 2000; Roşca et al., 2014) analyzed mixed convection flows involving nanofluids, with Literature . (Roşca et al., 2014) Focusing on a vertical plate in a porous medium and literature (Hossain et al., 2000) considering a stratified flow with internal heat generation/absorption and a magnetic field. (Ali J. Chamkha, 2004) Analyzed In the absence of a uniform contrary magnetic field and thermal and concentration buoyancy effects, a heat-absorbing, electrically conducting, viscous, incompressible fluid flows in an unsteady, two-dimensional laminar boundary-layer manner across a semi-infinite vertical permeable moving plate. (Noor et al., 2012) Studied Thermophoretic MHD flow over a radiate, inclined, isothermal permeable surface that has a sink and source of heat: Transfer of mass and heat.

Recent research has explored various aspects of boundary layer flows with heat and mass transfer. Literatures (Rahman, A.M., Alam, M.S. and Chowdhury, 2021; Seddeek et al., 2005) investigated the effects of variable properties (viscosity and thermal diffusivity) on mixed convection flows, with Literature (Seddeek et al., 2005) focusing on vertical stretching sheets and Literature (Rahman, A.M., Alam, M.S. and Chowdhury, 2021) considering a wedge geometry. Heat transfer mechanisms have also been a focus of study. The influence of thermal radiation on mixed convection in a porous medium was analyzed in Literature (Mukhopadhyay, 2009). Literature (Noor et al., 2012) examined the combined

effects of radiation and heat sources on thermophoretic MHD flow over an inclined surface.

Several studies have addressed forced convection flows with heat and mass transfer. Literatures (Adem, 2023; Ali J. Chamkha, 2004) analyzed laminar boundary layer flows past moving vertical plates, with Literature (Ali J. Chamkha, 2004) considering the absence of a magnetic field and Literature (Adem, 2023) focusing on flows along a porous wedge. The influence of combined effects like thermophoresis, variable properties, and magnetic fields has been explored in Literatures (Noor et al., 2012; Rahman, A., Alam, M. and Uddin, 2016; Rahman, A.M., Alam, M.S. and Chowdhury, 2021). These studies investigated flows over wedges and inclined surfaces, highlighting the role of these factors in heat and mass transfer. Other studies have examined mixed convection flows under different conditions. Literature (ABBAS et al., 2020) explored the combined effects of thermophoresis and temperature-dependent viscosity on a sphere. Literature (Khan et al., 2012) investigated mixed convection of a Newtonian fluid along a moving plate with chemical reactions. Literature (Ali J. Chamkha et al., 2001) analyzed natural convection from an inclined plate with internal heat generation and a magnetic field. The Soret effect, which occurs when a mixture's composition becomes inconsistent due to a temperature difference, is caused by a thermal process called thermophoresis or thermodiffusion. There is still much to learn regarding the nature of thermophoresis, and it keeps developing intensely debated, despite being a phenomenon that occurs pretty frequently in nature. Thermophoresis and heat convection together have the potential to reveal precursor accumulation in primordial settings, a critical mechanism for the genesis of life in the absence of any compartmentalization. In the presence of a changing

magnetic field and radiation effect, a convectively heated permeable vertically moving plate in the path of a two-dimensional steady forced convective flow of a Newtonian fluid has been studied (Ilias et al., 2020; Md. Jashim Uddin et al., 2013) Investigate the numerical solution of an inclined plate with leading edge accretion experiencing an unsteady aligned MHD flow of magnetic nanofluids. (Sheri, S.R., Chathilla, V. and Mahendar, 2018) Analyzed the effects of heat absorption, diffusion thermo effects, thermal-diffusion, and mass diffusion embedded in a porous medium on unsteady viscous incompressible MHD flow over a semi-infinite inclined permeable moving plate at different temperatures.

Graphs and tables are utilized to illustrate the effects of non-dimensional parameters on the profiles of temperature, velocity, and concentration as well as the Nusselt number, the Sherwood number, the magnetic parameter, the Prandtl number, the Brownain motion parameter, the thermophoresis parameter, and other driving parameters.

3.2. Mathematical problem, Governing equations and Boundary Conditions

Two-dimensional incompressible laminar systems with stable physical characteristics were studied. The x-axis measured along the plate; a uniformly strong magnetic field B_0 is applied in the y-direction (normal to the flow direction). The downward-acting gravitational acceleration g_e. Furthermore, buoyancy effects are included in momentum transfer with the conventional Boussinesq approximation. Similarly, convection from a hot fluid at a temperature T_f with a heat transfer coefficient h_f is expected to transfer heat to the plate's lower side.

It has been suggested that the base fluid and the nanoparticles are in thermal equilibrium with one another. Momentum, thermal, and nanoparticle volume boundary layers of three different types are generated close to the plate. After adding the fundamental assumptions to the discussion equations for mass, momentum, thermal energy, and species of nanoparticles, the dimensional set of governing equations is expressed as.

$$\frac{\partial u}{\partial x}+\frac{\partial v}{\partial y}=0 \tag{3.1}$$

$$\frac{\partial u}{\partial t}+\rho_f\left(u\frac{\partial u}{\partial x}+v\frac{\partial u}{\partial y}\right)=\mu\frac{\partial^2 u}{\partial y^2}-\sigma_{nf}B_0^2u+\frac{\partial U}{\partial t}+U\frac{\partial U}{\partial x} \tag{3.2}$$

$$\frac{\partial T}{\partial t}+u\frac{\partial T}{\partial x}+v\frac{\partial T}{\partial y}=\alpha_m\frac{\partial^2 T}{\partial y^2}+\tau[Db\frac{\partial \hat{\emptyset}}{\partial y}\frac{\partial T}{\partial y}+\frac{D_T}{T_\infty}\left(\frac{\partial T}{\partial y}\right)^2] \tag{3.3}$$

$$\frac{\partial \hat{\emptyset}}{\partial t}+u\frac{\partial \hat{\emptyset}}{\partial x}+v\frac{\partial \hat{\emptyset}}{\partial y}=Db\frac{\partial^2 \hat{\emptyset}}{\partial y^2}+\frac{D_T}{T_\infty}\frac{\partial^2 T}{\partial y^2} \tag{3.4}$$

Where T is the local temperature, $\emptyset\hat{}$ is the local solid volume fraction of the nanoparticles, β is the base fluid's volumetric thermal expansion coefficient, Db is the Brownian diffusion coefficient, D_T is the thermophoretic diffusion coefficient, and u and v are the velocity components parallel and perpendicular to the plate, respectively. Db coefficient of Brownian diffusion. Equations for nanofluids' continuity, momentum, thermal energy, and species of nanoparticles are represented by (3.1)-(3.4).

The boundary conditions may be written as:

$$u=U, v=0, \hat{\emptyset}=\hat{\emptyset}_w, T=T_f \; at \; y=0. \tag{3.5}$$

$$u=0, v=0, \hat{\emptyset}=\hat{\emptyset}_\infty, T=T_\infty at \; y\to\infty. \tag{3.6}$$

The continuity equation (1) is satisfied by introducing the steam function $\Psi(x,y)$. Such that

$$u = \frac{\partial \Psi}{\partial y}, v = -\frac{\partial \Psi}{\partial x}. \tag{3.7}$$

By introducing the following, the equations for momentum, thermal energy, and the species of nanoparticles can be converted to the corresponding ordinary differential equations. Similarity transformations:

$$\eta = \frac{y}{xt}(R_{a_x})^{1/4},\ \ \psi = \alpha_m (R_{a_x})^{1/4} f(\eta),\ \ \theta(\eta) = \frac{T - T_\infty}{T_f - T_\infty},\ \ \emptyset(\eta) = \frac{\widehat{\emptyset} - \emptyset_\infty}{\widehat{\emptyset}_w - \widehat{\emptyset}_\infty},$$

$$U = \frac{\alpha_m}{xt}(R_{a_x})^{1/2}. \tag{3.8}$$

The definition of the local Rayleigh number is

$$R_{a_x} = \frac{(1-\widehat{\emptyset}_\infty)\beta g_e (T_f - T_\infty) x^3 t^3}{\nu \alpha_m} \tag{3.9}$$

$$\frac{\partial \eta}{\partial x} = \frac{y}{t}(R_{a_x})^{\frac{1}{4}} \frac{\partial}{\partial x} x^{-1} = \frac{y}{t}(R_{a_x})^{\frac{1}{4}} \frac{\partial}{\partial x} x^{-1} = -\frac{y}{x^2 t}(R_{a_x})^{\frac{1}{4}}.$$

$$\frac{\partial \eta}{\partial y} = \frac{1}{xt}(R_{a_x})^{\frac{1}{4}} \frac{\partial}{\partial y} y = \frac{1}{xt}(R_{a_x})^{\frac{1}{4}}.$$

$$U = \frac{\alpha_m}{xt}(R_{a_x})^{1/2}.$$

$$\frac{\partial U}{\partial t} = \frac{\alpha_m}{x}(R_{a_x})^{1/2} \frac{\partial}{\partial t} t^{-1} = -\frac{\alpha_m}{xt^2}(R_{a_x})^{1/2}.$$

$$\frac{\partial U}{\partial x} = \frac{\alpha_m}{t}(R_{a_x})^{1/2} \frac{\partial}{\partial x} x^{-1} = -\frac{\alpha_m}{x^2 t}(R_{a_x})^{1/2}.$$

$$u = \frac{\partial \Psi}{\partial y} = \frac{\alpha_m}{xt}(R_{a_x})^{1/2} f'(\eta) = U f'(\eta).$$

$$\frac{\partial u}{\partial y} = \frac{1}{xt}\alpha_m (R_{a_x})^{\frac{1}{2}} \frac{\partial}{\partial y} f'(\eta) = \frac{1}{xt}\alpha_m (R_{a_x})^{\frac{1}{2}} f''(\eta) \frac{\partial \eta}{\partial y} = \frac{1}{xt}\alpha_m (R_{a_x})^{\frac{1}{2}} f''(\eta) \frac{1}{xt}(R_{a_x})^{\frac{1}{4}}.$$

$$= \frac{\alpha_m}{x^2 t^2}(R_{a_x})^{\frac{3}{4}} f''(\eta)\,.$$

$$\frac{\partial^2 u}{\partial y^2} = \frac{\alpha_m}{x^2 t^2}(R_{a_x})^{\frac{3}{4}} \frac{\partial}{\partial y} f''(\eta) = \frac{\alpha_m}{x^2 t^2}(R_{a_x})^{\frac{3}{4}} f'''(\eta) \frac{\partial \eta}{\partial y} = \frac{\alpha_m}{x^2 t^2}(R_{a_x})^{\frac{3}{4}} f'''(\eta)\ \frac{1}{xt}(R_{a_x})^{\frac{1}{4}}.$$

$$= \frac{\alpha_m}{x^3 t^3} R_{a_x} f'''(\eta)\,.$$

$$\frac{\partial u}{\partial x} = \frac{\alpha_m}{t}(R_{a_x})^{\frac{1}{2}} \frac{\partial}{\partial x}\left[\frac{f'(\eta)}{x}\right] = \frac{\alpha_m}{t}(R_{a_x})^{\frac{1}{2}}\left[f'(\eta)\frac{\partial}{\partial x} x^{-1} + \frac{1}{x}\frac{\partial}{\partial x} f'(\eta)\right].$$

$= \frac{\alpha_m}{t}\left(R_{a_x}\right)^{\frac{1}{2}}[f'(\eta)(-\frac{1}{x^2}) + \frac{1}{x}f''(\eta)\frac{\partial\eta}{\partial x}]\frac{\alpha_m}{t}\left(R_{a_x}\right)^{\frac{1}{2}}[-\frac{f'(\eta)}{x^2} + \frac{1}{x}f''(\eta)(-\frac{y}{x^2t}\left(R_{a_x}\right)^{\frac{1}{4}})].$

$= -\frac{\alpha_m}{x^2t}\left(R_{a_x}\right)^{\frac{1}{2}}f'(\eta) - \frac{y\alpha_m}{x^3t^2}\left(R_{a_x}\right)^{\frac{3}{4}}f''(\eta).$

$v = -\frac{\partial\psi}{\partial x} = -\alpha_m\left(R_{a_x}\right)^{\frac{1}{4}}\frac{\partial}{\partial x}[f(\eta)] = -\alpha_m\left(R_{a_x}\right)^{\frac{1}{4}}f'(\eta)\frac{\partial\eta}{\partial x}.$

$= -\alpha_m\left(R_{a_x}\right)^{\frac{1}{4}}f'(\eta)[-\frac{y}{x^2t}\left(R_{a_x}\right)^{\frac{1}{4}}] = \frac{y\alpha_m}{x^2t}\left(R_{a_x}\right)^{\frac{1}{2}}f'(\eta).$

$\frac{\partial u}{\partial t} = \frac{1}{x}\alpha_m\left(R_{a_x}\right)^{\frac{1}{2}}\frac{\partial}{\partial t}[\frac{f'(\eta)}{t}] = \frac{1}{x}\alpha_m\left(R_{a_x}\right)^{\frac{1}{2}}[f'(\eta)\frac{\partial}{\partial t}\frac{1}{t} + \frac{1}{t}\frac{\partial}{\partial t}f'(\eta)]..$

$= \frac{1}{x}\alpha_m\left(R_{a_x}\right)^{\frac{1}{2}}[f'(\eta)\left(-\frac{1}{t^2}\right) + \frac{1}{t}f''(\eta)\frac{\partial\eta}{\partial t}] = \frac{1}{x}\alpha_m\left(R_{a_x}\right)^{\frac{1}{2}}[-\frac{f'(\eta)}{t^2} + \frac{1}{t}f''(\eta)(-\frac{\eta}{t})].$

$= -\frac{1}{xt^2}\alpha_m\left(R_{a_x}\right)^{\frac{1}{2}}[f'(\eta) + \eta f''(\eta)].$

$u\frac{\partial u}{\partial x} = \frac{1}{xt}\alpha_m\left(R_{a_x}\right)^{\frac{1}{2}}f'(\eta)[-\frac{\alpha_m}{x^2t}\left(R_{a_x}\right)^{\frac{1}{2}}f'(\eta) - \frac{y\alpha_m}{x^3t^2}\left(R_{a_x}\right)^{\frac{3}{4}}f''(\eta)].$

$= -\frac{{\alpha_m}^2}{x^3t^2}R_{a_x}\,f'^2(\eta) - \frac{y{\alpha_m}^2}{x^4t^3}\left(R_{a_x}\right)^{\frac{5}{4}}f'(\eta)f''(\eta).$

$v\frac{\partial u}{\partial y} = \frac{y\alpha_m}{x^2t}\left(R_{a_x}\right)^{\frac{1}{2}}f'(\eta)\frac{\alpha_m}{x^2t^2}\left(R_{a_x}\right)^{\frac{3}{4}}f''(\eta) = \frac{y{\alpha_m}^2}{x^4t^3}\left(R_{a_x}\right)^{\frac{5}{4}}f'(\eta)f''(\eta).$

$U\frac{\partial U}{\partial x} = \frac{\alpha_m}{xt}\left(R_{a_x}\right)^{1/2}\left\{-\frac{\alpha_m}{x^2t}\left(R_{a_x}\right)^{1/2}\right\} = -\frac{{\alpha_m}^2}{x^3t^2}R_{a_x}.$

From equation (3.2), we get

$\frac{\partial u}{\partial t} + \rho_f\left(u\frac{\partial u}{\partial x} + v\frac{\partial u}{\partial y}\right) = \mu\frac{\partial^2 u}{\partial y^2} - \sigma_{nf}B_0^2u + \frac{\partial U}{\partial t} + U\frac{\partial U}{\partial x}$

Or, $-\frac{1}{xt^2}\alpha_m\left(R_{a_x}\right)^{\frac{1}{2}}[f'(\eta) + \eta f''(\eta)] +$

$\rho_f\left[-\frac{{\alpha_m}^2}{x^3t^2}R_{a_x}\,f'^2(\eta) - \frac{y{\alpha_m}^2}{x^4t^3}\left(R_{a_x}\right)^{\frac{5}{4}}f'(\eta)f''(\eta) + \frac{y{\alpha_m}^2}{x^4t^3}\left(R_{a_x}\right)^{\frac{5}{4}}f'(\eta)f''(\eta)\right] =$

$\mu\frac{\alpha_m}{x^3t^3}R_{a_x}f'''(\eta) - \sigma_{nf}B_0^2\frac{1}{xt}\alpha_m\left(R_{a_x}\right)^{\frac{1}{2}}f'(\eta) - \frac{{\alpha_m}^2}{x^3t^2}R_{a_x} - \frac{\alpha_m}{xt^2}\left(R_{a_x}\right)^{1/2}$

Or, $-\frac{\alpha_m}{xt^2}\left(R_{a_x}\right)^{\frac{1}{2}}[f'(\eta) + \eta f''(\eta)] - \rho_f\frac{{\alpha_m}^2}{x^3t^2}R_{a_x}\,f'^2(\eta) = \mu\frac{\alpha_m}{x^3t^3}R_{a_x}f'''(\eta)$

$-\sigma_{nf}B_0^2\frac{1}{xt}\alpha_m\left(R_{a_x}\right)^{\frac{1}{2}}f'(\eta) - \frac{{\alpha_m}^2}{x^3t^2}R_{a_x} - \frac{\alpha_m}{xt^2}\left(R_{a_x}\right)^{1/2}.$

$$\text{Or},-\frac{x^2t}{\mu}\left(R_{a_x}\right)^{\frac{-1}{2}}[f'(\eta)+\eta f''(\eta)]-\rho_f\frac{\alpha_m t}{\mu}f'^2(\eta)=f'''(\eta)-\frac{x^2t}{\mu}\left(R_{a_x}\right)^{\frac{-1}{2}}-\frac{\alpha_m t}{\mu}-$$

$$\frac{\sigma_{nf}B_0^2x^2t^2}{\mu}\left(R_{a_x}\right)^{\frac{-1}{2}}f'(\eta)$$

$$\text{Or},f'''(\eta)=-\frac{x^2t}{\mu}\left(R_{a_x}\right)^{\frac{-1}{2}}[f'(\eta)+\eta f''(\eta)]-\rho_f\frac{\alpha_m t}{\mu}f'^2(\eta)+\frac{x^2t}{\mu}\left(R_{a_x}\right)^{\frac{-1}{2}}+\frac{\alpha_m t}{\mu}+$$

$$\frac{\sigma_{nf}B_0^2x^2t^2}{\mu}\left(R_{a_x}\right)^{\frac{-1}{2}}f'(\eta)$$

$$\text{Or},f'''(\eta)+\frac{1}{E}(P)^{\frac{-1}{2}}[f'(\eta)+\eta f''(\eta)-1]+\frac{1}{Pr}f'^2-Mf'-RN=0 \qquad (3.10)$$

Where, $Pr(Modified\ Prandtl\ Number)=\frac{\mu}{\alpha_m\rho_f t}$

$M(Modified\ Magnetic\ field\ Parameter)=\frac{\sigma_{nf}B_0^2x^2t^2}{\mu(R_{a_x})^{\frac{1}{2}}}.$

$E(Viscosity\ of\ the\ nanofluid)=\mu.$

Unsteadiness parameter $P=\frac{(1-\widehat{\emptyset}_\infty)\beta g_e(T-T_\infty)}{\mu}.$

$Unsteadiness\ parameter, RN=\frac{\alpha_m t}{\mu}.$

$\theta(\eta)=\frac{T-T_\infty}{T_f-T_\infty}T=T_\infty+(T_f-T_\infty)\theta(\eta).$

$$\frac{\partial T}{\partial t}=0+(T_f-T_\infty)\frac{\partial}{\partial\eta}\theta(\eta)\frac{\partial\eta}{\partial t}=\left(T_f-T_\infty\right)\theta'(\eta)(-\frac{\eta}{t})=-\frac{\eta\theta'(\eta)}{t}(T_f-T_\infty).$$

$$\frac{\partial T}{\partial x}=0+(T_f-T_\infty)\frac{\partial}{\partial\eta}\theta(\eta)\frac{\partial\eta}{\partial x}=\left(T_f-T_\infty\right)\theta'(\eta)(-\frac{y}{x^2t}\left(R_{a_x}\right)^{\frac{1}{4}}).$$

$$=-\frac{y(T_f-T_\infty)}{x^2t}\,\theta'(\eta)\left(R_{a_x}\right)^{\frac{1}{4}}.$$

$$\frac{\partial T}{\partial y}=0+(T_f-T_\infty)\frac{\partial}{\partial\eta}\theta(\eta)\frac{\partial\eta}{\partial y}=\left(T_f-T_\infty\right)\theta'(\eta)\frac{1}{xt}\left(R_{a_x}\right)^{\frac{1}{4}}..$$

$$=\frac{(T_f-T_\infty)}{xt}\theta'(\eta)\left(R_{a_x}\right)^{\frac{1}{4}}.$$

$$\frac{\partial^2T}{\partial y^2}=\frac{(T_f-T_\infty)}{xt}\left(R_{a_x}\right)^{\frac{1}{4}}\frac{\partial}{\partial\eta}\theta'(\eta)\frac{\partial\eta}{\partial y}=\frac{(T_f-T_\infty)}{xt}\left(R_{a_x}\right)^{\frac{1}{4}}\theta''(\eta)\frac{1}{xt}\left(R_{a_x}\right)^{\frac{1}{4}}.$$

$$=\frac{(T_f-T_\infty)}{x^2t^2}\theta''(\eta)\left(R_{a_x}\right)^{\frac{1}{2}}.$$

$\emptyset(\eta) = \frac{\widehat{\emptyset}-\emptyset_\infty}{\widehat{\emptyset}_w-\widehat{\emptyset}_\infty} = \emptyset_\infty + (\widehat{\emptyset}_w-\widehat{\emptyset}_\infty)\emptyset(\eta)$.

$\frac{\partial\widehat{\emptyset}}{\partial t} = 0 + \left(\widehat{\emptyset}_w-\widehat{\emptyset}_\infty\right)\frac{\partial}{\partial\eta}\emptyset(\eta)\frac{\partial\eta}{\partial t} = \left(\widehat{\emptyset}_w-\widehat{\emptyset}_\infty\right)\emptyset'(\eta)(-\frac{\eta}{t}) = -\frac{\eta\,\emptyset\prime(\eta)}{t}\left(\widehat{\emptyset}_w-\widehat{\emptyset}_\infty\right).$

$\frac{\partial\widehat{\emptyset}}{\partial x} = 0 + \left(\widehat{\emptyset}_w-\widehat{\emptyset}_\infty\right)\frac{\partial}{\partial\eta}\emptyset(\eta)\frac{\partial\eta}{\partial x} = \left(\widehat{\emptyset}_w-\widehat{\emptyset}_\infty\right)\emptyset'(\eta)\,(-\frac{y}{x^2t}\left(R_{a_x}\right)^{\frac{1}{4}}).$

$= -\frac{y(\widehat{\emptyset}_w-\widehat{\emptyset}_\infty)}{x^2t}\left(R_{a_x}\right)^{\frac{1}{4}}\emptyset'(\eta)$.

$\frac{\partial\widehat{\emptyset}}{\partial y} = 0 + \left(\widehat{\emptyset}_w-\widehat{\emptyset}_\infty\right)\frac{\partial}{\partial\eta}\emptyset(\eta)\frac{\partial\eta}{\partial y} = \left(\widehat{\emptyset}_w-\widehat{\emptyset}_\infty\right)\emptyset'(\eta)\frac{1}{xt}\left(R_{a_x}\right)^{\frac{1}{4}} = \frac{(\widehat{\emptyset}_w-\widehat{\emptyset}_\infty)}{xt}\emptyset'(\eta)\left(R_{a_x}\right)^{\frac{1}{4}}.$

$\frac{\partial^2\widehat{\emptyset}}{\partial y^2} = \frac{(\widehat{\emptyset}_w-\widehat{\emptyset}_\infty)}{xt}\left(R_{a_x}\right)^{\frac{1}{4}}\frac{\partial}{\partial\eta}\emptyset'(\eta)\frac{\partial\eta}{\partial y}.$

$= \frac{(\widehat{\emptyset}_w-\widehat{\emptyset}_\infty)}{xt}\left(R_{a_x}\right)^{\frac{1}{4}}\emptyset''(\eta)\frac{1}{xt}\left(R_{a_x}\right)^{\frac{1}{4}} = \frac{(\widehat{\emptyset}_w-\widehat{\emptyset}_\infty)}{x^2t^2}\emptyset''(\eta)\left(R_{a_x}\right)^{\frac{1}{2}}.$

$u\frac{\partial T}{\partial x} = \frac{1}{xt}\alpha_m\left(R_{a_x}\right)^{\frac{1}{2}}f'(\eta)[-\frac{y(T_f-T_\infty)}{x^2t}\,\theta'(\eta)\left(R_{a_x}\right)^{\frac{1}{4}}].$

$= -\frac{y\alpha_m(T_f-T_\infty)}{x^3t^2}\left(R_{a_x}\right)^{\frac{3}{4}}f'(\eta)\theta'(\eta).$

$v\frac{\partial T}{\partial y} = \frac{y\alpha_m}{x^2t}\left(R_{a_x}\right)^{\frac{1}{2}}f'(\eta)\,\frac{(T_f-T_\infty)}{xt}\theta'(\eta)\left(R_{a_x}\right)^{\frac{1}{4}}.$

$= \frac{y\alpha_m(T_f-T_\infty)}{x^3t^2}\left(R_{a_x}\right)^{\frac{3}{4}}f'(\eta)\theta'(\eta).$

$\frac{\partial\widehat{\emptyset}}{\partial y}\frac{\partial T}{\partial y} = \frac{(\widehat{\emptyset}_w-\widehat{\emptyset}_\infty)}{xt}\emptyset'(\eta)\left(R_{a_x}\right)^{\frac{1}{4}}\frac{(T_f-T_\infty)}{xt}\theta'(\eta)\left(R_{a_x}\right)^{\frac{1}{4}}.$

$= \frac{(\widehat{\emptyset}_w-\widehat{\emptyset}_\infty)(T_f-T_\infty)}{x^2t^2}\left(R_{a_x}\right)^{\frac{1}{2}}\theta'(\eta)\emptyset'(\eta).$

From equation (3.3), we get

$\frac{\partial T}{\partial t} + u\frac{\partial T}{\partial x} + v\frac{\partial T}{\partial y} = \alpha_m\frac{\partial^2T}{\partial y^2} + \tau[Db\frac{\partial\widehat{\emptyset}}{\partial y}\frac{\partial T}{\partial y} + \frac{D_T}{T_\infty}\left(\frac{\partial T}{\partial y}\right)^2].$

Or, $-\frac{\eta\theta'(\eta)}{t}\left(T_f-T_\infty\right) - \frac{y\alpha_m(T_f-T_\infty)}{x^3t^2}\left(R_{a_x}\right)^{\frac{3}{4}}f'(\eta)\theta'(\eta) +$

$\frac{y\alpha_m(T_f-T_\infty)}{x^3t^2}\left(R_{a_x}\right)^{\frac{3}{4}}f'(\eta)\theta'(\eta) = \alpha_m\frac{(T_f-T_\infty)}{x^2t^2}\theta''(\eta)\left(R_{a_x}\right)^{\frac{1}{2}} +$

$\tau[\frac{(\widehat{\emptyset}_w-\widehat{\emptyset}_\infty)(T_f-T_\infty)Db}{x^2t^2}\left(R_{a_x}\right)^{\frac{1}{4}}\theta'(\eta)\emptyset'(\eta)+\frac{D_T}{T_\infty}(\frac{(T_f-T_\infty)}{xt}\theta'(\eta)\left(R_{a_x}\right)^{\frac{1}{4}})^2].$

Or, $-\frac{\eta\theta'(\eta)}{t}\left(T_f-T_\infty\right)=$

$\frac{\alpha_m}{x^2t^2}\left(T_f-T_\infty\right)\theta''(\eta)\left(R_{a_x}\right)^{\frac{1}{2}}+\tau\frac{\left(\widehat{\emptyset}_w-\widehat{\emptyset}_\infty\right)\left(T_f-T_\infty\right)Db}{x^2t^2}\left(R_{a_x}\right)^{\frac{1}{4}}\theta'(\eta)\emptyset'(\eta)$

$+\tau\frac{D_T}{T_\infty}\frac{\left(T_f-T_\infty\right)^2}{x^2t^2}\left(R_{a_x}\right)^{\frac{1}{2}}(\theta'(\eta))^2.$

Or, $-\frac{x^2t}{\alpha_m}\,\eta\theta'(\eta)\left(R_{a_x}\right)^{-\frac{1}{2}}=\theta''(\eta)+Nb\theta'(\eta)\emptyset'(\eta)+Nt(\theta'(\eta))^2.$

Or, $-\left(\frac{\left(1-\widehat{\emptyset}_\infty\right)\beta g_e(T-T_\infty)}{\mu}\right)^{-\frac{1}{2}}.\frac{1}{\alpha_m}\eta\theta'(\eta)=\theta''(\eta)+Nb\theta'(\eta)\emptyset'(\eta)+Nt(\theta'(\eta))^2.$

Or, $\theta''+Nb\theta'\emptyset'+Nt\theta'^2+\frac{1}{Bm}[P]^{-1/2}\eta\theta'=0.$ (3.11)

Where, $Nb(Brownian\ motion\ parameter)=\frac{\tau Db\left(\widehat{\emptyset}_w-\widehat{\emptyset}_\infty\right)}{\alpha_m}$

$Nt(thermophoresis\ parameter)=\frac{\tau D_T\left(T_f-T_\infty\right)}{T_\infty\alpha_m}.$

Bm $(thermal\ diffusivity\ parameter\ )=\alpha_m$

$u\frac{\partial\widehat{\emptyset}}{\partial x}=\frac{1}{xt}\alpha_m\left(R_{a_x}\right)^{\frac{1}{2}}f'(\eta)(-\frac{y\left(\widehat{\emptyset}_w-\widehat{\emptyset}_\infty\right)}{x^2t}\left(R_{a_x}\right)^{\frac{1}{4}}\emptyset'(\eta)).$

$=-\frac{y\alpha_m\left(\widehat{\emptyset}_w-\widehat{\emptyset}_\infty\right)}{x^3t^2}\left(R_{a_x}\right)^{\frac{3}{4}}f'(\eta)\emptyset'(\eta).$

$v\frac{\partial\widehat{\emptyset}}{\partial y}=\frac{y\alpha_m}{x^2t}\left(R_{a_x}\right)^{\frac{1}{2}}f'(\eta)\frac{\left(\widehat{\emptyset}_w-\widehat{\emptyset}_\infty\right)}{xt}\emptyset'(\eta)\left(R_{a_x}\right)^{\frac{1}{4}}.$

$=\frac{y\alpha_m\left(\widehat{\emptyset}_w-\widehat{\emptyset}_\infty\right)}{x^3t^2}\left(R_{a_x}\right)^{\frac{3}{4}}f'(\eta)\emptyset'(\eta).$

From equation (3.4), we get

$\frac{\partial\widehat{\emptyset}}{\partial t}+u\frac{\partial\widehat{\emptyset}}{\partial x}+v\frac{\partial\widehat{\emptyset}}{\partial y}=Db\frac{\partial^2\widehat{\emptyset}}{\partial y^2}+\frac{D_T}{T_\infty}\frac{\partial^2T}{\partial y^2}.$

Or, $-\frac{\eta\,\emptyset'(\eta)}{t}\left(\widehat{\emptyset}_w-\widehat{\emptyset}_\infty\right)-\frac{y\alpha_m\left(\widehat{\emptyset}_w-\widehat{\emptyset}_\infty\right)}{x^3t^2}\left(R_{a_x}\right)^{\frac{3}{4}}f'(\eta)\emptyset'^{(\eta)}+\frac{y\alpha_m\left(\widehat{\emptyset}_w-\widehat{\emptyset}_\infty\right)}{x^3t^2}\left(R_{a_x}\right)^{\frac{3}{4}}f'(\eta)\emptyset'(\eta)$

$=Db\frac{\left(\widehat{\emptyset}_w-\widehat{\emptyset}_\infty\right)}{x^2t^2}\emptyset''^{(\eta)}\left(R_{a_x}\right)^{\frac{1}{2}}+\frac{D_T}{T_\infty}\frac{\left(T_f-T_\infty\right)}{x^2t^2}\theta''(\eta)\left(R_{a_x}\right)^{\frac{1}{2}}.$

$$\text{Or},-\frac{\eta\,\emptyset'(\eta)}{t}\left(\widehat{\emptyset}_w-\widehat{\emptyset}_\infty\right)=Db\,\frac{\left(\widehat{\emptyset}_w-\widehat{\emptyset}_\infty\right)}{x^2t^2}\emptyset''(\eta)\left(R_{a_x}\right)^{\frac{1}{2}}+\frac{D_T}{T_\infty}\frac{\left(T_f-T_\infty\right)}{x^2t^2}\theta''(\eta)\left(R_{a_x}\right)^{\frac{1}{2}}.$$

$$\text{Or},\frac{\eta\,\emptyset'(\eta)}{t}\left(R_{a_x}\right)^{-\frac{1}{2}}\frac{x^2t^2}{Db}=\emptyset''(\eta)+\frac{Nt}{Nb}\,\theta''(\eta).$$

$$\text{Or},-\frac{1}{Db}\left(\frac{\left(1-\widehat{\emptyset}_\infty\right)\beta g_e(T-T_\infty)}{\mu}\right)^{-\frac{1}{2}}\eta\,\emptyset'(\eta)=\emptyset''(\eta)+\frac{Nt}{Nb}\,\theta''(\eta).$$

$$\text{Or},\ \emptyset''+\frac{Nt}{Nb}\theta''+\frac{1}{Db}[P]^{-1/2}\eta\emptyset'=0. \tag{3.12}$$

The following forms employ to the momentum, thermal energy, and species equations of nanoparticles:

$$f'''(\eta)+\frac{1}{E}(P)^{\frac{-1}{2}}[f'(\eta)+\eta f''(\eta)-1]+\frac{1}{Pr}f'^2-Mf'-RN=0 \tag{3.13}$$

$$\theta''+Nb\theta'\emptyset'+Nt\theta'^2+\frac{1}{Bm}[P]^{-1/2}\eta\theta'=0 \tag{3.14}$$

$$\emptyset''+\frac{Nt}{Nb}\theta''+\frac{1}{Db}[P]^{-1/2}\eta\emptyset'=0 \tag{3.15}$$

The corresponding boundary conditions are:

$$f(\eta)=0,\ f'(\eta)=0,\quad \emptyset(\eta)=1,\quad \theta(\eta)=1,\theta'(\eta)=0,\quad at\ \eta=0 \tag{3.16}$$

$$f'(\eta)=1,\ \theta(\eta)=0,\ \emptyset(\eta)=0\ \ as\ \ \eta\to\infty \tag{3.17}$$

Where the prime (') represents differentiation with respect to η.

Nusselt Number and Sherwood number assessment

Understanding heat and mass transfer at the wall serves as essential when analyzing the performance of nanofluidic systems. The engineering parameters that are significant to the current challenge are the local Nusselt number and Sherwood number, which differentiate for the wall deposition flux and the heat transfer rate, respectively. The local nanofluid Sherwood number and the local Nusselt number can be utilized to convey these values.

$$N_{u_x}=\frac{xq_w}{k(T_f-T_\infty)},\quad Sh_{x,n}=\frac{xq_{np}}{Db(\widehat{\emptyset_w}-\widehat{\emptyset_\infty})}$$

Where q_w and q_{np} represent the nano fluxes and wall heat, according to this order.

The following can be used to introduce and depict the modified Sherwood number $Sh_{x,n}$ for modified nanoparticles and the modified Nusselt number N_{u_x}.

$N_{ur} = (R_{a_x})^{\frac{1}{4}} N_{u_x} = -\theta'(0),\ Sh_{rn} = \left(R_{a_x}\right)^{\frac{1}{4}} Sh_{x,n} = \emptyset'(0).$

3.3. Numerical Solutions

A group of related nonlinear ordinary differential equations from (3.2) to (3.4), with boundary conditions as defined by (3.16) and (3.17). Higher order non-linear differential equations (3.13) to (3.15) must be simultaneously transformed into first order linear differential equations in order to solve the initial value problem numerically. Using the shooting method, the following results are obtained when integrating the Runge-Kutta integration scheme with the Nachtsheim-Swigert (1965) iteration technique:

After that, using a shooting technique that assumes a missing (undefined) initial condition at the starting point of the interval, at the terminal point, the differential equation is numerically integrated as an initial value problem. Next, by comparing the dependent variable's provided value at the conclusion line with its determined value, the accuracy of the presumed missing beginning condition is verified. Should a discrepancy appear, one must presume a different value for the absent initial condition and proceed with the testing process once more. The above process is carried out until the computed and provided requirements for the designated level of accuracy agree.

The Sherwood number and the Nusselt number are correlated with throughout the communication process. Figures and tables display the numerical results for a number of chosen values of the defined parameter. These graphs and

tables demonstrate how changes in the parameters under consideration have a substantial impact on heat transfer velocity, temperature, and concentration rate.

3.4. Results and Discussions

The temperature field (θ), concentration (∅), and velocity field (f') have all had numerical values calculated for a variety of physical parameters, including the nanofluid's viscosity, thermophoresis parameter, thermal diffusivity parameter, Prandtl number, magnetic field parameter, and Brownian motion and diffusion parameters, in order to look into the problem's mathematical representation. Where Pr=0.01 corresponds to liquid metals, can be chosen arbitrarily. Figures 3.1-3.26 provide an understandable summary of the problem's physics by offering a graphic representation of a representative set of numerical outcomes.

3.4.1 Velocity Profiles

As an illustration, 3.1–3.8 indicate the absence of dimension velocity profiles for the effects of multiple variables related to the Viscousity of the nanofluid (E), the thermophoresis parameter (Nt), thermal diffusivity (Bm), Prandtl number (Pr), Magnetic field (M), Brownian motion (Nb), and Unsteadiness parameters (P) & (RN). Figure 3.1 displays typical velocity profiles for various values of the magnetic field parameter (M). In an electrically conducting material, the Lorentz force rejects the flow during fluid when a magnetic field is introduced in the opposite guidance from the flow. Figure 3.1 indicates how, this resistive force tends to slow down the flow and fewer the fluid velocity as the magnetic field parameter (M) increases.. The Lorentz force increases with decreasing velocity. Both steady and unsteady cases are able to benefit from this. Considering that the magnetic field retards the forced convection flow, this result qualitatively reflects

the expectations. Figures 3.2, 3.4, and 3.8 exhibit the impact of the dimensionless velocity profiles' of the number Prandtl (Pr), the unsteadiness parameter (RN), and the Brownian motion parameter (Nb). It is apparent that the velocity profiles increase in proportion to the values of the Brownian motion parameter (Nb), the unsteadiness parameter (RN), and the Prandtl number (Pr). The effects of each of the following components on the dimensionless velocity profiles are presented in Figures 3.3, 3.5, 3.6, and 3.7: the thermal diffusivity parameter (Bm), the viscousity of the nanofluid (E), the unsteadiness parameter (P), and the thermophoresis parameter (Nt). It is evident that when the thermal diffusivity (Bm), viscosity of the nanofluid (E), unsteadiness (P), and thermophoresis (Nt) increase, the velocity profiles also decline.

3.4.2 Temperature Profiles

The measurement of temperature fluctuation with shifting altitude above the surface is called the temperature profile. There are temperature ranges across various altitudes above sea level rather than a constant rise or fall in temperature with altitude.

Figures 3.9–3.17 indicate the devoid of dimension temperature profiles for the effects of multiple variables related to the Viscousity of the nanofluid (E), Thermophoresis parameter (Nt), thermal diffusivity (Bm), Prandtl number (Pr), Motion of Brownian motion (Nb), Magnetic field (M), Brownian diffusion parameter (Db), and Unsteadiness parameter (P) and (RN). Images of the temperature profiles with different Magnetic field parameter (M) settings are displayed in Figure 3.9. It has been found that when the magnetic field parameter (M) increases, the temperature profile somewhat decreases. The temperature curve

with various Prandtl number (Pr) values appears in Figure 3.10. High fluids have less wealthy thermal conductivities, which reduces conduction heat transfer and increases temperature fluctuations at the wall, according to the definition of the Prandtl number. In accordance to this figure, an increase in the Prandtl number (Pr), so does the temperature distribution. Figure 3.11 demonstrates that the temperature distribution develops as the Thermal diffusivity parameter (Bm) value does.

Figures 3.12 and 3.14 exhibit how the unsteadiness parameters (RN) and (P) modify the temperature profile. The results presented here show that as the unsteadiness parameters (RN) and (P) increase, the temperature profiles correspondingly slightly rise and fall. Figure 3.13 indicates the x-axis's dimensionless temperature profiles for different degrees of the viscosity of the nanofluid (E) along with the impacts of the viscosity on the nanofluid (E). It is obvious that as the Viscosity of the nanofluid (E) improves, so do the temperature profiles.

Thermophoresis force is the force that causes nanoparticles to move into the fluid that surrounds them as a consequence of temperature gradients. Figure 3.15 explains that the ambient fluid is the result of a higher thermophoresis force, which causes temperature profiles to increase. The figure 3.16 illustrates the following effects on the temperature profiles of the Brownian diffusion parameter (Db). We determined that as the Brownian diffusion parameter (Db) increased, the temperature profiles reduced. Figure 3.17 shows the result of the temperature profiles on the Brownian motion parameter (Nb). We noticed that as the Brownian motion parameter (Nb) increased, the temperature profiles rise.

3.4.3 Concentration Profiles

For the purpose of offering a physical understanding of this issue, figures 3.18–3.26 graphically display the dimensionless concentration profiles' numerical results. Concentration profiles are shown to vary with the magnetic field parameter (M) in Figure 3.18. It has been discovered that applying an increase in the magnetic field parameter (M) is the outcome of a magnetic field parameter (M) by decreasing concentration profiles. Figure 3.19 shows the movement of the concentration profiles for various Prandtl number (Pr) levels. Concentration profiles are seen toslightly increase as Prandtl number (Pr) values increase. Figure 3.20 shows how distinct values of the Thermal diffusivity parameter (Bm) modify the concentration profiles. We note that the concentration profiles decline, but as the thermal diffusivity parameter (Bm) increases, the concentration profiles eventually reverse. Figures 3.21 and 3.23 exhibit the way the unsteadiness parameters (RN) and (P) affect the dimensionless concentration profiles. Evidently, as RN and P expand in both situations, the concentration profiles increase and decrease respectively.

Figure 3.22 demonstrates the concentration profiles for a range of viscosity of the nanofluid (E). It is being noted that concentration profiles marginally rise as the Viscosity of the nanofluid (E) rises. Figure 3.24 demonstrates how the Thermophoresis parameter (Nt) affects concentration profiles. In figure 3.24, it has been noted that the concentration profiles show an increase as a consequence of increase in the thermophoresis parameter (Nt). Figure 3.25 reveals the Brownian motion parameter (Nb) on concentration profiles. It has been notice the concentration profiles increase along with a rise in the thermophoresis parameter (Nt). While particles are small, Strong Brownian motion results in a high

;When particles are large, however, it is clear that Brownian motion greatly improves the concentration profiles. Figure 2.26 clarifies the difference of the dimensionless concentration profiles plotted for different values of the Brownian diffusion parameter (Db). Figure 3.26 illustrates how the concentration profiles quickly rise as the Brownian diffusion parameter (Db) increases.

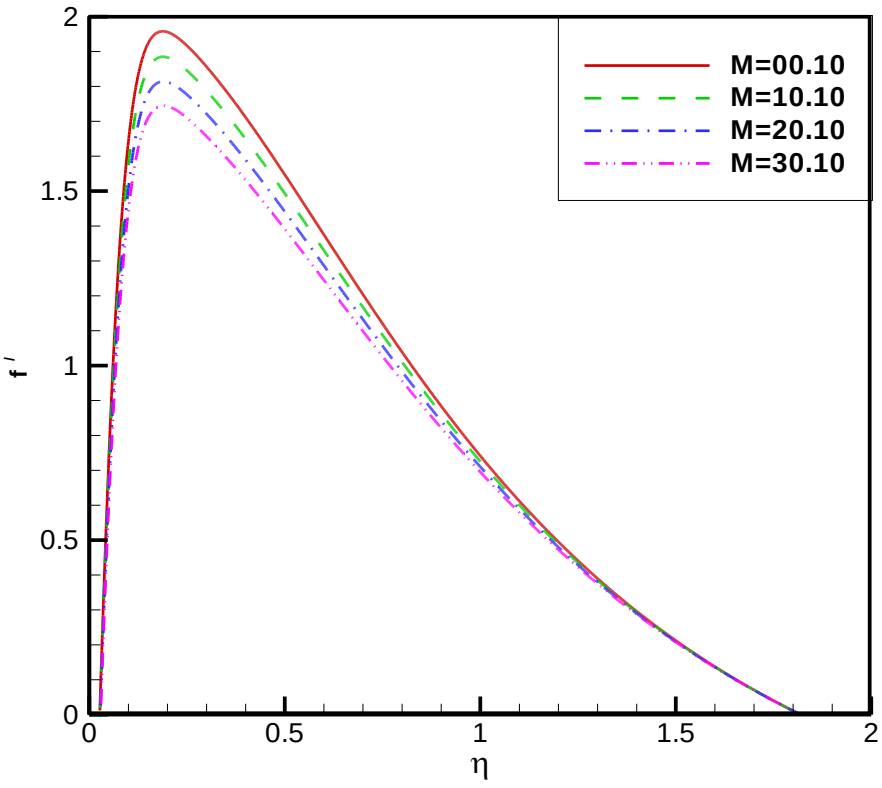

Fig. 3.1: Influence of multiple values of Magnetic field parameter M on velocity profiles, when Pr=00.01, RN=00.00, Bm=00.10, E=00.01, P=00.60, Nt=00.50, Nb=00.50, Db=00.10.

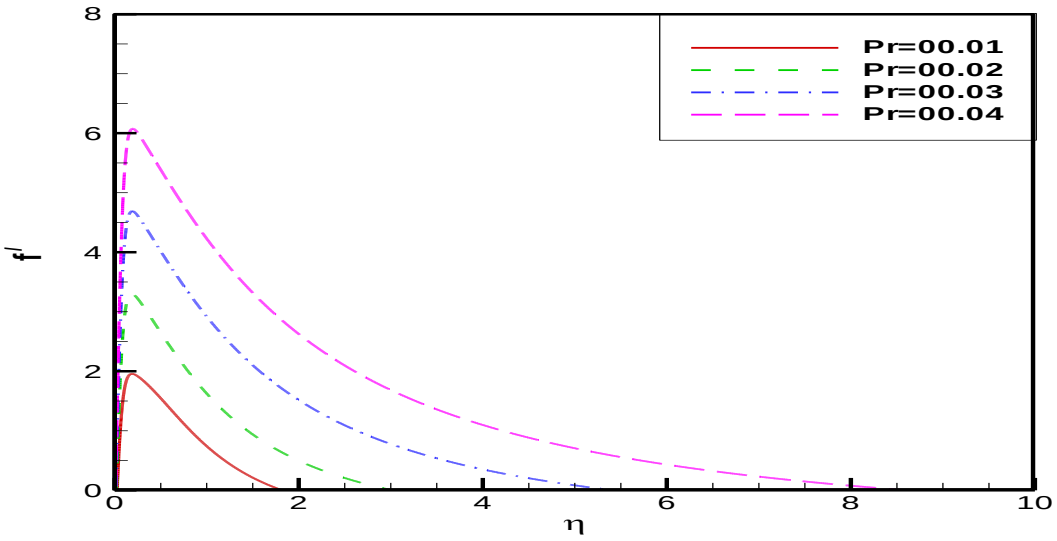

Fig. 3.2: Influence of multiple values on velocity profiles of Prandlt number Pr, when M=00.10, RN=00.00, Bm=00.10, E=00.01, P=00.60, Nt=00.50, Nb=00.50, Db=00.10.

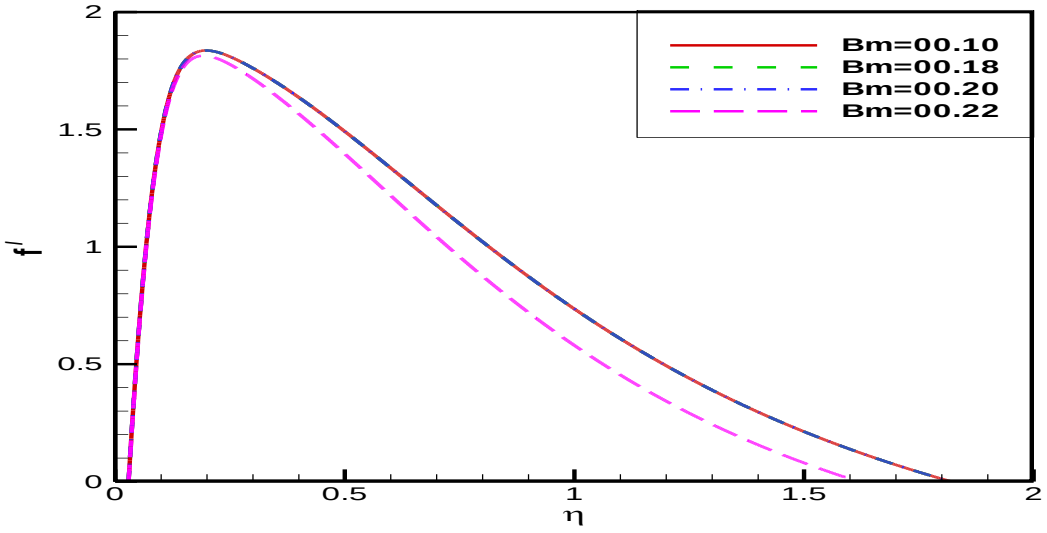

Fig. 3.3: Influence of multiple values of Thermal diffusivity parameter (Bm) on velocity profiles, when Pr=00.01, RN=00.00, M=00.10, E=00.01, P=00.60, Nt=00.50, Nb=00.50, Db=00.10.

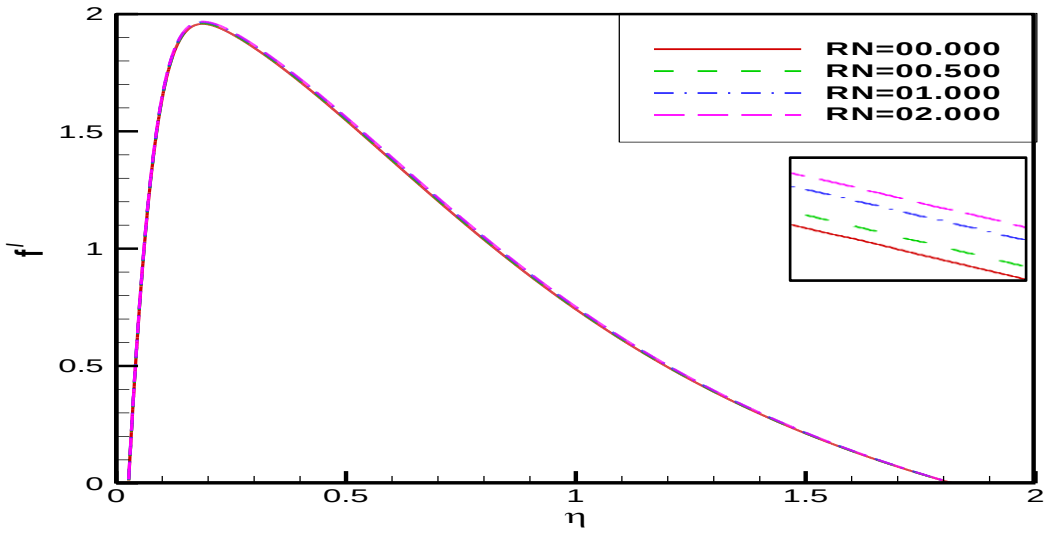

Fig. 3.4: Influence of multiple values of Unsteadiness parameter (RN) on velocity profiles, when Pr=00.01, M=00.10, Bm=00.10, E=00.01, P=00.60, Nt=00.50, Nb=00.50, Db=00.10.

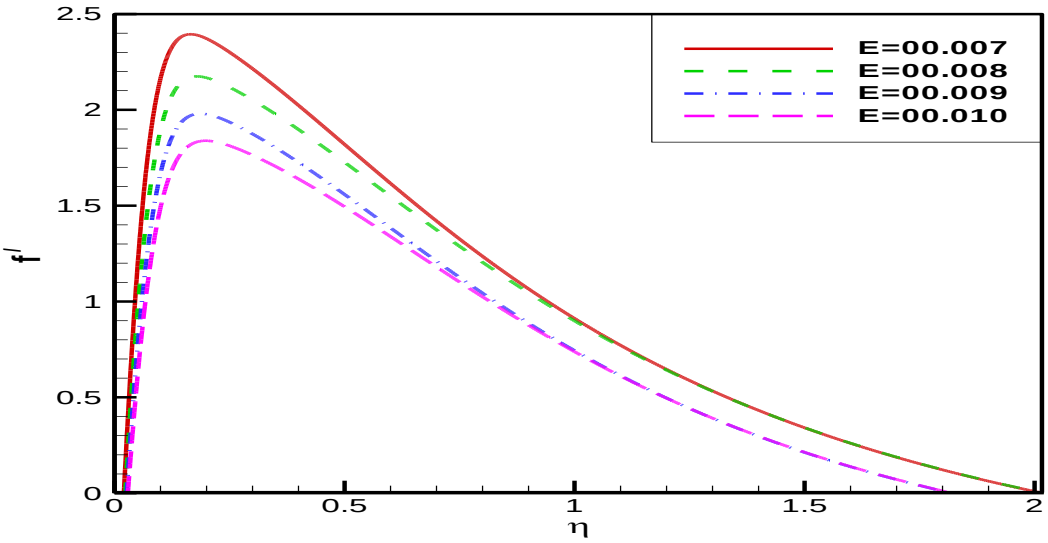

Fig. 3.5: Influence of multiple values of Viscosity of the nanofluid (E) on velocity profiles, when Pr=00.01, RN=00.00, Bm=00.10, M=00.10, P=00.60, Nt=00.50, Nb=00.50, Db=00.10.

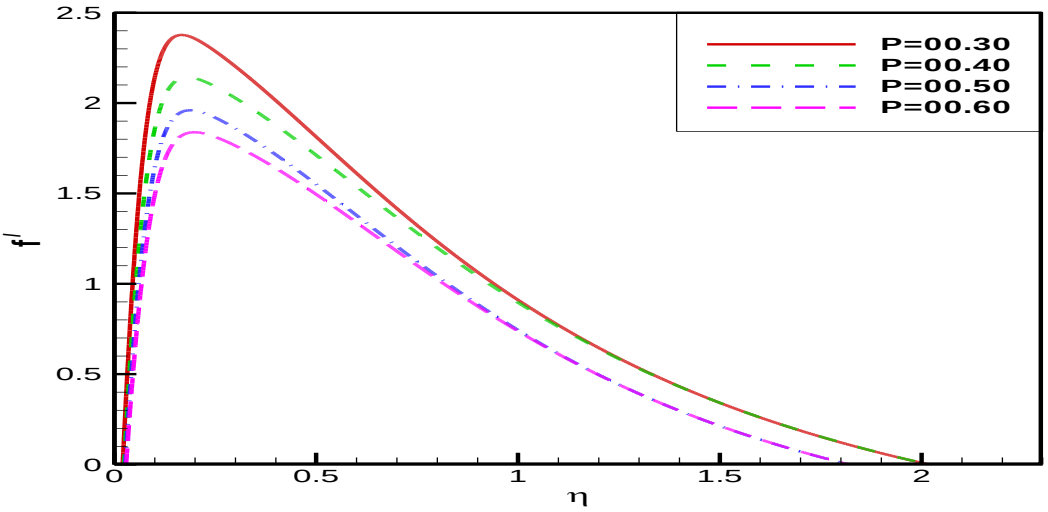

Fig. 3.6: Influence of multiple values of Unsteadiness parameter (P) on velocity profiles, when Pr=00.01, RN=00.00, Bm=00.10, E=00.01, M=00.10, Nt=00.50, Nb=00.50, Db=00.10.

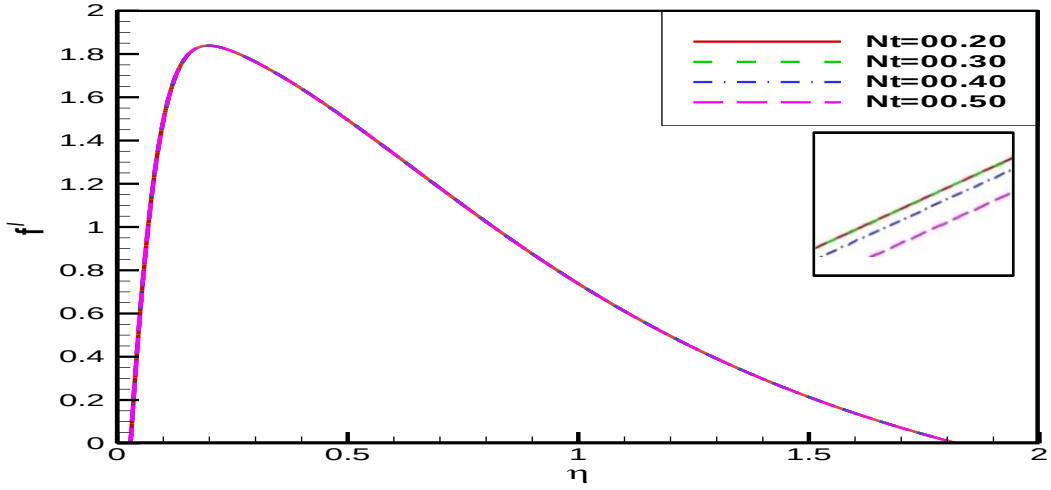

Fig. 3.7: Influence of multiple values of Thermophoresis parameter (Nt) on velocity profiles, when Pr=00.01, RN=00.00, Bm=00.10, E=00.01, P=00.60, M=00.10, Nb=00.50, Db=00.10.

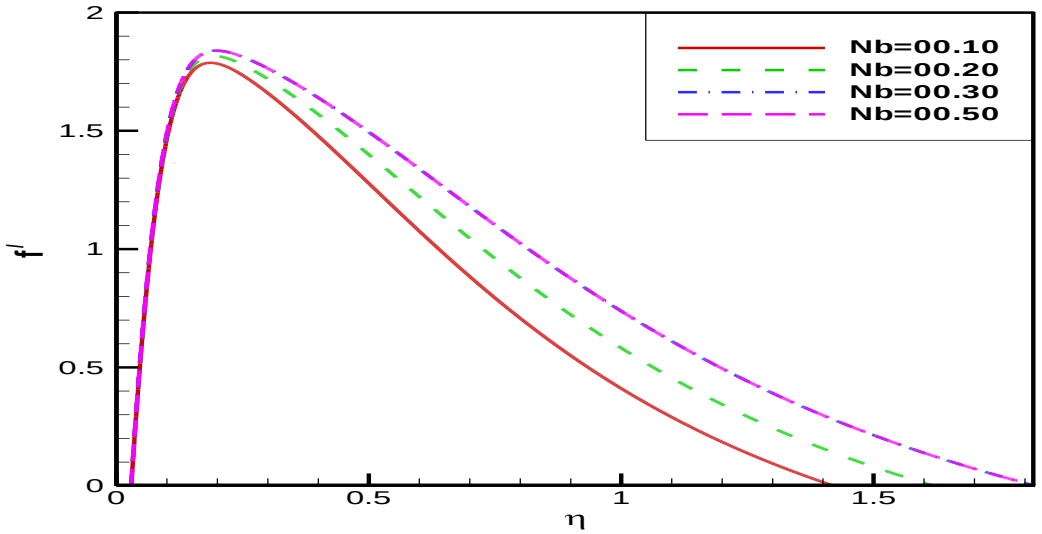

Fig. 3.8: Influence of multiple values of Brownian motion parameter (Nb) on velocity profiles, when Pr=00.01, RN=00.00, Bm=00.10, E=00.01, P=00.60, Nt=00.50, M=00.10, Db=00.10.

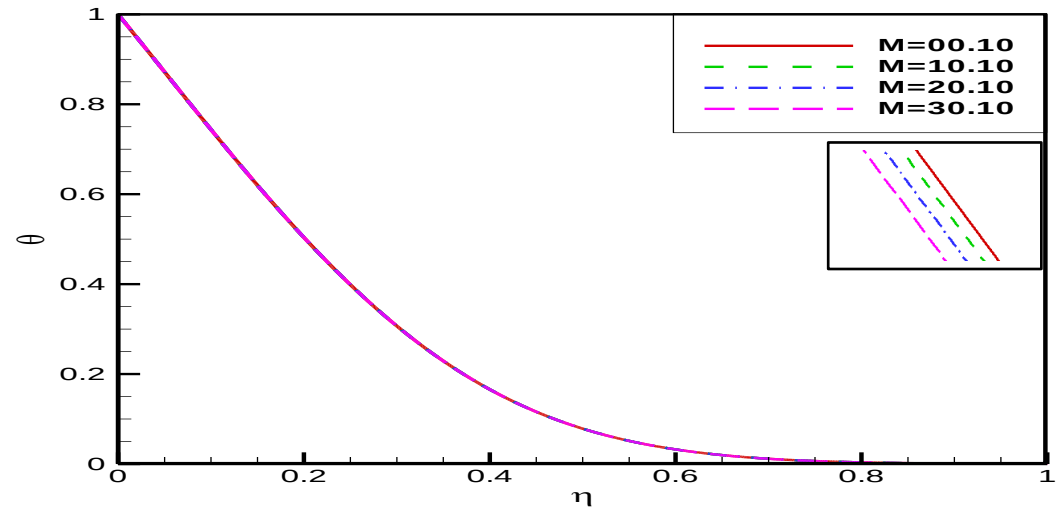

Fig. 3.9: Multiple values' of Magnetic parameter (M) effects on Temperature profiles, when Pr=00.01, RN=00.00, Bm=00.10, E=00.01, P=00.60, Nt=00.50, M=00.10, Db=00.10.

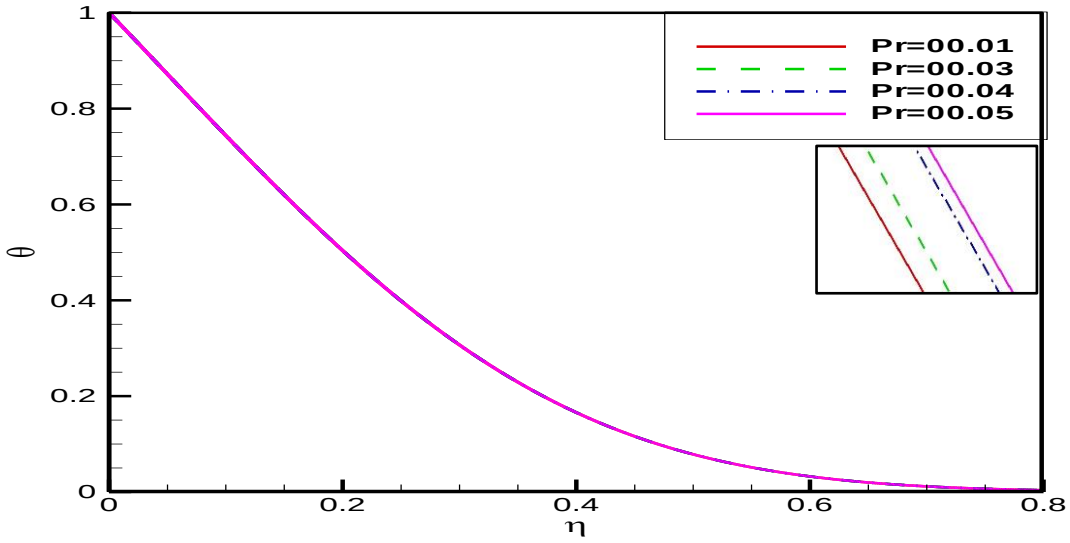

Fig. 3.10: Multiple values' of Prandlt number (Pr) effects on Temperature profiles, when M=00.10, RN=00.00, Bm=00.10, E=00.01, P=00.60, Nt=00.50, Nb=00.50, Db=00.10.

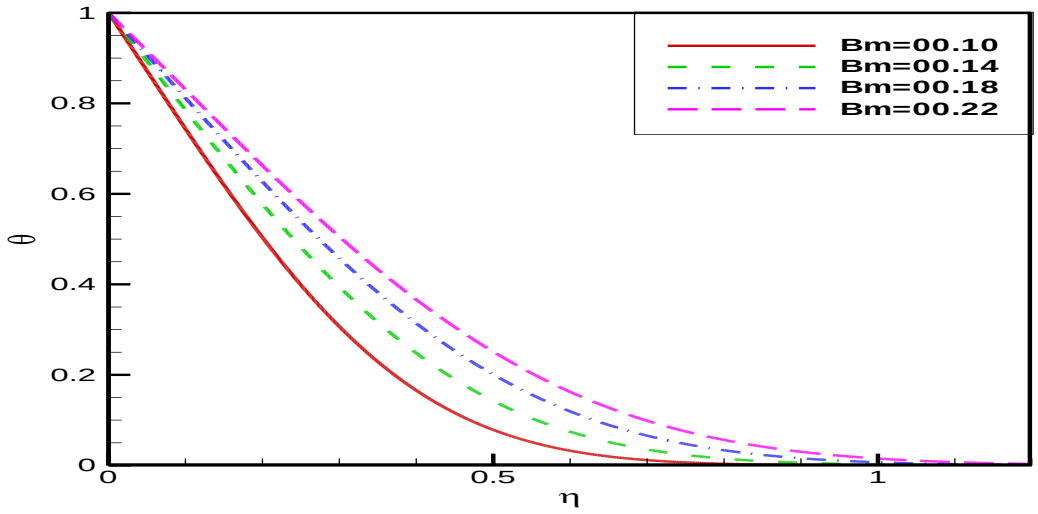

Fig. 3.11: Multiple values' of Thermal diffusivity parameter (Bm) effects on Temperature profiles, when Pr=00.01, RN=00.00, M=00.10, E=00.01, P=00.60, Nt=00.50, Nb=00.50, Db=00.10.

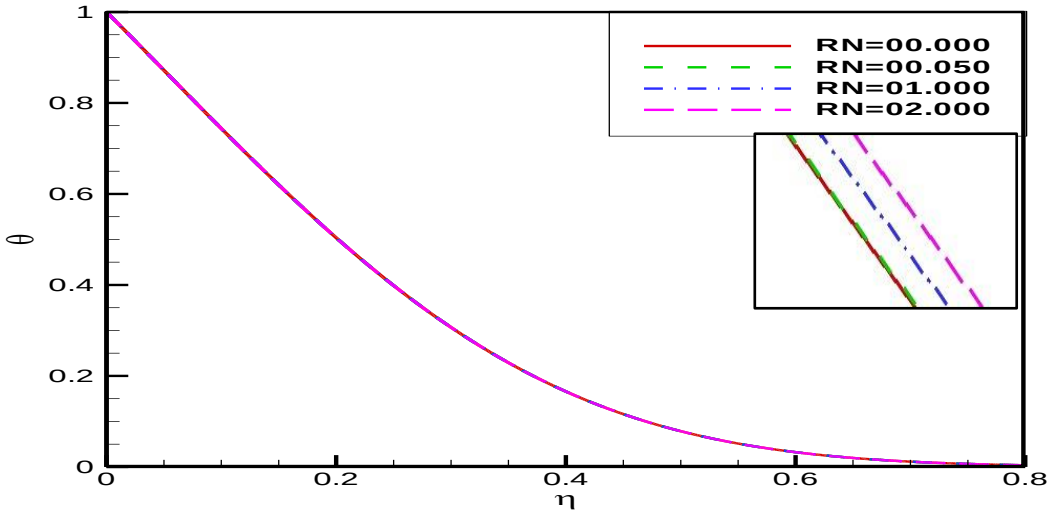

Fig. 3.12: Multiple values' of Unsteadiness parameter (RN) effects on Temperature profiles, when Pr=00.01, M=00.10, Bm=00.10, E=00.01, P=00.60, Nt=00.50, Nb=00.50, Db=00.10.

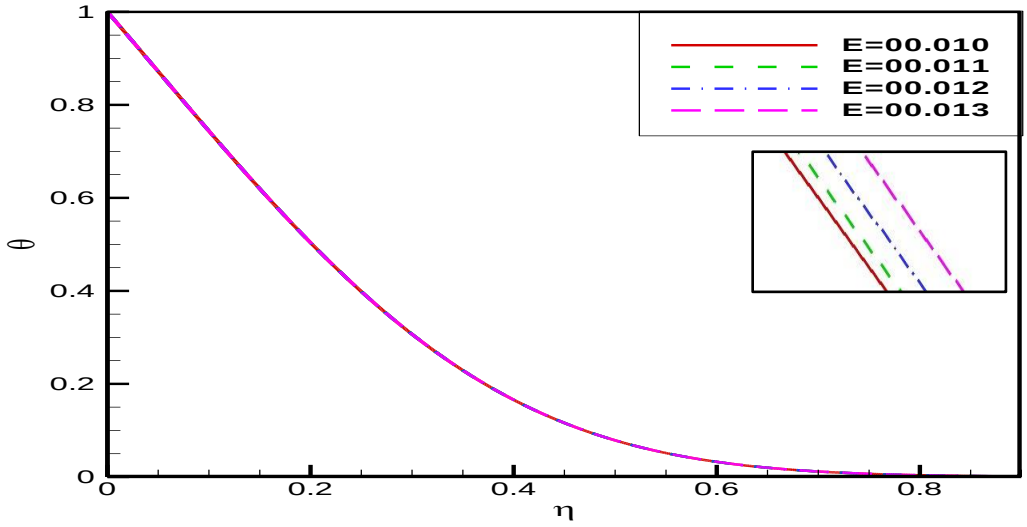

Fig. 3.13: Multiple values' of Viscosity of the nanofluid (E) effects on Temperature profiles, when Pr=00.01, RN=00.00, Bm=00.10, M=00.10, P=00.60, Nt=00.50, Nb=00.50, Db=00.10.

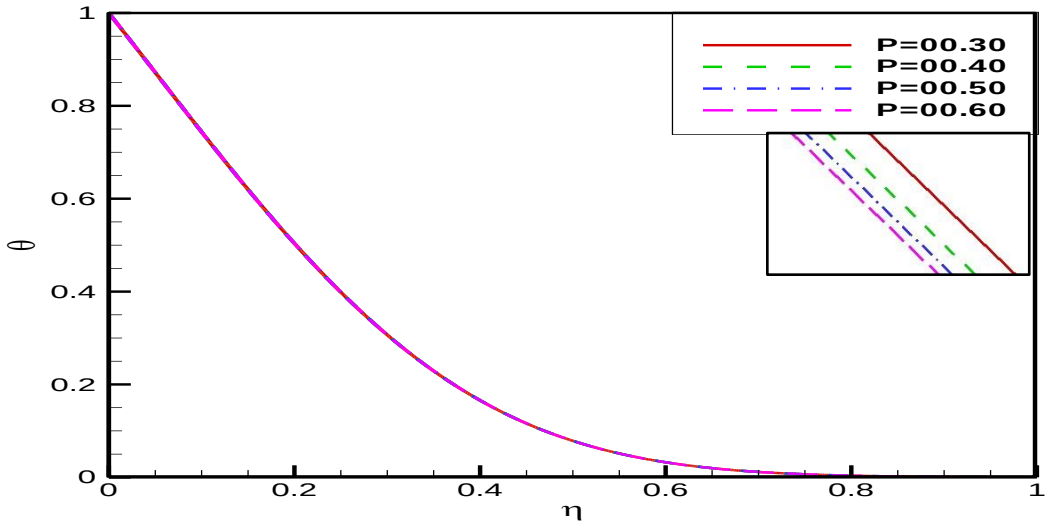

Fig. 3.14: Multiple values' of Unsteadiness parameter (P) effects on Temperature profiles, when Pr=00.01, RN=00.00, Bm=00.10, E=00.01, M=00.10, Nt=00.50, Nb=00.50, Db=00.10.

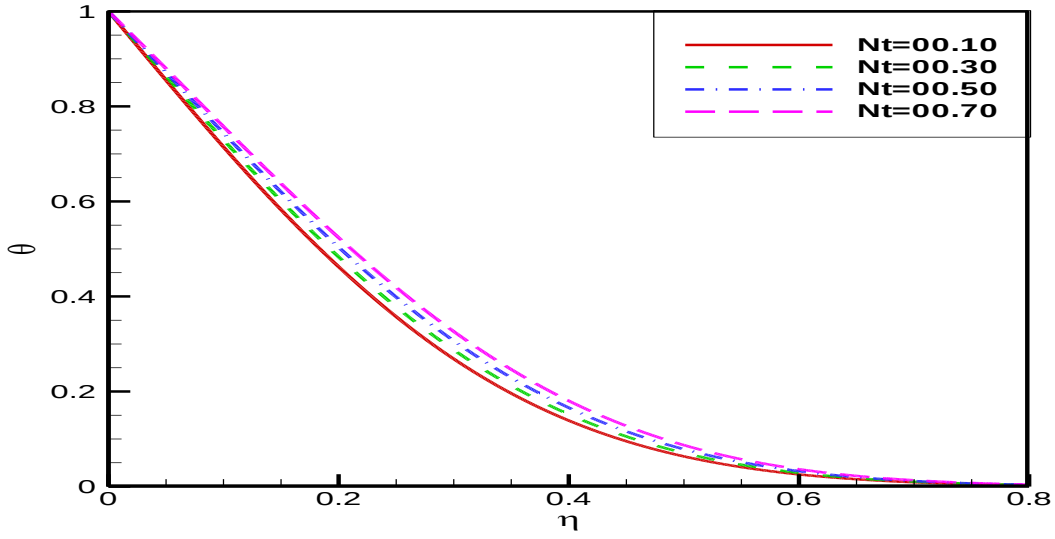

Fig. 3.15: Multiple values' Thermophoresis parameter (Nt) effects on Temperature profiles, when Pr=00.01, RN=00.00, Bm=00.10, E=00.01, P=00.60, Nb=00.50, M=00.10, Db=00.10.

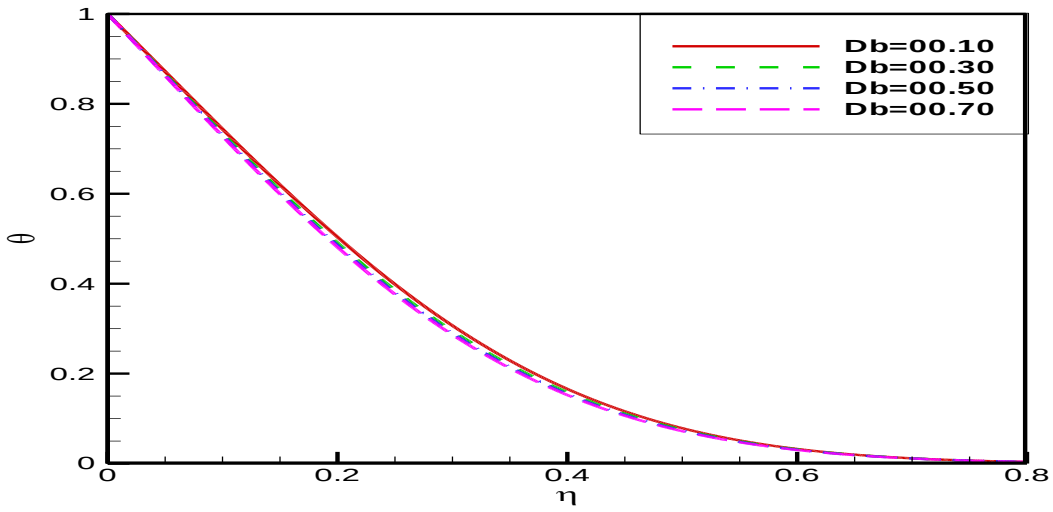

Fig. 3.16: Multiple values' of Brownian diffusion parameter (Db) effects on Temperature profiles, when Pr=00.01, RN=00.00, Bm=00.10, E=00.01, P=00.60, Nt=00.50, Nb=00.10, M=00.10.

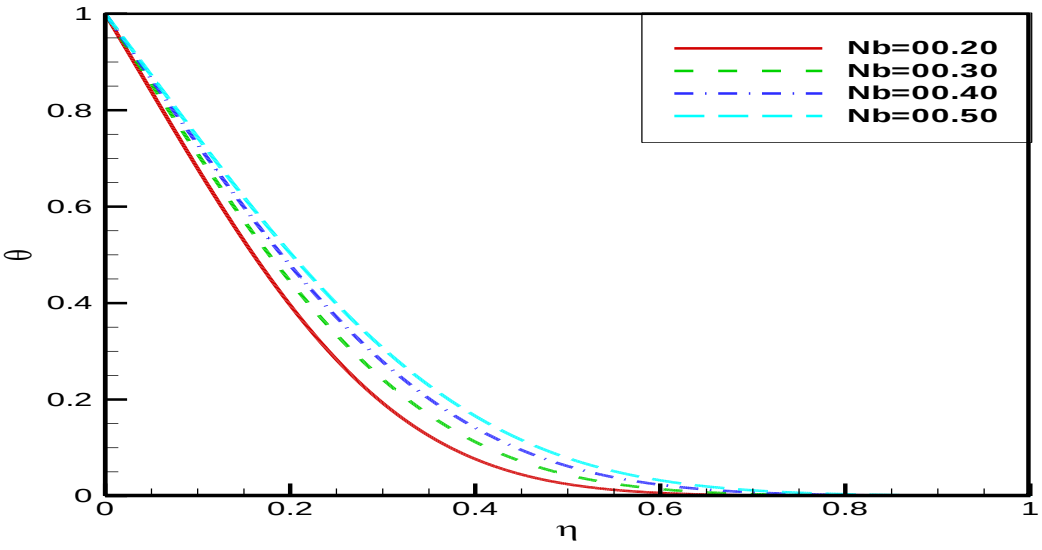

Fig. 3.17: Multiple values' of Brownian motion parameter (Nb) effects on Temperature profiles, when Pr=00.01, RN=00.00, Bm=00.10, E=00.01, P=00.60, Nt=00.50, M=00.10, Db=00.10.

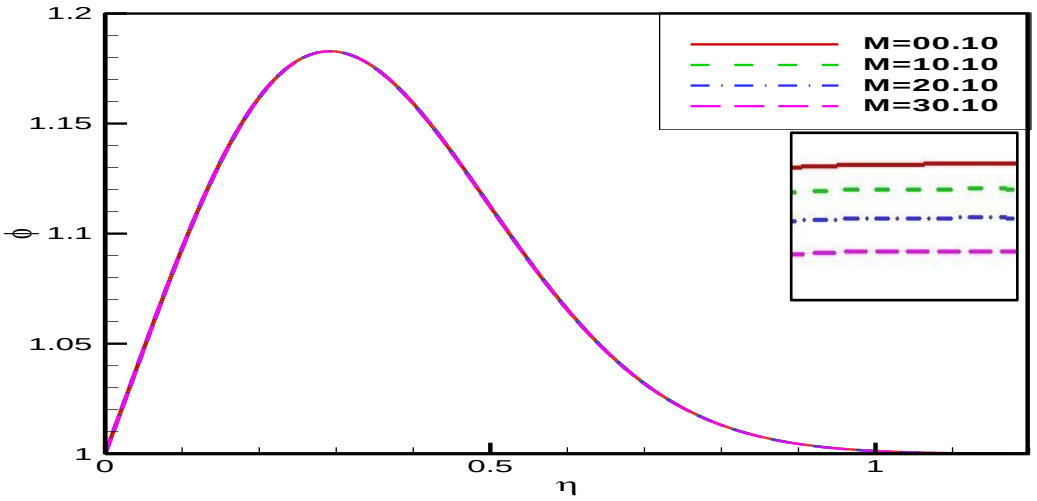

Fig. 3.18: Variations in values' of Magnetic parameter (M) effects on Concentration, when Pr=00.01, RN=00.00, Bm=00.10, E=00.01, P=00.60, Nt=00.50, Nb=00.10, Db=00.10.

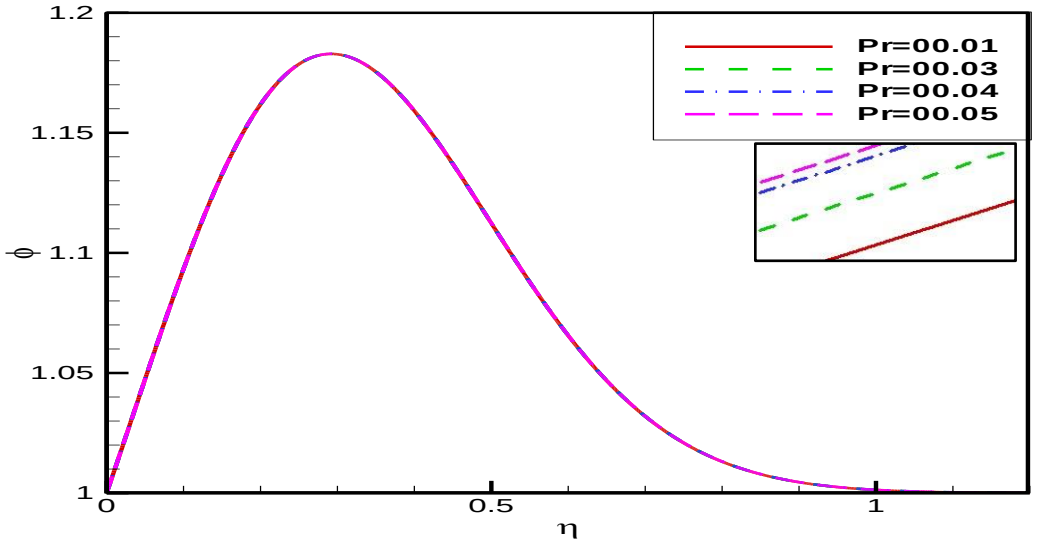

Fig. 3.19: Variations in values' of Prandlt number (Pr) effects on Concentration profiles, when M=00.10, RN=00.00, Bm=00.10, E=00.01, P=00.60, Nt=00.50, Nb=00.10, Db=00.10.

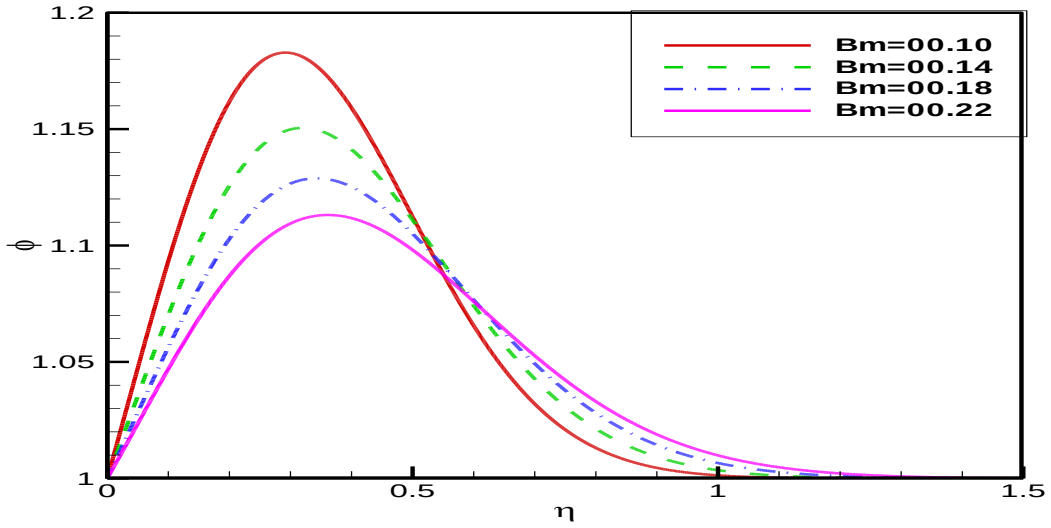

Fig. 3.20: Variations in values' of Thermal diffusivity parameter (Bm) effects on Concentration profiles, when Pr=00.01, RN=00.00, M=00.10, E=00.01, P=00.60, Nt=00.50, Nb=00.50, Db=00.10.

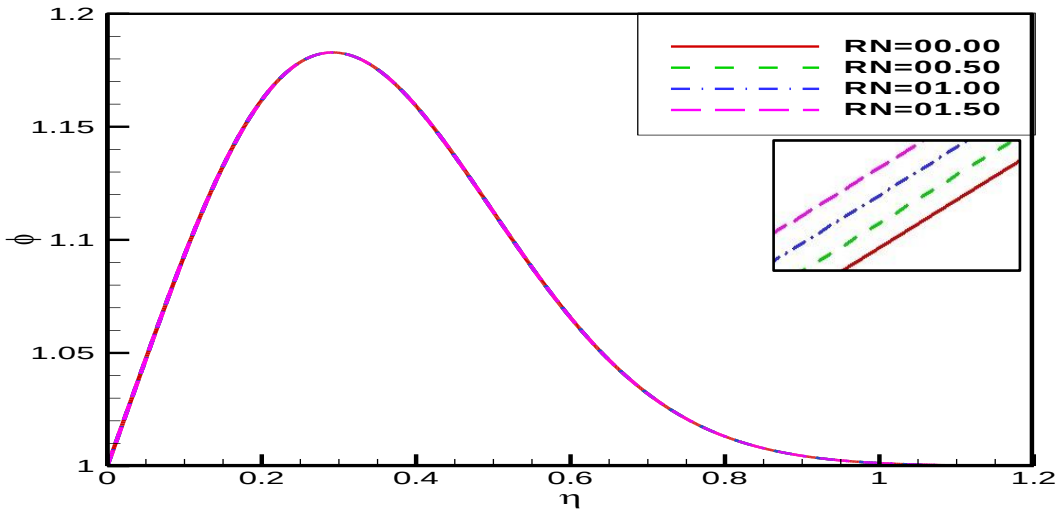

Fig. 3.21: Variations in values' of Unsteadiness parameter (RN) effects on Concentration profiles, when Pr=00.01, M=00.10, Bm=00.10, E=00.01, P=00.60, Nt=00.50, Nb=00.50, Db=00.10.

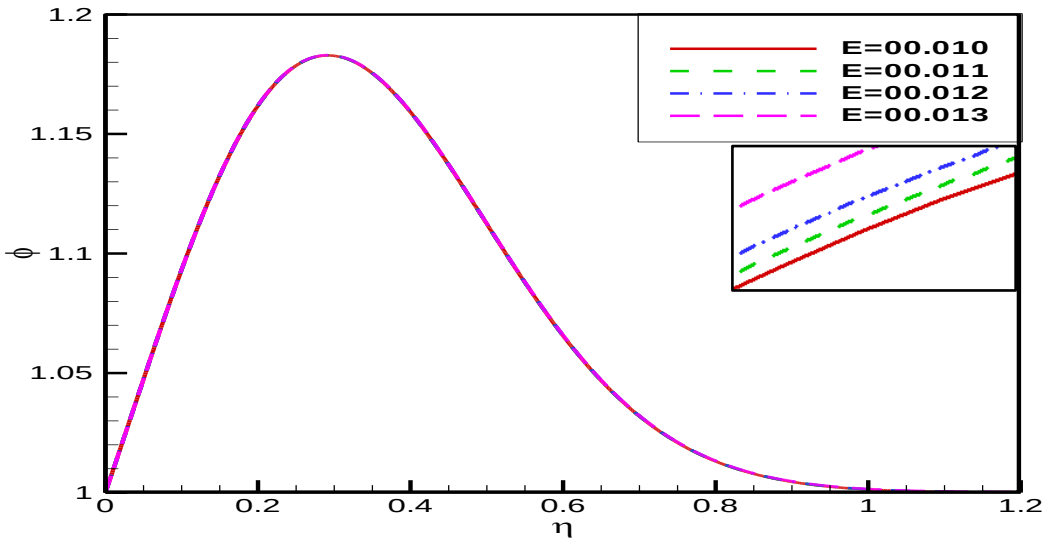

Fig. 3.22: Variations in values' of Viscosity of the nanofluid (E) effects on Concentration profiles, when Pr=00.01, RN=00.00, Bm=00.10, M=00.10, P=00.60, Nt=00.50, Nb=00.50, Db=00.10.

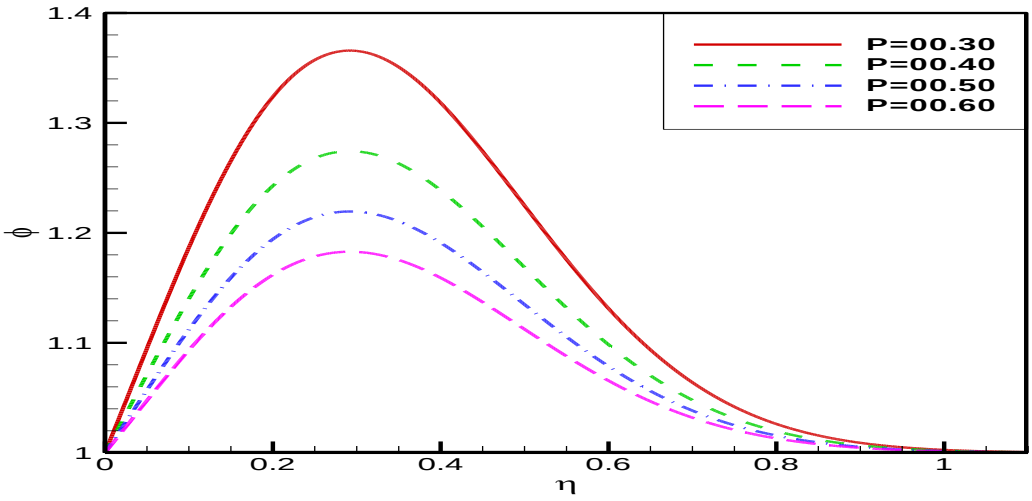

Fig. 3.23: Variations in values' of Unsteadiness parameter (P) effects on Concentration profiles, when Pr=00.01, RN=00.00, Bm=00.10, E=00.01, M=00.10, Nt=00.50, Nb=00.50, Db=00.10.

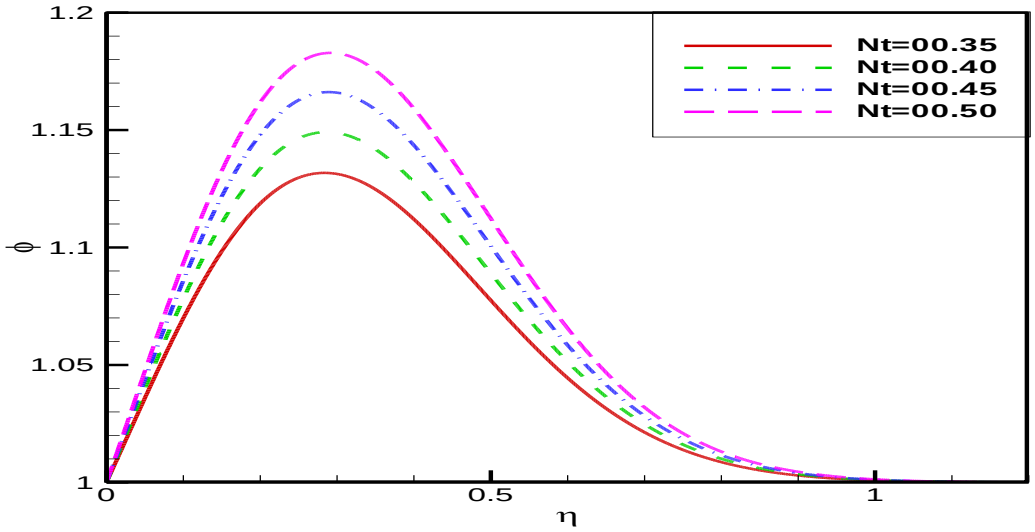

Fig. 3.24: Variations in values' of Thermophoresis parameter (Nt) effects on Concentration profiles, when Pr=00.01, RN=00.00, Bm=00.10, E=00.01, M=00.10, P=00.60, Nb=00.50, Db=00.10.

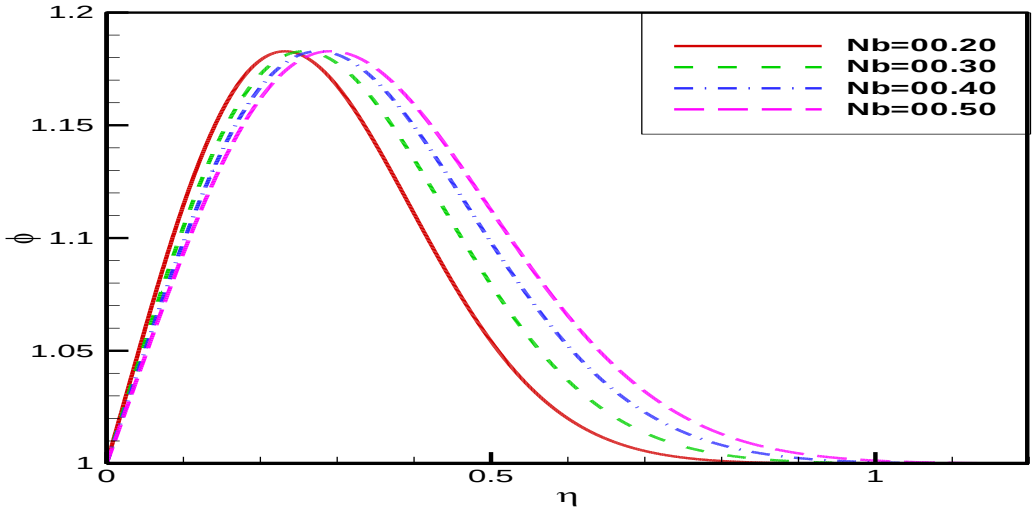

Fig. 3.25: Variations in values' of Brownian motion parameter (Nb) effects on Concentration profiles, when Pr=00.01, RN=00.00, Bm=00.10, E=00.01, M=00.10, Nt=00.50, P=00.60, Db=00.10.

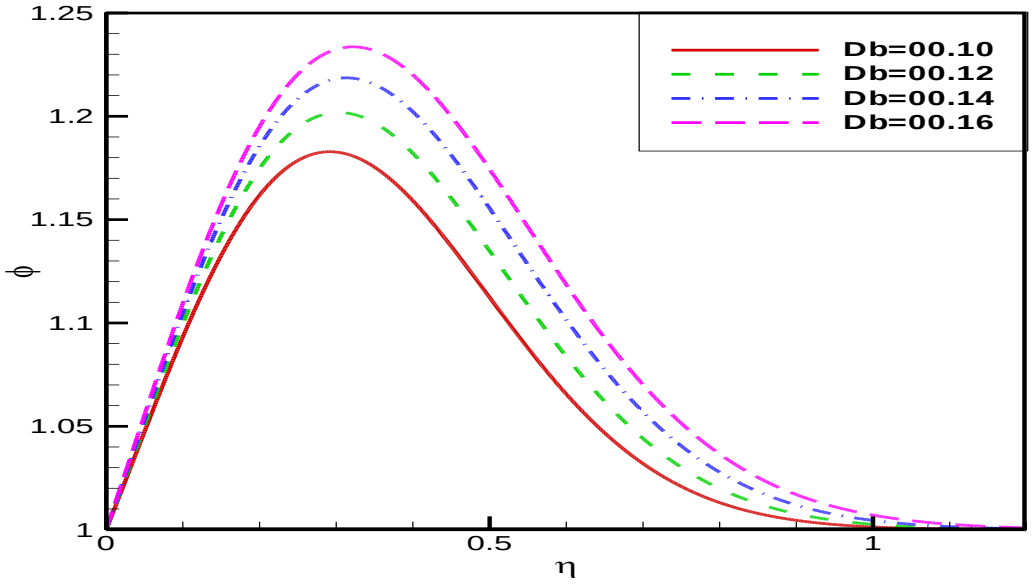

Fig. 3.26: Variations in values' of Brownian diffusion parameter (Db) effects on Concentration profiles, when Pr=00.01, RN=00.00, Bm=00.10, E=00.01, P=00.60, Nt=00.50, Nb=00.50, M=00.10.

Table 3.1 displays the calculated Sherwood number ∅'(0) values, which are contrasted with the published findings of (Aziz et al., 2012; Goyal et al., 2018). There is strong agreement between the results.

Table 3.1. Comparison values of $[\emptyset'(\mathbf{0})]$for, $Pr = 0.01$, $M = 0.10$, $E = 0.01, Nb = 0.50$, $P = 0.60$, $Nt = 0.50$, $Bm = 0.10$, $Db = 0.10, RN = 00.00$.

Nb	(Aziz et al., 2012)	(Goyal et al., 2018)	Present
0.10	0.9954	0.9955	1.1682
0.12	0.9828	0.9830	1.0556
0.14	0.9697	0.9699	0.9826
0.16	0.9559	0.9563	0.9294

The wall heat transfer coefficient θ'(0) and the wall deposition flux ∅'(0), which are determined by the Sherwood and Nusselt number, respectively, are significant physical parameters. The tables are listed below.

Table: 3.2. The Nusselt Number$-\theta'(0)$ and Sherwood number $\emptyset'(0)$ for distinct values of M.

M	$-\boldsymbol{\theta'(0)}$	$\emptyset'(\mathbf{0})$
00.10	2.531766136	0.929411577
10.10	2.531793997	0.929238629
20.10	2.531826324	0.929037880
30.10	2.531863342	0.928807926

Table: 3.3. The Nusselt Number$-\theta'(0)$ and Sherwood number $\emptyset'(0)$ for distinct values of P.

P	$-\boldsymbol{\theta'(0)}$	$\emptyset'(\mathbf{0})$
00.30	2.531711383	1.859074593
00.40	2.531744357	1.394249834
00.50	2.531759663	1,115348500
00.60	2.531766136	0.929411577

Table: 3.4. The Nusselt Number $-\theta'(0)$ and Sherwood number $\emptyset'(0)$ for different values of Nt.

Nt	$-\boldsymbol{\theta'(0)}$	$\emptyset'(\mathbf{0})$
00.10	2.900195525	0.235889973
00.30	2.709396677	0.629696190
00.50	2.531766136	0.929411577
00.70	2.366615155	1.146840653

Table: 3.5. The Nusselt Number $-\theta'(0)$ and Sherwood number $\emptyset'(0)$ for different values of Pr.

Pr	$-\boldsymbol{\theta'(0)}$	$\emptyset'(\mathbf{0})$
00.01	2.531766136	0.929411577
00.03	2.531739440	0.929576792
00.04	2.531727462	0.929651484
00.05	2.531724324	0.919671076

Table: 3.6. The Nusselt Number $-\theta'(0)$ and Sherwood number $\emptyset'(0)$ for different values of RN.

RN	$-\boldsymbol{\theta'(0)}$	$\emptyset'(\mathbf{0})$
00.00	2.531766136	0.929411577
00.50	2.531764902	0.929419242
01.00	2.531763676	0.929426872
00.05	2.531761235	0.929442024

Table: 3.7. The Nusselt Number$-\theta'(0)$ and Sherwood number $\emptyset'(0)$ for different values of E.

E	$-\boldsymbol{\theta'(0)}$	$\boldsymbol{\emptyset'(0)}$
00.010	2.531766136	0.929411577
00.011	2.531732402	0.929621077
00.012	2.531683823	0.929911652
00.013	2.531524251	0.930558870

Table: 3.8. The Nusselt Number$-\theta'(0)$ and Sherwood number $\emptyset'(0)$ for distinct values of Bm.

Bm	$-\boldsymbol{\theta'(0)}$	$\boldsymbol{\emptyset'(0)}$
00.10	2.531766136	0.929411577
00.16	1.96870300	0.612546640
00.18	1.849220574	0.550094704
00.22	1.662691727	0.456685257

Table: 3.9. The Nusselt Number$-\theta'(0)$ and Sherwood number $\emptyset'(0)$ for different values of Nb.

Nb	$-\boldsymbol{\theta'(0)}$	$\boldsymbol{\emptyset'(0)}$
00.20	3.183602364	1.168290074
00.30	2.876696878	1.055684330
00.40	2.677028927	0.982663849
00.50	2.531766136	0.929411577

Table: 3.10. The Nusselt Number$-\theta'(0)$ and Sherwood number $\emptyset'(0)$ for distinct values of Db.

Db	$-\boldsymbol{\theta'(0)}$	$\emptyset'(\mathbf{0})$
00.10	2.531766136	0.929411577
00.12	2.541930314	0.992132628
00.14	2.564808149	1.046003290
00.16	2.578496623	1.093120687

Lastly, Tables 3.2–3.10 present quantitative results illustrating the the consequences of several variables on the Sherwood number and Nusselt number. It is clear from Tables 3.2, 3.3, and 3.4 that the Nusselt number increases while the Sherwood number decreases as the thermophoresis parameter (Nt), unsteadiness parameter (P), and magnetic field parameter (M) expand. Tables 3.5, 3.6, and 3.7 demonstrate how, as the Prandtl number (Pr) increases, the Sherwood number expands and the Nusselt number falls. Unsteadiness parameter (RN), and Viscosity of the nanofluid (E) increase. Tables 3.8 and 3.9 show the fact that as the thermal diffusivity parameter (Bm) and the Brownian motion parameter (Nb) increase, the Sherwood number and the Nusselt number also decrease. Table 3.10 conveys that when the Brownian diffusion parameter (Db) increases, the Sherwood number and the Nusselt number increase concurrently.

3.5 Conclusions

An analytic study of unsteady MHD flow of a Nanofluid for Forced convection over a plate. Brownian diffusion parameter, Brownian motion parameter, viscosity of the nanofluid, Prandtl number, magnetic field parameter, thermal diffusivity parameter, unsteadiness parameter, and thermophoresis parameter, Nusselt number, and Sherwood number are among the physical characteristics that are analyzed in the analysis. Tables and graphs have been utilized for presenting the numerical results. The particular findings of this investigation can be expressed up as follows:

- Fluid velocity, temperature profiles, concentration profiles, and the magnetic field parameter M all decrease as they increase. The fluid's velocity is retarded by the magnetic field.
- The profiles of temperature, concentration, and velocity increase with the increase in Prandtl number and unsteadiness parameter.
- When temperature and concentration profiles increase, the viscosity of the nanofluid and the thermophoresis parameter rise as well, but velocity profiles fall.
- The thermal diffusivity parameter increases with a decrease in velocity profiles and concentration profiles, but temperature profiles increase.
- As the thermophoresis, unsteadiness, and magnetic field parameters improve, the Sherwood number decreases and the Nusselt number increases.
- If the nanofluid's viscosity and Prandtl number both increase, the Sherwood number increases and the Nusselt number falls.

- The Sherwood number and Nusselt number decrease in together with increases in the Brownian motion parameter (Nb) and thermal diffusivity parameter (Bm).

Chapter 4

Concluding Remarks and Future Works

4.1 Concluding Remarks

This study investigates the unsteady magnetohydrodynamic (MHD) boundary layer flow of a nanofluid for combined free and forced convection around an inclined plate using similarity solutions. The governing nonlinear partial differential equations are transformed into a system of ordinary differential equations via similarity transformations. These equations are then solved numerically using the Nachtsheim-Swigert iteration technique implemented in FORTRAN software. The effects of various dimensionless parameters on the temperature, velocity, and concentration gradients are presented and analyzed from a physical perspective in tabular format. The key findings are summarized as follows:

I. The Nachtsheim-Swigert iteration technique was employed to obtain numerical solutions, which are presented graphically.
II. An increase in the Brownian diffusion coefficient leads to a decrease in fluid temperature and an increase in fluid velocity and concentration. Conversely, increasing the thermal diffusivity parameter results in a rise in fluid temperature and a decrease in both velocity and concentration.
III. The thermophoresis parameter exhibits a positive influence on all three profiles, leading to an increase in fluid velocity, temperature, and concentration.

IV. The effect of the Brownian motion parameter on the temperature, concentration, and velocity profiles mirrors that of the thermophoresis parameter.

V. The fluid velocity and concentration decline while the fluid temperature stays mostly constant as a result of the increase in the unsteadiness parameter.

VI. Through the increased viscosity of the nanofluid, the fluid velocity increased while the fluid temperature and concentration did not significantly change. Angle has the same influence on velocity, temperature, and concentration profiles as the thermophoresis parameter.

VII. The fluid velocity increased while the fluid temperature showed no significant variation, and the fluid concentration increment was very small because of the buoyancy ratio parameter's increase.

VIII. The fluid temperature increased very little as a result of the increase in the magnetic parameter, and the fluid velocity decreased while the fluid concentration did not change significantly.

IX. The Sherwood number, Nusselt number, and Skin-friction coefficient drop as the thermal and magnetic diffusivity parameters increase.

X. As the consequence of an increase in the Bouyancy-ratio parameter, the viscosity of the nanofluid, and the skin friction coefficient, the Brownian motion parameter, and the Sherwood and Nusselt numbers go down.

XI. The skin friction coefficient lowers as the Prandlt number increases, but the Sherwood and Nusselt numbers remain fixed.

XII. The thermal diffusivity parameter increases with a decrease in velocity profiles and concentration profiles, but temperature profiles increase.

XIII. As can be the thermophoresis parameter increases, while the Nusselt number decreases, the skin friction coefficient and Sherwood number increase.

4.2 Future works based on the thesis

The current studies may be extended further

(a) The author has considered an unsteady two-dimensional MHD nanofluid flow past an inclined plate. This work can be extended to an unsteady three-dimensional MHD nanofluid flow past an inclined plate.

(b) The author has considered free and forced convection boundary layer flow on an inclined plate in this thesis. One can consider mixed convection boundary layer flow an inclined plate.

ABBAS, A., & ASHRAF, M. (2020). Combined Effects of Variable Viscosity and Thermophoretic Transportation on Mixed Convection Flow Around the Surface of a Sphere. *Thermal Science*, *24*(6 PART B), 4089–4101. doi: 10.2298/TSC1190518137A

Abin John*, Jithin Thomas*, Jose S Kattukaran*, Relno Baby M*, C. (2014). Solar Powered Heat Control System for Cars. *Abin John et Al Int Journal of Engineering Research and Applications*, 49–54.

Adem, G. A. (2023). Influence of inclined magnetic field and cross diffusion on transient forced convective heat and mass transfer flow along a porous wedge with variable Prandtl number. *Numerical Heat Transfer, Part B: Fundamentals*, 1–22. doi: 10.1080/10407790.2023.2267174

Alam, M. S. (2013). A Similarity Approach for an Unsteady Two-dimensional Forced Convective Heat Transfer Boundary Layer Flow along a Convergent Channel. *Thammasat International Journal of Science and Technology*, *18*(1), 1–9.

Alam, M. S., Rahman, M. M., & Sattar, M. A. (2009). On the effectiveness of viscous dissipation and Joule heating on steady Magnetohydrodynamic heat and mass transfer flow over an inclined radiate isothermal permeable surface in the presence of thermophoresis. *Communications in Nonlinear Science and Numerical Simulation*, *14*(5), 2132–2143. doi: 10.1016/j.cnsns.2008.06.008

Aldoss, T. K., Al-Nimr, M. A., Jarrah, M. A., & Al-Sha'er, B. J. (1995). MAGNETOHYDRODYNAMIC MIXED CONVECTION FROM A VERTICAL PLATE EMBEDDED IN A POROUS MEDIUM. *Numerical Heat Transfer, Part A: Applications*, *28*(5), 635–645. doi: 10.1080/10407789508913766

ALFVÉN, H. (1942). Existence of Electromagnetic-Hydrodynamic Waves. *Nature*, *150*(3805), 405–406. doi: 10.1038/150405d0

Ali, F., Khan, I., Samiulhaq, & Shafie, S. (2013). Conjugate Effects of Heat and Mass Transfer on MHD Free Convection Flow over an Inclined Plate Embedded in a Porous Medium. *PLoS ONE*, *8*(6). doi: 10.1371/journal.pone.0065223

Ali, M. Y., Uddin, M. J., Uddin, M. N., & Zahed, N. M. R. (2016). Similarity Solutions for Unsteady Hydromagnetic Free Convection Boundary Layer Flow over Flat Plates with Thermophoresis. *Journal of Scientific Research*, *8*(3), 287–307. doi: 10.3329/jsr.v8i3.27347

Ali, M. Y., Zahed, N. M. R., Uddin, M. N., & Uddin, M. J. (2016). Similarity Solutions for an Internal Heat Generation, Thermal Radiation and Free Convection Unsteady Boundary Layer Flow over a Vertical Plate. *Journal of Scientific Research*, *8*(3), 341–353. doi: 10.3329/jsr.v8i3.27851

Ali, Md. Yeakub, Uddin, M. N., Uddin, M. J., & Zahed, N. M. R. (2015). Similarity Solutions of Unsteady Convective Boundary Layer Flow along Isothermal Vertical Plate with Porous Medium. *Open Journal of Fluid Dynamics*, *05*(04), 391–406. doi: 10.4236/ojfd.2015.54038

Ali, N., Teixeira, J. A., & Addali, A. (2018). A Review on Nanofluids: Fabrication, Stability, and Thermophysical Properties. *Journal of Nanomaterials*, *2018*. doi: 10.1155/2018/6978130

Anghel, M., Hossain, M.A., Zeb, S. and Pop, I. (2001). Combined heat and mass transfer by free convection past an inclined flat plate. *Applied Mechanics and Engineering*, 473–487.

Aziz, A., & Khan, W. A. (2012). Natural convective boundary layer flow of a nanofluid past a convectively heated vertical plate. *International Journal of Thermal Sciences*, *52*, 83–90. doi: 10.1016/j.ijthermalsci.2011.10.001

Bazukyan, I.L., Rostomyan, A.V., Hovhannisyan, A.G., Aleksanyan, T.M., Hakobyan, L.L., Dallakyan, A.M. and Haertlé, T. (2022). The effects of ultraviolet, gamma-and X-ray irradiation on the growth, antibacterial activity and radio-protective of Lactobacill. *Oxfod Academe*, *1151–1159*.

Çengel, Y. A., Cimbala, J. M., & Turner, R. H. (2017). Fundamentals of fluid-thermal sciences. In Fundamentals of Thermal Fluid Sciences.

Chamkha, A. J., & Aly, A. M. (2010). MHD FREE CONVECTION FLOW OF A NANOFLUID PAST A VERTICAL PLATE IN THE PRESENCE OF HEAT GENERATION OR ABSORPTION EFFECTS. *Chemical Engineering Communications*, *198*(3), 425–441. doi: 10.1080/00986445.2010.520232

Chamkha, Ali J. (2004). Unsteady MHD convective heat and mass transfer past a semi-infinite vertical permeable moving plate with heat absorption. *International Journal of Engineering Science*, *42*(2), 217–230. doi: 10.1016/S0020-7225(03)00285-4

Chamkha, Ali J., & Khaled, A.-R. A. (2001). Similarity solutions for hydromagnetic simultaneous heat and mass transfer by natural convection from an inclined plate with internal heat generation or absorption. *Heat and Mass Transfer*, *37*(2–3), 117–123. doi: 10.1007/s002310000131

Chamkha, Ali J., & Khaled, A. R. A. (2000). Similarity solutions for hydromagnetic mixed convection heat and mass transfer for Hiemenz flow through porous media. *International Journal of Numerical Methods for Heat and Fluid Flow*, *10*(1), 94–115. doi: 10.1108/09615530010306939

Chen, C.-H. (2004). Heat and mass transfer in MHD flow by natural convection from a permeable, inclined surface with variable wall temperature and concentration. *Acta Mechanica*, *172*(3–4), 219–235. doi: 10.1007/s00707-004-0155-5

Chiou, M. C. (1998). Effect of thermophoresis on submicron particle deposition from a forced laminar boundary layer flow onto an isothermal moving plate. *Acta Mechanica*, 219–229.

Chiou, M. C., & Cleaver, J. W. (1996). Effect of thermophoresis on sub-micron particle deposition from a laminar forced convection boundary layer flow onto an isothermal cylinder. *Journal of Aerosol Science*, *27*(8), 1155–1167. doi: 10.1016/0021-8502(96)00045-6

Choi, S.U. and Eastman, J. . (1995). Enhancing thermal conductivity of fluids with nanoparticles. *U.S. Department of Energy*, 951135–29.

Choi, S. U. (2008). Nanofluids: A new field of scientific research and innovative applications. Heat transfer engineering. *Heat Transfer Enginneering*, 429–431. Retrieved from https://www.researchgate.net/publication/271995654_Nanofluids_A_New_Field_of_Scientific_Research_and_Innovative_Applications

Dai, W. J., Gan, Y. X., & Hanaor, D. (2016). Effective Thermal Conductivity of Submicron Powders: A Numerical Study. *Applied Mechanics and Materials*, *846*, 500–505. doi: 10.4028/www.scientific.net/AMM.846.500

Goyal, M., & Bhargava, R. (2013). Numerical Solution of MHD Viscoelastic Nanofluid Flow over a Stretching Sheet with Partial Slip and Heat Source/Sink. *ISRN Nanotechnology*, *2013*, 1–11. doi: 10.1155/2013/931021

Goyal, M., & Bhargava, R. (2014a). Boundary layer flow and heat transfer of viscoelastic nanofluids past a stretching sheet with partial slip conditions. *Applied Nanoscience (Switzerland)*, *4*(6), 761–767. doi: 10.1007/s13204-013-0254-5

Goyal, M., & Bhargava, R. (2014b). Numerical study of thermodiffusion effects on boundary layer flow of nanofluids over a power law stretching sheet. *Microfluidics and Nanofluidics*, *17*(3), 591–604. doi: 10.1007/s10404-013-1326-2

Goyal, M., & Bhargava, R. (2018). Simulation of Natural Convective Boundary Layer Flow of a Nanofluid Past a Convectively Heated Inclined Plate in the Presence of Magnetic Field. *International Journal of Applied and Computational Mathematics*, *4*(2), 1–24. doi: 10.1007/s40819-018-0483-0

Haile, E. and Shankar, B. (2015). Boundary-layer flow of nanofluids over a moving surface in the presence of thermal radiation, viscous dissipation and chemical reaction. Applications and Applied Mathematics. *An International Journal*, P 21.

Hamad, M. A. A., & Pop, I. (2011). Unsteady MHD free convection flow past a vertical permeable flat plate in a rotating frame of reference with constant heat source in a nanofluid. *Heat and Mass Transfer/Waerme- Und Stoffuebertragung*, *47*(12), 1517–1524. doi: 10.1007/s00231-011-0816-6

Hamad, M. A. A., Pop, I., & Md Ismail, A. I. (2011). Magnetic field effects on free convection flow of a nanofluid past a vertical semi-infinite flat plate. *Nonlinear Analysis: Real World Applications*, *12*(3), 1338–1346. doi: 10.1016/j.nonrwa.2010.09.014

Hed, G. and Bellander, R. (2006). Mathematical modelling of PCM air heat exchanger. Energy and Buildings. *Elsevier*, *82–89*.

Hetnarski, R.B., Eslami, M.R. and Gladwell, G. M. L. (2009). Thermal stresses: advanced theory and applications. *Springer*, 227–231.

Hossain, M. A., & Munir, M. S. (2000). Mixed convection flow from a vertical flat plate with temperature dependent viscosity. *International Journal of Thermal Sciences*, *39*(2), 173–183. doi: 10.1016/S1290-0729(00)00237-4

Ibrahim, S. M., & Bhashar Reddy, N. (2013). Similarity Solution of Heat and Mass Transfer for Natural Convection over a Moving Vertical Plate with Internal Heat Generation and a Convective Boundary Condition in the Presence of Thermal Radiation, Viscous Dissipation, and Chemical Reaction. *ISRN Thermodynamics*, *2013*, 1–10. doi: 10.1155/2013/790604

Ibrahim, W., & Makinde, O. D. (2014). Double-Diffusive in Mixed Convection and MHD Stagnation Point Flow of Nanofluid Over a Stretching Sheet. *Journal of Nanofluids*, *4*(1), 28–37. doi: 10.1166/jon.2015.1129

Ilias, M. R., Ismail, N. S. aidah, Raji, N. H. A., Rawi, N. A., & Shafie, S. (2020). Unsteady aligned mhd boundary layer flow and heat transfer of a magnetic nanofluids past an inclined plate. *International Journal of Mechanical Engineering and Robotics Research*, *9*(2), 197–206. doi: 10.18178/ijmerr.9.2.197-206

Johnson, C. H., & Ping, C. (1978). Possible similarity solutions for free convection boundary layers adjacent to flat plates in porous media. *International Journal of Heat and Mass Transfer*, *21*(6), 709–718. doi: 10.1016/0017-9310(78)90032-7

Khan, W. A., Uddin, M. J., & Ismail, A. I. M. (2012). Similarity solutions of MHD mixed convection flow with variable reactive index, magnetic field, and velocity slip near a moving horizontal plate: A group theory approach. *Mathematical Problems in Engineering*, *2012*. doi: 10.1155/2012/183029

Kim, Y. J. (2000). Unsteady MHD convective heat transfer past a semi-infinite vertical porous moving plate with variable suction. *International Journal of Engineering Science*, *38*(8), 833–845. doi: 10.1016/S0020-7225(99)00063-4

Kirkwood, P.E. and Parker-Gibson, N. T. (2013). *Informing chemical engineering decisions with data, research, and government resources*. Gibson: Morgan & Claypool Publishers.

Kumari, M., Slaouti, A., Takhar, H.S., Nakamura, S. and Nath, G. (1996). Unsteady free convection flow over a continuous moving vertical surface. *Acta Mechanica*, 75–82.

Kuznetsov, A. V., & Nield, D. A. (2010). Natural convective boundary-layer flow of a nanofluid past a vertical plate. *International Journal of Thermal Sciences*, *49*(2), 243–247. doi: 10.1016/j.ijthermalsci.2009.07.015

Li, L., Zhang, Y., Ma, H. and Yang, M. (2008). An investigation of molecular layering at the liquid-solid interface in nanofluids by molecular dynamics simulation. Physics Letters A. *Elsevier*, 4541–4544. Retrieved from https://www.researchgate.net/publication/243259040_An_investigation_of_molecular_layering_at_the_liquid-solid_interface_in_nanofluids_by_molecular_dynamics_simulation

Mosallanezhad, S., Rahimpour, H. R., & Rahimpour, M. R. (2024). Acid gases properties and characteristics in companion with natural gas. In Advances in Natural Gas: Formation, Processing, and Applications. Volume 2: Natural Gas Sweetening (pp. 75–88). Elsevier. doi: 10.1016/B978-0-443-19217-3.00015-5

Mukhopadhyay, S. (2009). Effect of thermal radiation on unsteady mixed convection flow and heat transfer over a porous stretching surface in porous medium. *International Journal of Heat and Mass Transfer*, *52*(13–14), 3261–3265. doi: 10.1016/j.ijheatmasstransfer.2008.12.029

Mustafa, M., Mushtaq, A., Hayat, T., & Ahmad, B. (2014). Nonlinear radiation heat transfer effects in the natural convective boundary layer flow of nanofluid past a vertical plate: A numerical study. *PLoS ONE*, *9*(9). doi: 10.1371/journal.pone.0103946

Nandy, S. K., Sidui, S., & Mahapatra, T. R. (2014). Unsteady MHD boundary-layer flow and heat transfer of nanofluid over a permeable shrinking sheet in the presence of thermal radiation. *Alexandria Engineering Journal*, *53*(4), 929–937. doi: 10.1016/j.aej.2014.09.001

Narahari, M., Akilu, S. and Jaafar, A. (2013). Free convection flow of a nanofluid past an isothermal inclined plate. *Applied Mechanics and Materials*, 129–133.

Nasrin, R., Parvin, S., & Alim, M. A. (2013). Effect of Prandtl number on free convection in a solar collector filled with nanofluid. *Procedia Engineering*, *56*(December 2013), 54–62. doi: 10.1016/j.proeng.2013.03.088

Noor, N. F. M., Abbasbandy, S., & Hashim, I. (2012). Heat and mass transfer of thermophoretic MHD flow over an inclined radiate isothermal permeable surface in the presence of heat source/sink. *International Journal of Heat and Mass Transfer*, *55*(7–8), 2122–2128. doi: 10.1016/j.ijheatmasstransfer.2011.12.015

Rahman, A., Alam, M. and Uddin, M. (2016). Influence of magnetic field and thermophoresis on transient forced convective heat and mass transfer flow along a porous wedge with variable thermal conductive and variable thermal conductivity and variable Prandt. *Int. J. of Advances in Applied Mathematics and Mechanics,* 49–64.

Rahman, A.M., Alam, M.S. and Chowdhury, M. . (2021). Thermophoresis particle deposition on unsteady two-dimensional forced convective heat and mass transfer flow along a wedge with variable viscosity and variable Prandtl number. *International Communication*, 541–550.

Rahman, A.T.M.M., Alam, M.S. and Chowdhury, M. K. (2012). Local similarity solutions for unsteady two-dimensional forced convective heat and mass transfer flow along a wedge with thermophoresis. *Int. J. App. Math. Mech*, 86–112.

Rana, P., & Bhargava, R. (2012). Flow and heat transfer of a nanofluid over a nonlinearly stretching sheet: A numerical study. *Communications in Nonlinear Science and Numerical Simulation*, *17*(1), 212–226. doi: 10.1016/j.cnsns.2011.05.009

Roşca, N. C., Roşca, A. V., Groşan, T., & Pop, I. (2014). Mixed convection boundary layer flow past a vertical flat plate embedded in a non-Darcy porous medium saturated by a nanofluid. *International Journal of Numerical Methods for Heat and Fluid Flow*, *24*(5), 970–987. doi: 10.1108/HFF-09-2012-0199

Seddeek, M. A., & Salem, A. M. (2005). Laminar Mixed Convection Adjacent to Vertical Continuously Stretching Sheets With Variable Viscosity and Variable Thermal Diffusivity. *Heat and Mass Transfer*, *41*(12), 1048–1055. doi: 10.1007/s00231-005-0629-6

Selim, A., Hossain, M. A., & Rees, D. A. S. (2003). The effect of surface mass transfer on mixed convection flow past a heated vertical flat permeable plate with thermophoresis. *International Journal of Thermal Sciences*, *42*(10), 973–982. doi: 10.1016/S1290-0729(03)00075-9

Sheri, S.R., Chathilla, V. and Mahendar, D. (2018). Unsteady mhd flow over an inclined porous plate embedded in porous medium with heat absorption and Soret-Dufour effects. *Int J Pure Appl Math*, 8021–8049.

Shit, G. C., Haldar, R., & Ghosh, S. K. (2016). Convective Heat Transfer and MHD Viscoelastic Nanofluid Flow Induced by a Stretching Sheet. *International Journal of Applied and Computational Mathematics*, *2*(4), 593–608. doi: 10.1007/s40819-015-0080-4

Slaouti, A., Takhar, H. S., & Nath, G. (1998). Unsteady free convection flow in the stagnation-point region of a three-dimensional body. *International Journal of Heat and Mass Transfer*, *41*(22), 3397–3408. doi: 10.1016/S0017-9310(98)00080-5

Sreelakshmy, K.R., Nair, A.S., Vidhya, K.M., Saranya, T.R. and Nair, S. C. (2014). INTERNATIONAL RESEARCH JOURNAL OF PHARMACY. *INTERNATIONAL RESEARCH JOURNAL OF PHARMACY.*, 1–5.

Sun, H., Li, R., Chénier, E., & Lauriat, G. (2012). On the modeling of aiding mixed convection in vertical channels. *Heat and Mass Transfer*, *48*(7), 1125–1134. doi: 10.1007/s00231-011-0964-8

Talbot, L.R.K.R.W.D.R., Cheng, R.K., Schefer, R.W. and Willis, D. R. (1980). Thermophoresis of particles in a heated boundary layer. Journal of fluid mechanics. *Fluid Machanics*, 737–758.

Uddin, M. N., Ali, M. Y., Zahed, N. M. R., & Uddin, M. J. (2016). Similarity Solutions of Unsteady Mixed Convective Boundary Layer Flow of Viscous Incompressible Fluid along Isothermal Horizontal Plate. *Open Journal of Fluid Dynamics*, *06*(04), 279–302. doi: 10.4236/ojfd.2016.64022

Uddin, Md. Jashim, & Ali, M. Y. (2016). Effects of Hydromagnetic and Thermophoresis of Unsteady Forced Convection Boundary Layer Flow over Flat Plates. *Journal of Applied Mathematics and Physics*, *04*(09), 1756–1776. doi: 10.4236/jamp.2016.49182

Uddin, Md. Jashim, Khan, W. A., & Ismail, A. I. M. (2013). MHD Forced Convective Laminar Boundary Layer Flow from a Convectively Heated Moving Vertical Plate with Radiation and Transpiration Effect. *PLoS ONE*, *8*(5), e62664. doi: 10.1371/journal.pone.0062664

Uddin, Mohammed J., Khan, W. A., & Ismail, A. I. (2012). MHD Free Convective Boundary Layer Flow of a Nanofluid past a Flat Vertical Plate with Newtonian Heating Boundary Condition. *PLoS ONE*, *7*(11), 1–8. doi: 10.1371/journal.pone.0049499

Venkatasubbaiah, K., & Sengupta, T. K. (2009). Mixed convection flow past a vertical plate: Stability analysis and its direct simulation. *International Journal of Thermal Sciences*, *48*(3), 461–474. doi: 10.1016/j.ijthermalsci.2008.03.019

Walker, K.L., Homsy, G.M. and Geyling, F. T. (1979). Thermophoretic deposition of small particles in laminar tube flow. *Journal of Colloid and Interface Science*, 138–147.

Wang, G., Zhang, Z., Wang, R., & Zhu, Z. (2020). A review on heat transfer of nanofluids by applied electric field or magnetic field. *Nanomaterials*, *10*(12), 1–24. doi: 10.3390/nano10122386